ORSAY
n° d'ordre : 2648

UNIVERSITE DE PARIS-SUD

CENTRE D'ORSAY

THESE

présentée

Pour obtenir

Le grade de DOCTEUR es Sciences Physiques

PAR

MANTRACH Abdelhaq

SUJET : INTERACTIONS FORTES ET CHROMODYNAMIQUE A L'APPROXIMATION DES LOGARITHMES DOMINANTS

soutenue le 15 novembre 1982 devant la Commission d'examen

MM. Alessandrini V. Président

Chadan K.

Cohen-Tannoudji G.

Davier M.

Fontannaz M.

Morel A.

ORSAY
n° d'ordre :

UNIVERSITE DE PARIS-SUD

CENTRE D'ORSAY

THESE

présentée

Pour obtenir

Le grade de DOCTEUR es Sciences Physiques

PAR

MANTRACH Abdelhaq

SUJET : INTERACTIONS FORTES ET CHROMODYNAMIQUE A L'APPROXIMATION DES LOGARITHMES DOMINANTS

soutenue le 15 novembre 1982 devant la Commission d'examen

MM. Alessandrini V. Président

Chadan K.

Cohen-Tannoudji G.

Davier M.

Fontannaz M.

Morel A.

UNIV.
LEIDEN
BIBL.

Remerciements

Je remercie Messieurs Khosrow Chadan et Michel Fontannaz qui m'ont accueilli au Laboratoire de Physique Théorique et Hautes Energies d'Orsay et ont accepté de faire partie du jury de soutenance.

Je tiens à témoigner ici du grand plaisir que j'ai eu à travailler avec G. Cohen-Tannoudji. Je suis heureux de pouvoir lui dire ici combien son amitié et ses conseils m'ont été précieux tout au long de cette année.

Je remercie également tous les physiciens des Laboratoires de Physique Théorique et Hautes Energies d'Orsay et de Saclay avec les quels j'ai eu de nombreuses et fructueuses discussions, en particulier Monsieur H. Navelet et Madame D. Schiff.

Je remercie Monsieur le Professeur V. Alessandrini d'avoir accepté la présidence de mon jury de thèse, ainsi que Monsieur le Professeur M. Davier et Monsieur A. Morel d'avoir bien voulu en faire partie.

Je remercie enfin M.T. Pillet et M. Calvet pour la gentillesse avec laquelle elles ont pris soin du travail de frappe, ainsi que Mesdames J. Bellone, L. Bourdois et D. Piton pour l'aide qu'elles m'ont apportée dans l'impression de cette thèse.

ABSTRACT

This thesis is a contribution to the study of Quantum Chromodynamics (QCD) at the leading logarithm approximation (LLA). We have used the interpretation of the LLA in terms of the generalized parton model to propose tests of elementary processes of QCD in large transverse momentum photoproduction reactions. We have used the LLA to sum gluon radiation effects induced in high energy hadronic reactions. We have obtained this way a rise of the nucleon-nucleon total cross section of 15 mb from 60 GeV to 540 GeV. We have exploited the existence of a preconfinement transition in the LLA to study scaling violations in the framework of the dual parton model.

Digitized by the Internet Archive
in 2026

https://archive.org/details/IA41543522_0001

S O M M A I R E

Introduction

Chapitre I : Chromodynamique quantique et modèle des partons généralisés.

I.1. Le groupe de renormalisation.
I.2. Diffusion inélastique profonde (méthode standard ou développement de Wilson).
I.3. La méthode diagrammatique et modèle des partons généralisés.
I.4. Photoproduction des hadrons de grande impulsion transverse P_T et tests de QCD.

Chapitre II : La radiation des gluons et la montée de la section efficace totale hadronique inélastique.

Chapitre III : Q.C.D. à l'approximation des logarithmes dominants et le modèle dual des partons.

III.1. Le préconfinement.
III.2. Confinement et développement topologique.
III.3. DTU et le modèle dual des partons.

Introduction

La théorie des particules élémentaires a connu durant les années 70 de véritables mutations grâce à la compréhension améliorée des théories de jauge. L'un des progrès les plus importants a été l'élaboration d'une théorie de jauge candidate à être la théorie de l'interaction forte, la chromodynamique quantique (QCD). QCD est une théorie de jauge non abélienne, dont le groupe de jauge est le groupe SU(3) de couleur, dont les champs fermioniques de matière sont les quarks et les champs de jauge les gluons.

QCD est une théorie renormalisable satisfaisant la propriété de liberté asymptotique (le couplage effectif s'annule à grand transfert d'impulsion). C'est cette propriété fondamentale qui justifie le choix de QCD comme la théorie sous-jacente de la structure hadronique car elle apporte une explication théorique cohérente aux phénomènes observés dans les réactions à grand transfert d'impulsion.

Cependant des problèmes importants restent ouverts. Les quanta des champs fondamentaux de QCD, les quarks et les gluons ne sont pas observables à l'état libre, seuls sont observables les hadrons, états liés de quarks et de gluons, singulet du groupe de couleur. Il est généralement admis que ce "confinement" des quarks et des gluons est lié, de manière non perturbative, au comportement singulier de QCD dans l'infrarouge. C'est pourquoi il est indispensable de dépasser les simples méthodes perturbatives si l'on veut disposer d'une description globale et cohérente de l'interaction forte avec QCD.

D'ailleurs, même pour tester QCD au niveau perturbatif, c'est-à-dire pour isoler les processus élémentaires au niveau des partons (les quarks et les gluons), il apparaît nécessaire de faire appel à des resommations de termes perturbatifs. La méthode des logarithmes dominants (approximation des logarithmes dominants ALD) permet de justifier la factorisation des singularités de masse et conduit à une interprétation physique simple (modèle des partons généralisé)

des processus à grand transfert d'impulsion. C'est cette méthode qui est à l'origine de tous les tests des processus élémentaires de QCD dans les réactions "dures" impliquant des hadrons, des leptons ou des photons. Dans la première partie du travail sont présentés des tests de QCD dans les réactions de photoproduction inclusive à grande impulsion transverse.

Nous avons étudié l'application de QCD perturbatif à la photoproduction des hadrons à grand moment transfert. Nous avons montré que la section efficace différentielle inclusive à une particule est insensible aux effets de mouvement de Fermi intrinsèque, et nous avons montré en particulier comment cette réaction permet de tester QCD et de déterminer les fonctions de structure et de fragmentation des gluons.

D'importantes similarités ont été observées dans les distributions d'état multihadronique obtenues dans des réactions purement hadroniques et dans des réactions dures impliquant des leptons : accroissement des multiplicités et du moment transverse moyen, corrélations de longue portée en rapidité, etc. Puisque QCD est le cadre théorique adapté à la description des observables dans les réactions à grand transfert d'impulsion, les similarités observées suggèrent que QCD pourrait aussi expliquer certains aspects des réactions purement hadroniques sans grand transfert d'impulsion. Dans la deuxième partie du présent travail nous nous sommes intéressés à la description par QCD du comportement des sections efficaces totales en fonction de l'énergie. L'ALD permet de resommer toutes les corrections radiatives (émission bremstrahlung de gluons) en terme d'échange d'un gluon dans une collision parton-parton. Nous avons ainsi calculé à l'ALD, la somme de toutes les sections efficaces de production multiple de parton induites dans une collision hadronique à haute énergie. Nous avons pu montrer que cette somme contribue à une part importante de la section efficace totale : bien que chaque section efficace individuelle soit petite et décroissante, l'accroissement rapide des multiplicités de partons conduit à une section efficace totale importante et croissante.

Une estimation quantitative de cet effet est présentée dans la deuxième partie : à l'aide d'un seul paramètre concentrant tous les effets non perturbatifs et qui peut être fixé à une valeur raisonnable puisqu'il s'agit de la masse du quark constituant (de l'ordre du tiers de la masse du nucléon) nous avons trouvé une montée de la section efficace totale nucleon-nucleon de 15 mb entre 60 GeV (energie des ISR) et 540 GeV (energie des collisions $p\bar{p}$ au SPS).

Un tel succès encourage de tenter de prolonger la méthode ALD, qui est une méthode de resommation à couplage faible, jusqu'à la région des couplages forts c'est-à-dire la région où l'on s'attend au confinement des partons. Ainsi dans le processus d'annihilation e^+e^- en hadrons, il apparaît que les graphes dominants, dans la jauge axiale, à l'ALD, sont des diagrammes en arbres ordonnés : un quark de virtualité maximum perd cette virtualité successivement par l'émission de gluons presque colinéaires jusqu'à une virtualité de transition Q_T où les partons produits commencent à s'organiser en amas singulets de couleur. On appelle préconfinement ce phénomène ; les amas singulets de couleur de masse Q_T sont des sortes de "pré-hadrons" dont l'évolution postérieure dépend d'effets non perturbatifs à couplage fort. La meilleure technique adaptée à la description de tels effets est celle du développement topologique. Initiée par 't Hooft cette méthode a l'avantage d'opérer la jonction avec le schéma d'unitarisation topologique dual (DTU) qui s'est révélée très efficace pour la description des réactions à petit transfert d'impulsion. Il convient de remarquer que la topologie planaire des configurations de pré-hadrons permet d'opérer une transition vers le développement topologique de DTU. C'est cette transition que nous avons étudié dans la troisième partie du travail.

a) Les fonctions de fragmentation des quarks

Nous avons derivé un modèle pour les fonctions invariantes d'échelle de fragmentation des quarks u,d,s et c en mesons pseudo-scalaires et vectoriels à partir de DTU en utilisant l'interprétation partonique de la composante planaire de la section efficace inclusive à une particule. La comparaison avec l'expérience est satisfaisante.

b) Les fonctions de structure de quark et de gluon

Nous proposons une paramétrisation simple pour les fonctions de structure de valence, de quarks de la mer et du gluon dans le nucléon à tout x et tout Q^2. Nous utilisons le modèle dual des partons pour fixer cette paramétrisation à un point de référence ($Q_T^2 = 1.25\ GeV^2$) et nous obtenons l'évolution prédite par QCD en remplaçant les paramètres dimensionés de DTU par des fonctions dépendantes de Q^2, un excellent accord en comparaison avec les données expérimentales est obtenu.

C H A P I T R E I

I Chromodynamique quantique et modèle des partons généralisés.

I.1. Le groupe de renormalisation.

I.2. Diffusion inélastique profonde (méthode standard ou développement de Wilson).

I.3. La méthode diagrammatique et modèle des partons généralisés.

I.4. Photoproduction des hadrons de grande impulsion transverse P_T et tests de QCD.

C H A P I T R E I

I.1. Le groupe de renormalisation[1].

Considérons la fonction de Green renormalisée (Nq quarks et N_G gluons externes) qu'on peut écrire sous la forme suivante

$$\Gamma_R^{N_q,N_G}(P_j,g,\mu) = Zq^{Nq/2}\, Z_G^{N_G/2}\, \Gamma_{reg}^{Nq,N_G}(P_j,g_o,\varepsilon) \qquad (I.1)$$

où ε est le paramètre introduit pour la régularisation[2] dimensionnelle. Z_q et Z_G sont respectivement les constantes de renormalisation des fonctions d'ondes de quark et de gluon. La structure multiplicative de la renormalisation des fonctions de Green nous donne les équations du groupe de renormalisation de Callan-Symanzik (C-S), qui expriment le fait que les quantités physiques ne dépendent pas du choix du point de renormalisation μ.

$$(\mu\partial/\partial\mu + \beta(g)\frac{\partial}{\partial g} - N_q\gamma_q(g) - N_G\gamma_G(g))\,\Gamma_R^{N_q,N_G}(P_j,g,\mu) = 0 \qquad (I.2)$$

$$\gamma_q(g) = \frac{1}{2}\,\mu\,\frac{1}{Zq}\,\frac{\partial Z_q}{\partial \mu}$$

$$\gamma_G(g) = \frac{1}{2}\,\mu\,\frac{1}{Z_G}\,\frac{\partial Z_G}{\partial \mu} \qquad (I.3)$$

$$\beta(g) = \mu\,\frac{\partial g}{\partial \mu}$$

Appelons d la dimension de $\Gamma_R^{Nq,\,N_G}$ en unité de masse. Sous l'effet d'une dilatation des impulsions P_j par un facteur λ et par le théorème d'Euler, on a

$$(\lambda\partial/_{\partial\lambda} + \mu\ \partial/_{\partial\mu} - d)\ \Gamma_R^{Nq,N_G}(\lambda P_j, g, \mu) = 0 \qquad (I.4)$$

Combinant les équations (I.2) et (I.4) et notant $t = \log \lambda$, on obtient

$$\left(-\frac{\partial}{\partial t} + \beta(g)\frac{\partial}{\partial g} - N_q\gamma_q(g) - N_G\gamma_G(g) + d\right)\ \Gamma_R^{N_q,N_G}(e^t P_j, g, \mu) = 0$$

(I.5)

la solution de cette équation exprime la dépendance par rapport aux dilatations de la fonction de Green considérée :

$$\Gamma_R^{Nq,N_G}(e^t P_j, g, \mu) = \lambda^d\ \Gamma_R^{Nq,N_G}(P_j, \bar{g}(t), \mu)\ \exp -\int_g^{g(t)} \frac{(Nq\gamma_q(g') + N_G\gamma_G(g'))}{\beta(g')}\,dg'$$

(I.6)

où la constante de couplage $\bar{g}$ est la solution de l'équation différentielle suivante :

$$\frac{d\bar{g}^2}{dt} = \bar{g}\beta(\bar{g}) \ , \ \bar{g}(t=0) = g \ , \qquad (I.7)$$

et γ_q, γ_G sont les dimensions anormales. Dans la jauge de Feynman elles sont données par [3-4]

$$\left.\begin{aligned} \gamma_q(g) &= \frac{4}{3}\ g^2/16\pi^2 = \gamma_q^o\ g^2/16\pi^2 + O(g^4) \\ \gamma_G(g) &= \frac{g^2}{16\pi^2}\left(5 - \frac{2}{3}N_F\right) = \gamma_G^o\ g^2/16\pi^2 + Q(g^4) \end{aligned}\right\} \qquad (I.8)$$

$$\beta(g) = -\beta_o \frac{g^3}{16\pi^2} + O(g^5)$$

$$\beta_o = 11 - 2N_f/Nc \qquad (I.9)$$

N_f et N_C sont respectivement le nombre de saveur et de couleur. Il est facile de montrer à l'ordre dominant, en utilisant les équations (I.7) et (I.8), que la constante de couplage dépendant de l'échelle t est :

$$4\pi\bar{\alpha}_s(t) = \bar{g}^2(t) = \frac{g^2}{1 + \frac{g^2\beta_o t}{16\pi^2}} \qquad (1.10)$$

Pour $N_f \leq 16$ et $N_c = 3, \bar{g}^2(t)$ décroit lorsque t croit. Ceci implique

d'une part que (voir I.6) les fonctions de Green des champs en interaction à grande impulsion s'expriment en fonction d'une quantité $\Gamma(P_j, \bar{g}(t),\mu)$ calculable perturbativement. (la théorie dans laquelle les fonctions de Green ont un tel comportement est asymptotiquement libre). D'autre part, la violation de la loi de l'invariance d'échelle pour ces fonctions de Green est logarithmique. (l'exponentielle de la relation (I.6) à l'ordre dominant est proportionnelle à $(\log\lambda)^C$ où $C = -(N_G\gamma_G^{\,o} + N_q\gamma_q^{\,o})/2\beta_o$)

I.2. Diffusion inélastique profonde[1],[4-9]:(méthode standard ou développement de Wilson)

Dans cette section nous allons montrer brièvement comment le développement sur le cône de lumière du produit de deux courants[10] et les équations de groupe de renormalisation nous conduisent à des violations de la loi d'invariance d'échelle sous forme d'une dépendance logarithmique en Q^2 (carré du transfert du moment) pour les processus de diffusion profondément inélastiques. Ces violations sont en bon accord avec l'expérience[11].

Considérons la diffusion profondément inélastique sur le proton figure 1.

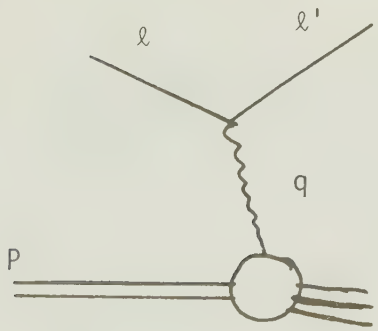

$(q^2 = -Q^2)$ Fig. 1

L'étude de cette diffusion nous amène à étudier le tenseur hadronique défini par :

$$W_{\mu\nu}(P,q) = \int d^4z\, e^{iqz} < P| \left[J_\mu(z), J_\nu^+(0) \right] |P >$$

$$= \ell_{\mu\nu} \frac{\nu W_L}{2x} (\nu, Q^2) + d_{\mu\nu} \frac{\nu W_2(\nu, Q^2)}{2X} \qquad (I.11)$$

$$- i\, \varepsilon_{\mu\ \nu\alpha\beta} \frac{P_\alpha q_\beta}{\nu} \nu\, W_3(\nu, Q^2)$$

où J_μ est le courant electromagnétique (W_3=0) ou le courant faible, les tenseurs $\ell_{\mu\nu}$ et $d_{\mu\nu}$ sont donnés par

$$\ell_{\mu\nu} = g_{\mu\nu} - \frac{q_\mu q_\nu}{q^2}$$

$$d_{\mu\nu} = - \frac{P_\mu P_\nu}{\nu^2} q^2 + \frac{P_\mu q_\nu + P_\nu q_\mu}{\nu} - g_{\mu\nu} \qquad (I.12)$$

$$\nu = p.q \qquad Q^2 = - q^2$$

$$x = Q^2 / p.q$$

Le tenseur hadronique $W_{\mu\nu}$ est exprimé à partir de l'amplitude compton élastique vers l'avant par

$$W_{\mu\nu}(P,q) = \frac{1}{2\pi} \mathrm{Im}\, T_{\mu\nu}(P,q) \qquad (I.13)$$

$$\text{où} \quad T_{\mu\nu}(P,q) = i \int d^4z\, e^{iqz} < P|T\, J_\mu(z) J_\nu^+(0)|P > \qquad (I.14)$$

Si nous nous intéressons à la limite de Bjorken ($Q^2 \to \infty$, $p.q \to \infty$;

x fixé), la région $z^2 \to 0$ domine l'intégrale du membre de droite[1]. Ceci amène à développer le produit ordonné dans le temps de deux courants au voisinage du cône de lumière (développement de Wilson). Après transformée de Fourier, il vient :

$$T_{\mu\nu}(P,q) = \sum_{n,i} \{(g_{\mu\nu} - \frac{q_\mu q_\nu}{q^2})\, q_{\mu_1}\, q_{\mu_2}\, C^i_{L,n}\,(Q^2/\mu^2,\, g^2)$$

$$-(g_{\mu\mu_1}\, g_{\nu\mu_2}\, q^2 - g_{\mu\mu_1}\, q_\nu q_{\mu_2} - g_{\nu\mu_2}\, q_\mu q_{\mu_1} + g_{\mu\nu}\, q_{\mu_1}\, q_{\mu_2}) C^i_{2,n}\,(Q^2/\mu^2,\, g^2)$$

$$-i\varepsilon_{\mu\nu\alpha\beta}\, g_{\alpha\mu_1} q_\beta q_{\mu_2}\, C^i_{3,n}\,(Q^2/\mu_2, g^2)\} q_{\mu_3} \ldots q_{\mu_n} (2/Q^2)^n \langle P|O_i^{\mu_1 \ldots \mu_n}|P\rangle$$

(I.15)

où les $C^i_K(Q^2/\mu^2, g^2)$ sont les transformées de Fourier des coefficients de Wilson (K=L,2,3).

En se limitant à la contribution dominante on peut définir l'opérateur O_i (twist deux) entre les états de proton par :

$$\langle P|O_i^{\mu_1 \ldots \mu_n}|P\rangle = A^i_n(\mu^2) P^{\mu_1 \ldots} P^{\mu_n} \qquad \text{(I.16)}$$

$A^i_n(\mu^2)$ est l'amplitude réduite. i(i = q_{NS},q,G) correspond respectivement à un opérateur du quark non singlet et aux opérateurs singulet de quark et de gluon. L'indice n est le spin de l'opérateur $O_i^{\mu_1 \ldots \mu_n}$. Substituant la relation (I.16) dans (I.15) nous obtenons

$$T_{\mu\nu}(Q^2,x) = \sum_n \left(\frac{1}{x}\right)^n \{ \ell_{\mu\nu}\, C^i_{L,n}\,(Q^2/\mu^2,g^2) + d_{\mu\nu}\, C^i_{2,n}\,(Q^2,g^2)$$

$$-i\,\varepsilon_{\mu\nu\alpha\beta}\,\frac{p_\alpha q_\beta}{\nu}\; C^i_{3,n}\left(\frac{Q^2}{\mu^2},g^2\right)\} A^i_n(\mu^2) \qquad \text{(I.17)}$$

Tenant compte de relations (I.11), (I.13) et (I.17) on peut relier les moments de fonctions de structure aux coefficients de Wilson par

$$M_K(n,Q^2) = \int_0^1 dx\, x^{n-2}\, F_K(x,Q^2) = \sum_i A^i_n(\mu^2) C^i_{K,n}\,(Q^2/\mu^2,\, g^2) \qquad \text{(I.18)}$$

$(K = 2,L)$

$$M_3(n,Q^2) = \int_0^1 dx\, x^{n-1}\, F_3(x,Q^2) = \sum_i A^i_n\,(\mu^2) C^i_{3,n}(Q^2/\mu^2,\, g^2) \qquad \text{(I.19)}$$

$(F_{2,3,L} = \nu W_{2,3,L})$

Il est bien connu que les coefficients $C^i_{K,n}$ de Wilson obeissent à l'équation de C-S, dont la solution est donnée dans le cas non singlet par [13,14]

$$M^{NS}_K(n,Q^2) = \delta^{NS}_K\, A^{NS}_n(\mu^2 = Q^2_o)\, \exp(-d^n_{NS}\, V(Q^2)) \qquad \text{(I.20)}$$

avec $d^n_{NS} = \dfrac{\gamma^{o,n}_{NS}}{2\beta_o}$ $\qquad (\gamma^{o,n}_{NS} = \dfrac{6\pi^2}{g^2}\,\gamma^n_{NS}(g^2))$

δ_K^{NS} est un facteur dépendant du processus (l'interaction électromagnétique ou faible)

$$V(Q^2) = \log\left(\frac{\log \frac{Q^2}{\Lambda^2}}{\log \frac{Q_o^2}{\Lambda^2}}\right) \qquad (I.21)$$

Λ est le paramètre d'échelle de QCD.

Les $A_n^i(Q_o^2)$ de l'équation (I.20) ne sont pas calculables par QCD perturbatif mais peuvent s'interpréter comme les moments des distributions du parton i dans le proton mesurées à $Q^2 = Q_o^2$. Les coefficients $C_{K,n}^i$ prédisent l'évolution en Q^2 des moments des fonctions de structure. Les coefficients de Wilson pour la partie singlet obéissent également à l'équation du groupe de renormalisation dont la solution est une combinaison linéaire de $(\bar{g}^2(Q^2)/\bar{g}^2(Q_o^2))^{d_\pm^n}$ où $d_\pm^n = \lambda_\pm^n/2\beta_o$

$\lambda_\pm^n$ sont les valeurs propres de la matrice 2x2 (q,G) des dimensions anormales des opérateurs singlets du quark et du gluon (O_q^n, O_G^n).

Il se trouve que malheureusement on ne peut pas appliquer une analyse semblable aux processus durs pour lesquels Q^2 est du genre temps (c'est à dire là on ne peut pas utiliser le développement sur le cône de lumière). La méthode diagrammatique pour ces processus est très féconde et permet de justifier le modèle des partons (voir I.3).

I.3. La méthode diagrammatique[15-20] et le modèle des partons généralisés[21-25].

Le point central dans cette approche consiste à reconnaître les diagrammes donnant les termes logarithmiques dominants, c'est à dire qu'à chaque ordre du développement en perturbation nous retenons seulement les termes qui sont de type $(\alpha_s \log Q^2)^n$ pour des grands Q^2, plus précisément :

$\alpha_s(Q_o^2)/\pi << 1$, $(\alpha_s/\pi) \log (Q^2/Q_o^2) \sim 1$.

Considérons la fonction non singlet $F_3^{\nu N}$. Dans le modèle des partons naifs :

$$F_3^{\nu N}(x) = \sum_i q_i(x)$$

où $q_i(x)$ sont les distributions de quarks de valence (u,d) dans le proton.

En théorie de perturbation à l'ALD on peut écrire :

$$F_3^{\nu N}(x,Q^2) = \sum_i \int_x^1 \frac{dy}{y}\ q_i(y)\ d\sigma_i(x/y,Q^2) \qquad \text{(I.22)}$$

$$d\sigma_i = d\sigma_{q_i\gamma^* \to q_i} + d\sigma_{q_i\gamma^* \to q_i g} + \ldots$$

C'est à dire, en prenant la virtualité de quark q_i égal à à $-p^2$,

$$F_3^{\nu N}(x,Q^2) = \sum_i \int_x^1 \frac{dy}{y}\ q_i(y)\ e_{q_i}^2 \left[\delta(1-x/y) + \alpha_s\ P_{qq}(x/y)\ \log\left(\frac{Q^2}{-p^2}\right)\right.$$

$$\left. + O(1/Q^2)\right] \qquad \text{(I.23)}$$

Lorsque P^2 tend vers zero, la relation (I.23) n'a plus de sens puisqu'elle contient une singularité de masse. La démonstration de la factorisation revient en fait à démontrer qu'on peut regrouper ces facteurs divergents dans une fonction de distribution dependant de Q^2.

En effet le moment de $F_3^{\nu N}$ s'écrit,

$$F_3^{\nu N}(n,Q^2) = \int_0^1 dx\, x^{n-1} F_3^{\nu N}(x,Q^2) = \sum_i \int_0^1 dy\, y^{n-1} q_i(y) \int_0^1 dz\, z^{n-1} d\sigma_i(z,Q^2)$$

(I.24)

avec

$$\int_0^1 dz\, z^{n-1}\, d\sigma_i(z,Q^2) = e^2 q_i (1+\alpha_s P_{qq}(n) \log Q^2/-p^2 + \ldots)$$

$$= (1 + \alpha_s\, P_{qq}(n) \log (Q_o^2/-p^2 + \ldots)(1 + \alpha_s\, P_{qq}(n) \log Q^2/Q_o^2 + \ldots)$$

(I.25)

$$\int_0^1 dy\, y^{n-1} q_i(y)(1+\alpha_s P_{qq}(y) \log Q_o^2/-p^2+\ldots) \equiv \int_0^1 dy\, y^{n-1} q_i(y,Q_o^2)$$

(I.26)

$$F_3^{\nu N}(n,Q^2) = \sum_i e_{q_i}^2 \int_0^1 dy\, y^{n-1} q_i(y,Q_o^2)(1+\alpha_s\, P_{qq}(n) \log Q^2/Q_o^2 + \ldots)$$

$$\equiv \sum_i \int_0^1 dy\, y^{n-1} q_i(y,Q^2) \qquad \text{(I.27)}$$

La deuxième partie de (I.27) $(1+\alpha_s P_{qq}(n) \log Q^2/Q_o^2 + \ldots)$ est alors parfaitement finie mais contient des $\log Q^2/Q^2_o$ qu'on resomme à tous les ordres ; la structure générale du modèle de parton n'est pas affectée puisqu'il suffit de remplacer $q_i(x)$ par une fonction dépendant de Q^2 $q_i(x,Q^2)$.

La méthode diagrammatique peut être étendue à des processus durs. Par exemple la section efficace de production d'un pion à grand P_T peut s'écrire

$$E \frac{d\sigma}{d^3P} (AB \to \pi X) = \sum_{abc} \int dx_a \, dx_b \, \frac{dz}{z} \, G_{a/A}(x_q, Q^2)$$

$$G_{b/B}(x_b, Q^2) \, D_{\pi/c}(z, Q^2) \, E_c \frac{d\sigma}{d^3P_c} (ab \to cX) \qquad (I.28)$$

où les quantités $G_{a/A}(x,Q^2)$ sont les mêmes que celles qui apparaissent dans la diffusion inélastique profonde et les facteurs $E_c \frac{d\sigma}{d^3P}$ dépendent de la réaction envisagée et sont calculés avec la constante de couplage $\alpha_s(Q^2)$.

la formule (I.28) se réécrit sous la forme[25]

$$E \frac{d\sigma}{d^3P} (AB \to \pi X) = \sum_{abc} \int dx_a \, dx_b \, \frac{dz}{z^2} \, G_{a/A}(x_a, Q^2) \, G_{b/B}(x_b, Q^2)$$

$$D_{\pi/c}(z, Q^2) \, \delta(\hat{s}+\hat{t}+\hat{u}) \, \frac{1}{\pi} \frac{d\sigma}{d\hat{t}} (\hat{s}, \hat{t}, \hat{u}, \alpha_s(Q^2))$$

(I.29)

I.4. Photoproduction des hadrons de grande impulsion transverse P_T et tests de QCD.

La phénoménologie de la chromodynamique quantique a accompli un progrès énorme dans l'étude de la leptoproduction (ℓN), l'annihilation e^+e^- et la production hadronique de pair de leptons. Cependant dans ces réactions QCD ne se manifeste que par des corrections à un terme de Born impliquant des quarks. L'observation de jets de gluons est cruciale pour la vérification de QCD perturbatif et la structure en trois jets découverte dans l'annihilation e^+e^- a été la meilleure confirmation de l'existence de gluons. Il est cependant difficile d'aller très loin dans cette réaction et d'étudier les propriétés des gluons, mais le cas de la photoproduction à grand P_T est différent puisque les gluons apparaissent dès le terme de Born. Dans ce schéma le photon est considéré comme ponctuel (l'interaction directe avec le proton), ou comme composite (description à l'aide de la fonction de structure). L'idée fondamentale est de tirer profit de la nature ponctuelle du photon et de son couplage au quark proportionnel à la charge éléctrique. On sait alors que parmi les graphes de couplage direct (fig. 2) seul le graphe Compton contribue à une

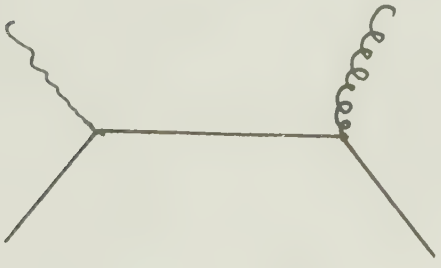

graphe Compton

fig. 2

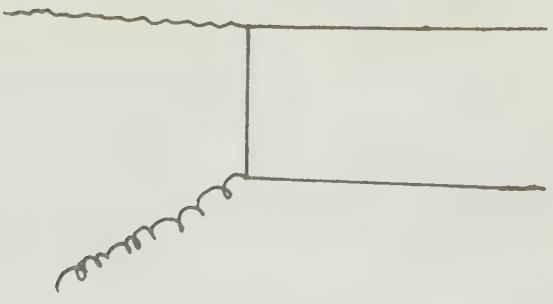

graphe de Fusion

difference de section efficace du type $d\sigma(\gamma P \to h^+X) - d\sigma(\gamma P \to h^-X)$. En fait, seule la partie valence de la fonction de structure et la fonction de fragmentation du quark intervient dans ce calcul. Il est évident que les effets de mouvement de Fermi intrinsèque seront moins importants ici que dans l'hadroproduction. Nous avons montré qu'ils étaient négligeables.

Dans les ref. (26) et (27) nous avons présenté une étude complète des conséquences de l'application de la chromodynamique quantique perturbative à la photoproduction de particule de grande impulsion transverse. Nous avons montré comment on peut isoler les contributions des différents sous-processus (couplage direct du photon par les termes de Compton ou de fusion, couplage indirect du photon par l'intermédiaire de la composante anormale ou par la composante hadronique de sa fonction de structure). Les résultats expérimentaux de la collaboration WA4 au CERN sont analysés. Ils indiquent une intéressante convergence entre la théorie et l'expérience vers des impulsions transverse,de 2.5 GeV/c. Les ref.(28) et (29) abordent une étude spécifique de la physique des gluons qu'on peut effectuer dans les réactions de photoproduction à grande impulsion transverse. On peut mesurer la fonction de fragmentation du gluon en hadrons, y compris sa variation en Q^2 telle qu'elle est prédite par la chromodynamique quantique. On peut ensuite mesurer la fonction de structure du gluon dans le proton, en isolant la contribution du sous-processus de fusion $\gamma g \to q\bar{q}$; les ordres de grandeur obtenus sont amplement suffisants à une bonne détermination de cette fonction dont diverses formes ont été proposées dans la littérature[30].

En conclusion nous pouvons dire que la photoproduction à grande impulsion transverse est un bon candidat pour tester la validité de QCD perturbatif.

REFERENCES

(1) D.J. Gross, in Methods in Field Theory, Les Houches 1975, edited by R. Balian and J. Zinn-Justin (North-Holland, Amsterdam, 1976)

E. De Rafael, Ecole d'ete de Physique des Particules - Gif/Yvette Tome 2 (1978) - France

V. Alessandrini, Deuxième Rencontre de Rabat, 1979, Maroc.

J. Ellis, in weak and electromagnetic interactions at high energies Les Houches, 1976, edited by R. Balian and C.H. Llewellyn Smith (North-Holland, Amsterdam, 1977).

(2) G. 'T Hooft, Nucl. Phys. B61, 455 (1973)

(3) D.J. Gross and F. Wilczek, Phys. Rev. Lett. 30, 1343 (1973) ; Phys. Rev. D8, 3633 (1973).

H.D. Politzer, Phys. Rev. Lett. 30, 1346 (1973).

(4) H.D. Politzer, Phys. Reports 14C, 129 (1974)

C.H. Llewellyn Smith, Acta Physica Austriaca, suppl. XIX (1978) 331.

(5) F.E. Close, An introduction to quarks and partons, Academic Press, 1979.

(6) A.J. Buras, Rev. Mod. Phys. 52, 199 (1980)

(7) A. Peterman, Phys. Reports 53, 157 (1978)

(8) E. Reya, Desy preprint 79/88

(9) J. Ellis and C.T. Sachrajda, Cargese Summer Institute on quarks and leptons (1979)

(10) R.G. Wilson, Phys. Rev. 179, 1499 (1969)

(11) J.G.H. de Groot et al., Z. Phys. C1, 143 (1979)

P.C. Bossetti et al., Nucl. Phys. B142, 1 (1978)

(12) N. Christ, B. Hasslacher and A. Muller, Phys. Rev. D6, 3543 (1972)

(13) H. Georgi and H.D. Politzer, Phys. Rev. D9, 416 (1974).

(14) D.J. Gross and G. Wilczek, Phys. Rev. D9, 980 (1974)

(15) Yu. L. Dokshister, D.I. Dyakanov and S.I. Troyan, Phys. Reports 58, 271 (1980) ; Phys. Lett. 79B, 269, (1978)

(16) K.H. Craig and C.H. Llewellyn Smith, Phys. Lett. 72B, 349 (1978)

(17) C.H. Llewellyn Smith, Schladming Lectures, 1979, Acta Physica Austriaca XIX, 331 (1978)

(18) W.R. Frazer and J.F. Gunion, Phys. Rev. D19, 2447 (1979)

(19) M. Gourdin, Lectures at Rencontre de Rabat (Maroc) 1979 ; Lectures at Kupari Summer School (1979)

(20) L.N. Lipatov, Sov. J. Nuclear Phys. 20 (1975) 94.
Yu. L. Dokshitzev, JETP (Sov. Phys.) 46 (1977) 641.

(21) R. Ellis et al, Phys. Lett. 78B (1978) 281, Nucl. Phys. B152 (1979) 285

(22) H.D. Politzer, Nucl. Phys. B129 301 (1977)

(23) A.V. Radyushkin, Phys. Lett. 69B, 245 (1977)

(24) C.T. Sachrajda, Phys. Lett. 82B, 79 (1979)

(25) S.M. Berman, J.D. Bjorken and J.B. Kogut, Phys. Rev. D4? 3388 (1971) ; S.D. Ellis and M.B. Kislinger, Phys. Rev. D9, 2027 (1974) ; D. Sivers, S.J. Brodsky and R. Blankenbecler, Physics Reports 23C, 1 (1976)

(26) M. Fontannaz, A. Mantrach, B. Pire et D. Schiff, Phys. Lett. 89B (1980) 263.

(27) M. Fontannaz, A. Mantrach, B. Pire et D. Schiff, Particles and Fields C6 (1980) 241.

(28) M. Fontannaz, A. Mantrach, B. Pire et D. Schiff, Phys. Lett. 94B (1980) 509.

(29) M. Fontannaz, A. Mantrach, B. Pire et D. Schiff, Particles and Fields C6 (1980) 357.

(30) G. Cohen-Tannoudji, A. Mantrach, E.G. Oudrhiri-Safiani, Particles and Fields C14 (1982) 171.

A CLEAR TEST OF PERTURBATIVE QCD IN LARGE-p_T PHOTOPRODUCTION

M. FONTANNAZ [a], A. MANTRACH [a,1], B. PIRE [b] and D. SCHIFF [a]
[a] *LPTHE[2], Université Paris Sud, 91405 Orsay, France*
[b] *CPT[3], Ecole Polytechnique, 91128 Palaiseau Cédex, France*

Received 29 October 1979

It is shown that measurement of the cross-section differences $E\,d\sigma/d^3p\,(\gamma p \to h^+X) - E\,d\sigma/d^3p\,(\gamma p \to h^-X)$ at large transverse momentum provides a good test of perturbative QCD. Such differences are insensitive to the parton Fermi motion and to the poorly known sea-quark and gluon distribution functions. Moreover the hadronized photon component is shown to contribute little compared to the point-like one. Presently available photon beams at the CERN-SPS and FNAL are sufficient to test QCD in large-p_T photoproduction.

Introduction. The phenomenology of Quantum Chromodynamics [1] has achieved tremendous progress in the understanding of leptoproduction, e^+e^- annihilation and lepton-pair hadro-production. However, in these reactions QCD manifests itself as a higher-order correction to the Born terms involving only quarks. As pointed out by Fritzsch and Minkowski [2], the case of large-p_T photoproduction [3] is different since gluons appear already at the Born term level.

The purpose of this letter is to show that the study of the quantity Δ^h defined as:

$$\Delta^h(p) = \frac{E\,d\sigma}{dp}(\gamma p \to h^+X) - \frac{E\,d\sigma}{dp}(\gamma p \to h^-X)\,, \qquad (1)$$

is a very clear way of isolating the QCD Compton effect: $\gamma q \to gq$. We shall find indeed that subtracting cross sections as in eq. (1) allows to get rid of most of the hadronized photon contribution which is not well under control. Let us notice that this component is completely negligible in the case of an isoscalar target. Moreover, we shall show that the theoretical predictions for $\Delta^h(p)$ are not obscured by the uncertainties encountered in large-p_T hadronic collisions, namely those due to the treatment of the internal Fermi motion of the partons inside hadrons and those implied by the current ignorance of the gluon structure and fragmentation functions. If experiment confirms the presence of the QCD Compton effect, further studies of two-particle correlations will provide direct information on the gluon fragmentation function [4]. Indeed, in the only graph contributing to $\Delta^h(p)$ (fig. 1a) a gluon jet recoils in the hemisphere opposite to the trigger.

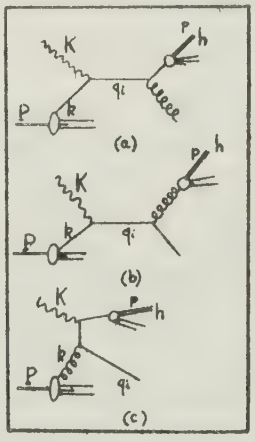

Fig. 1. The Born graphs for photoproduction at large p_T.

The Born term. The graphs of fig. 1 (and their crossed versions) represent the Born approximation to the photoproduction of a large-p_T pion. The differential cross section may be written as

[1] On leave from LPT, Faculté des Sciences de Rabat, Maroc.
[2] Laboratoire associé au CNRS.
[3] Equipe de Recherche associée au CNRS.

$$E\frac{d\sigma}{d^3p}(\gamma p \to hX) = \frac{d\sigma}{dY\, d\boldsymbol{p}_T} \qquad (2)$$

$$= \sum_{\alpha\beta}\frac{1}{\pi}\int dx\, dz\, G_\alpha(x,Q^2)\hat{s}\frac{d\hat{\sigma}_{\alpha\beta}}{dt}\delta(\hat{s}+\hat{t}+\hat{u})\frac{D_\beta^h(z)}{z^2},$$

with obvious notations and taking (Y is the center-of-mass rapidity):

$$\hat{t} = (p - K)^2/z = -\sqrt{s}p_T e^{-Y}/z .$$

The subprocess cross sections are given by (figs. 1a,b,c)

$$\frac{d\hat{\sigma}_{q_iq_i}}{d\hat{t}} = \frac{8\pi e_i^2\alpha\alpha_s(Q^2)}{3\hat{s}^2}\left(-\frac{\hat{t}}{\hat{s}}-\frac{\hat{s}}{\hat{t}}\right), \qquad (3a)$$

$$\frac{d\hat{\sigma}_{q_ig}}{d\hat{t}} = \frac{8\pi e_i^2\alpha\alpha_s(Q^2)}{3\hat{s}^2}\left(-\frac{\hat{u}}{\hat{s}}-\frac{\hat{s}}{\hat{u}}\right), \qquad (3b)$$

$$\frac{d\hat{\sigma}_{gq_i}}{d\hat{t}} = \frac{\pi e_i^2\alpha\alpha_s(Q^2)}{\hat{s}^2}\left(\frac{\hat{t}}{\hat{u}}+\frac{\hat{u}}{\hat{t}}\right). \qquad (3c)$$

The running coupling constant is defined as

$$\alpha_s(Q^2) = 12\pi/(33-2N_f)\log(Q^2/\Lambda^2) . \qquad (4)$$

Throughout the paper Λ is taken as 500 MeV and $N_f = 4$.

In eq. (2) the parton transverse momentum has been neglected. We now briefly show that this is justified. It is well known that in large-p_T hadronic collisions the parton transverse momentum may play an important [5] but controversial [6] role, its effect being strongly model dependent. In the reaction considered here we expect a smaller effect since one incident parton, the photon, has no transverse momentum. To test the model independence of our results, we considered on-shell and off-shell kinematics. In both cases we use a gaussian distribution for the parton transverse momentum K_T within the proton. For simplicity we restrict ourselves to the jet production cross section; for the hadron cross section very similar results are expected.

On-shell kinematics. All parton masses are neglected; the initial and final partons are on shell. The divergences which may appear in $d\hat{\sigma}/d\hat{t}$ (eqs. (3a,b,c)) are cured by the substitution $\hat{s}, \hat{t}, \hat{u} \to \hat{s}+M^2, \hat{t}-M^2, \hat{u}-M^2$, with M of the order of a hadronic mass.

Off-shell kinematics. We take the outgoing partons on shell with zero masses. We use off-shell kinematics [7] for the incident parton and put $k^2 \approx -\lambda K_T^2 - \mu^2$; this approximation is valid when the fractional longitudinal momentum x is small. The parameter λ may be estimated from the behaviour of $G_\alpha(x, K_T)$ for small x and large K_T; $\lambda \approx 1.5$ is a reasonable value. The mass μ is taken different from zero so as to prevent divergences from appearing in $d\hat{\sigma}/d\hat{t}$.

Table 1
The ratio r for the jet cross section calculated with off-shell kinematics; $\mu^2 = 0.1$ GeV^2 and $s = 200$ GeV^2.

$\langle K_T\rangle$ (MeV/c)	graph	p_T ($Y=0$)			Y ($p_T=2$)		
		2	3	4	−1	0	+1
900	1a	0.86	0.93	0.97	0.93	0.86	0.71
	1b	1.25	1.09	1.08	1.56	1.25	0.84
500	1a	0.94	0.97	0.99	0.98	0.94	0.88
	1b	1.06	1.03	1.03	1.10	1.06	0.95

Our results for the subprocesses of figs. 1a and b are summarised in table 1 where we show the ratio r of the jet cross section calculated with and without parton transverse momentum. Even with a very large mean value $\langle|K_T|\rangle \approx 900$ MeV/c and a small mass cut off, $\mu^2 = 0.1$ GeV^2, the Fermi motion effect is weak. We get very similar results (within 20%) with on-shell kinematics (with $M^2 \approx 1$ GeV^2). Notice, however, that we found a higher value of r (~ 2–4) for subprocess 1c. This is due to the stronger decrease of the gluon structure function compared to the quark. Anyhow, this subprocess does not contribute to $\Delta^h(p)$. Thus contrarily to the case of hadronic collisions at medium p_T, the effects of parton transverse momenta are well under control in photoproduction.

The input gluon structure and fragmentation functions are unknown and thus a lot of perturbative QCD calculations are somewhat arbitrary. In π^+ photoproduction also, the evaluation of graphs 1b and 1c suffers from this difficulty. A method to circumvent this problem consists in focusing on the difference of cross sections $\Delta^h(p)$ defined in eq. (1), which depends only on graph 1a. Moreover only photon–valence-quark scattering contributes. As is well known, the Q^2 evolution of the valence part is decoupled from the evolution of the sea and gluon part. $\Delta^h(p)$ is thus completely independent of the poorly determined sea and gluon structure functions.

We shall restrict here on the $\pi^+ - \pi^-$ difference. The resulting $\Delta^\pi(p)$ is shown in figs. 2 and 3. In eq. (2) we have used the Buras–Gaemers [8] scale-violating valence structure functions. As there is no experimental

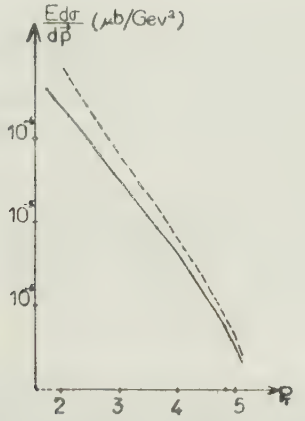

Fig. 2. The p_T dependence of $\Delta^\pi(p)$ (full curve) and of π^+ photoproduction (dashed curve) at $s = 200\,\mathrm{GeV}^2$ and $Y = 0.5$ (Born terms).

indication of sizable scale violation in the fragmentation functions, we have taken the scaling forms proposed by Field and Feynman [9]. The definition of Q^2 is arbitrary in such a lowest-order calculation. Following Feynman et al. [5] we have taken

$$Q^2 = 2\hat{s}\hat{t}\hat{u}/(\hat{s}^2 + \hat{t}^2 + \hat{u}^2)\,. \tag{5}$$

In fig. 2, we add for comparison the π^+ photoproduction cross section where the three graphs of fig. 1 contribute. For this process we must specify the sea and gluon content of the proton. We have taken the scale-violating parametrization obtained by Owens and Reya [10] as an improvement of the Buras–Gaemers method [8]. At Q_0^2 these structure functions are of the form

$$xG(x, Q_0^2) \sim (1-x)^5\,, \quad xs(x, Q_0^2) \sim (1-x)^7\,. \tag{6}$$

For the gluon fragmentation we have chosen a scale-invariant form,

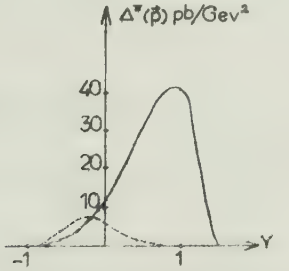

Fig. 3. The angular dependence of $\Delta^\pi(p)$ at $p_T = 3$ GeV/c and $s = 200\,\mathrm{GeV}^2$. Y is the center-of-mass rapidity, the full curve corresponds to the Born terms and the dashed one to the anomalous part of the hadronized photon.

$$zD_g^{\pi^+}(z) = 2(1-z)^3/3\,. \tag{7}$$

Let us comment on the results:

Due to the charge coefficients in eqs. (3a, b, c), the difference $\Delta^\pi(p)$ is a large fraction of the π^+ cross section.

The angular distribution is easily understood since the photon interacts with its full energy $\sqrt{s}/2$ with a parton carrying less energy $x\sqrt{s}/2$.

The p_T dependence at fixed s can be described by $p_T^{-n_{\mathrm{eff}}}$ with $n_{\mathrm{eff}} = 5.9$ for $2 < p_T < 4\,\mathrm{GeV}/c$.

The hadronized photon contribution. In addition to the point-like photon Born terms, the hadronic-like terms in the photon should be taken into account. The photon structure function [11] may be viewed as the sum of two terms: the vector dominance contribution and the anomalous component which is derived from the point-like photon coupling to quarks and antiquarks renormalized by the strong interactions. This last component, proportional to $\log Q^2$, is exactly calculated from QCD and is generally believed to dominate [11] at large Q^2. In the Q^2 domain which is investigated here, the VDM component is not negligible. An estimate of its relative importance based on Witten's discussion [11] is of the order of 50%. This spoils the confidence one might have in the predictions for π^+ and π^- cross sections for the medium-p_T range. On the other hand, a favourable situation is obtained by taking the difference of these cross sections where most of both hadronic-like components gets cancelled contrary to the point-like case where the charge factors ensure a sizable value for $\Delta^h(p)$. We have calculated the contribution of the anomalous component to $\Delta^h(p)$. The only subprocesses which survive involve valence quarks in the proton and either quarks, antiquarks and gluons in the photon. They are drawn in fig. 4. Their cross sections are given in numerous references and were first calculated by Combridge et al. [12]. We use the parametrization of Nicolaidis [13][‡1] for the leading-log photon structure functions. The result of the calculation is plotted in fig. 3 and is indeed found to be small with respect to the Born-term contri-

[‡1] This parametrization gives the quark and gluon distributions correctly summed over color (a factor of 8 is missing for the gluon distribution in Llewellyn Smith's paper of ref. [11]).

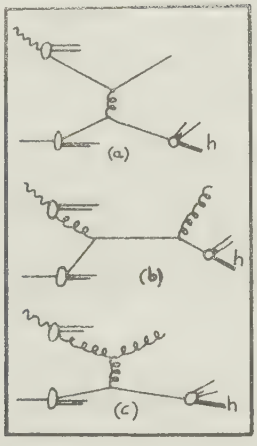

Fig. 4. The graphs with a hadronized photon contributing to $\Delta^h(p)$.

bution. Thus even doubling this result in order to roughly take into account the VDM part, we still get a small hadronized photon contribution (negligible at large Y).

Conclusion. The overall value for $\Delta^\pi(p)$ is measurable in the conditions of the soon to come experiments at the CERN SPS [14]. As discussed at length, it is free from a list of ambiguities which appear in either π^+ or π^-. On the basis of Owens' calculations of the jet cross section [3] we have estimated that the hadronized photon contribution to the π^+ cross section for $p_T \approx 3$ GeV/c is about twice that of the Born term. This gives $(\pi^+ - \pi^-)/\pi^+ \sim 15$–$25\%$, which means that $\Delta^\pi(p)$ is a well-measurable quantity.

It is not easy to determine at which value of p_T the QCD Compton effect will take over from other contributions of the CIM/higher-twist type. We expect a smooth transition from a low-p_T region where a $d\sigma/dp_T \approx Cp_T^{-12}$ law seems to dominate [15] to a QCD region characterized by a p_T^{-6} decreasing law (at fixed s) and the magnitude calculated above. One should keep in mind, however, that all these estimates have been performed in the frame of the leading-log approximation. The problem of incorporating terms beyond the leading log is very delicate. They affect in particular the definition of Q^2 and the value of Λ; for instance, taking $Q^2 = (\hat{s}\hat{t}\hat{u})^{1/3}$ in place of eq. (5) lowers our result by some 30%.

As a final remark, let us stress the fact that we may get completely rid of the hadronized photon contribution by measuring $\Delta^h(p)$ on an isoscalar target. In that case also the Born contribution remains sizable due to the charge factors in eq. (3).

We would like to thank the members of the WA4 collaboration at the CERN SPS, especially F. Richards, F. Gorski and D. Treille, for useful discussions.

References

[1] For a recent review, see, for instance: R. Field, lectures at La Jolla Institute Summer Workshop (1978), and references therein.
[2] H. Fritzsch and P. Minkowski, Phys. Lett. 69B (1977) 316.
[3] Tu T.-S., CERN preprint TH 2690 (1979);
J. Owens, Florida State Univ. preprint FSU 790731 (1979).
[4] M. Fontannaz, A. Mantrach, B. Pire and D. Schiff, preprint in prepration.
[5] A. Contogouris, R. Gaskell and S. Papadopoulos, Phys. Rev. D17 (1978) 2314;
R. Feynman, R. Field and G. Fox, Phys. Rev. D18 (1978) 3320.
[6] M. Fontannaz and D. Schiff, Nucl. Phys. B132 (1978) 457;
R. Horgan and P. Sharbach, Phys. Lett. 81B (1979) 215.
[7] D. Sivers, R. Blankenbecler and S. Brodsky, Phys. Rep. 23C (1976) 1, Appendix A.
[8] A. Buras and K. Gaemers, Nucl. Phys. B132 (1978) 249.
[9] R. Field and R. Feynman, Phys. Rev. D15 (1977) 2590.
[10] J. Owens and E. Reya, Phys. Rev. D17 (1978) 3003.
[11] E. Witten, Nucl. Phys. B120 (1977) 189;
C. Llewellyn Smith, Phys. Lett. 79B (1978) 83;
R. de Witt et al., Phys. Rev. D19 (1979) 2046.
[12] B. Combridge, J. Kripfganz and J. Ranft, Phys. Lett. 70B (1977) 234.
[13] A. Nicolaidis, Nucl. Phys. B., to be published.
[14] CERN–Imperial College–LAL Orsay–Saclay–Southampton Collaboration.
[15] A. Eisner et al., Phys. Rev. Lett. 33 (1974) 865.

Z. Physik C, Particles and Fields 6, 241–250 (1980)

Zeitschrift für Physik C Particles and Fields
© by Springer-Verlag 1980

Large p_T Photoproduction and Tests of QCD

M. Fontannaz, A. Mantrach*, and D. Schiff
Laboratoire de Physique Théorique et Hautes Energies**, Université Paris-Sud, F-91405 Orsay, France

B. Pire
Centre de Physique Théorique ***, Ecole Polytechnique, F-91128 Palaiseau Cedex, France

Received 30 April 1980

Abstract. A complete investigation of large p_T hadron photoproduction is carried out aiming to isolate and study QCD predictions concerning both direct coupling and anomalous photon components. Comparison with experimental data shows that these components may be disentangled from a large hadron-like background, provided cross-section differences or symmetric pair correlations are measured. The production of jets is also examined with emphasis on gluon jets.

Introduction

The interest of photon initiated processes for producing large p_T particles and testing QCD has been emphasized in many places [1–10]. We investigate in this paper what photoproduction of large p_T particles tells us about two aspects of the photon interaction: the direct coupling and the photon structure function contributions, as shown in Fig. 1, which are predicted and exactly calculable in the framework of perturbative QCD at sufficiently large Q^2.

In a recent paper [8] we already proposed a way of isolating, among the direct coupling terms, the QCD compton effect (Fig. 1a) by studying the cross-section differences

$$\Delta^h(\mathbf{p}) = E\frac{d\sigma}{d\mathbf{p}}(\gamma p \to h^+ X) - E\frac{d\sigma}{d\mathbf{p}}(\gamma p \to h^- X).$$

The photon structure function contributes very little to $\Delta^h(\mathbf{p})$ and in lowest order, the prediction of QCD is free from the arbitrariness connected with ill-determined gluon structure and fragmentation functions, so that the measure of $\Delta^H(\mathbf{p})$ is a clear test of the theory. Moreover, studying, in a second step, differences of double inclusive cross sections is a way of determining specifically the properties of gluon fragmentation [11].

Furthermore, it is also very interesting to measure the photon structure function [2, 12, 13] which is completely calculable at large Q^2. It is usually described as consisting of two terms: the anomalous and hadron-like components. The photon point-like coupling to $q\bar{q}$, renormalized by QCD, generates the anomalous component with a specific $\log Q^2$ behaviour, already present at the Born term level. This ensures, at large enough Q^2, the dominance of the anomalous component over the hadron-like component which has the same scaling behaviour as usual hadronic structure functions. At experimentally accessible Q^2, however, both components are at work and we shall be interested in this paper to investigate under which conditions the anomalous component is experimentally accessible, which will provide a stringent test of QCD. We shall thus essentially handle the problems of disentangling the various contributions: the direct photon coupling and the anomalous and hadron-like components of the photon structure function.

Preliminary experimental results [14] for π^+ and π^- photoproduction are already available in the energy domain $45\ \text{GeV} < E^{\gamma}_{\text{lab}} < 70\ \text{GeV}$ and $p_T < 2.5\ \text{GeV}/c$. We shall show that one-particle inclusive cross-sections are dominated by the hadron-like component, commonly estimated in the VDM framework. This is in some sense a background to the QCD calculable components and forbids a meaningful comparison with the theory. In contrast, the measure of $\Delta^{\pi}(\mathbf{p})$ is a way of subtracting a large

* On leave of absence from L.P.T., Faculté des Sciences de Rabat, Maroc
** Laboratoire associé au C.N.R.S.
*** Groupe de Recherche du C.N.R.S.

0170-9739/80/0006/0241/$02.00

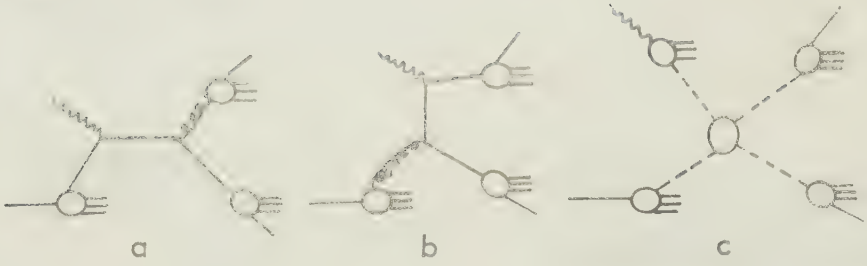

Fig. a-c. The graphs contributing to large p_T photoproduction: a, b direct coupling terms; c photon structure function terms (the dashed lines represent quarks or gluons)

fraction of the hadron-like background; in this sense, this paper contains, in addition to [8], a very detailed study of the background in $A^{\pi}(\mathbf{p})$ and re-emphasizes the interest of this quantity. Comparison with existing data for A^{π} is indeed satisfactory.

In the next-to-come experiment [15] energy and p_T domain ($E_{\text{lab}} \cong 100\,\text{GeV}$, $p_T \lesssim 5\,\text{GeV/c}$), we shall find that one particle cross-sections have still an important hadron-like background, so that again, it is very difficult to extract the anomalous component of the photon structure function. Should we wait for higher energies in order to perform this task? We shall show that a possible way at presently accessible energy is to analyze symmetric pair correlations which are little affected by the hadron-like background.

Finally, we shall study jet cross-sections at very high energies. They provide a stringent test of the non-abelian nature of the theory, being essentially determined by the 3 and 4 gluon couplings. Moreover, they are very sensitive to the gluon content of the photon.

The specificity of the present paper, among others already published on the subject, is the emphasis put on the possibility of isolating each photon component in order to obtain clear tests of QCD. Preliminary experimental data are used to discuss the difficulties of this approach. In particular, we study in detail the hadron-like background which clouds predictions for one-particle cross-sections at presently accessible energies. This problem had been ignored or underestimated by previous authors. Finally, we mainly focus on particle production in view of the difficulties connected with the experimental definitions of jets in large p_T reactions.

Let us outline the contents of this paper: Section I is devoted to establishing the formalism in order to calculate the direct coupling term and the anomalous component. The hadron-like contribution is discussed and evaluated in the framework of VDM in Sect. II. Section III deals with comparing theoretical calculations to preliminary experimental data on large p_T π^+ and π^- photoproduction. Theoretical predictions are also given, in the next-to-come experiment energy and p_T domain. A complete discussion of the hadron-like background is given. Section IV is devoted to the study of jets, and in particular to the possibility of observing gluon jets after having separated 3 and 4 jet samples. Section V discusses the symmetric pair correlations which provide the way to extract the anomalous component at presently accessible energies. Section VI is devoted to higher energies and Sect. VII is the conclusion.

I. Basic Calculations in QCD

In this section we present basic formulae for the inclusive cross-section for producing a large p_T hadron. Here, we limit ourselves to the two components that are exactly calculable in QCD, namely the direct coupling terms and the anomalous photon structure function contribution. We perform calculations in the leading logarithm approximation. We also give the relevant equations for differences of cross-section of the type $d\sigma(\gamma p \to h^+ X) - d\sigma(\gamma p \to h^- X)$ which will turn out to provide the most testable predictions.

a) Direct Coupling Terms

In contradistinction with the case of hadron–hadron scattering where both incident particles scatter through their constituents the photon may interact as a whole with the proton partons. The lowest order direct coupling terms which we consider are drawn in Fig. 1. The one-particle inclusive cross-section may be written as:

$$E\frac{d\sigma^h}{d\mathbf{p}} = \frac{1}{\pi}\sum_{a,b,c}\int dx\,dz\,G_{a/p}(x,Q^2)\hat{s}\frac{d\hat{\sigma}}{d\hat{t}}(\gamma a \to bc)\cdot\frac{D_b^h(z)}{z^2}\delta(\hat{s}+\hat{t}+\hat{u}) \tag{1}$$

where

$$\frac{d\hat{\sigma}}{d\hat{t}}(\gamma q \to qg) = \left[\frac{4}{3}\right]\frac{2\pi e_q^2\alpha\alpha_s(Q^2)}{\hat{s}^2}\left(-\frac{\hat{t}}{\hat{s}}-\frac{\hat{s}}{\hat{t}}\right)$$

$$\frac{d\hat{\sigma}}{d\hat{t}}(\gamma g \to q\bar{q}) = \left[\frac{1}{2}\right]\frac{2\pi e_q^2\alpha\alpha_s(Q^2)}{\hat{s}^2}\left(\frac{\hat{t}}{\hat{u}}+\frac{\hat{u}}{\hat{t}}\right) \tag{2}$$

numbers in brackets being colour factors, $\hat{s},\hat{t}$ and $\hat{u}$ being the subprocess Mandelstam variables

$$\hat{s} = (p_\gamma + p_a)^2 \quad \hat{t} = (p_\gamma - p_b)^2 \quad \hat{u} = (p_\gamma - p_c)^2$$

The running coupling constant is, as usual, given by

$$\alpha_s(Q^2) = 12\pi/(33 - 2N_f)\,\text{Log}\,(Q^2/\Lambda^2)$$

with $N_f = 4$. The definition of Q^2 and Λ is arbitrary in such a leading log calculation. We take $Q^2 = 2\hat{s}\hat{t}\hat{u}/(\hat{s}^2 + \hat{t}^2 + \hat{u}^2)$ following [16] and $\Lambda = 0.5$ GeV. The trigger rapidity is defined through

$$t = (p - p_\gamma)^2 = -\sqrt{s}\, p_T e^{-y}$$

where p_T is the transverse momentum of the observed hadron.

In (1) we have neglected the Fermi motion of partons in the proton. It is well known that such an approximation is unjustified in the case of hadron–hadron scattering. The situation is however very different in photoproduction. We have indeed shown in [8] that for direct coupling terms the inclusion of this effect leaves the result unchanged for $p_T \gtrsim 2.5$ GeV/c, in a model independent way. We refer the reader to this work for more details.

The G's are the gluon and quark structure functions in the proton. The valence quark structure functions are the only well determined ones; we use the Buras–Gaemers [17] parametrization derived in agreement with experiment and renormalization group equations. Various choices are possible for the sea and gluon content of the proton; we choose the Owens–Reya [18] forms which behave as $(1-x)^7$ and $(1-x)^5$ respectively at $Q_0^2 = 1.8\,\text{GeV}^2$ and x near 1. We neglect charmed quarks in the proton. The D's are fragmentation functions. Here again only the quark ones are well-known; we take the Field–Feynman [19] parametrization in agreement with experiment. For gluon fragmentation we adopt the scale invariant parametrization

$$D_g^{\pi^+}(z) = \frac{2(1-z)^3}{3z} \tag{3}$$

In the following we shall comment on the implication of other choices for gluon functions.

It is important to notice, as emphasized in [8], that only graph 1a (QCD Compton Effect) contributes to $\Delta^h(\mathbf{p}) = E\,d\sigma(\gamma p \to h^+ X)/d\mathbf{p} - E\,d\sigma(\gamma p \to h^- X)/d\mathbf{p}$ and only valence quarks in the proton are to be taken into account. Remembering that the Q^2 evolution of the valence is disconnected from the Q^2 evolution of sea and gluons, one concludes that $\Delta^h(\mathbf{p})$ does not depend on ill-determined structure or fragmentation functions, at the level of direct processes studied here. Moreover, this difference of cross-sections is not small because of the electric charge coupling of the photon to the quarks.

b) Anomalous Photon Structure Function Contribution

The photon may also interact through its constituents with the target proton. Both the renormalization group [12] and perturbative QCD [13] approaches lead to distinguish two components in the photon structure function: (i) the anomalous part, exactly calculable which results from renormalization of the point-like photon coupling to quark–anti-quark through strong interactions with the specific log Q^2 behaviour as in the free quark model. *ii*) the "hadronic" part which has the same scaling properties as usual hadron structure functions and is commonly parametrized in the framework of Vector Dominance as will be done in detail in Sect. III.

The anomalous part is dominant for large enough Q^2 which makes the photon structure function such an interesting QCD object. Its contribution to the photoproduction cross-section is written under the form

$$E\frac{d\sigma^h}{d\mathbf{p}} = \frac{1}{\pi}\sum_{a,b,c}\int dx_a\, dx_b\, G_{a/\gamma}(x_a, Q^2) G_{b/p}(x_b, Q^2) \cdot \int \frac{dz}{z^2} D_c^h(z)\hat{s}\frac{d\hat{\sigma}}{d\hat{t}}(ab \to cd)\,\delta(\hat{s} + \hat{t} + \hat{u}) \tag{4}$$

The various subprocesses cross-sections have been calculated several times [20]. Three independent photon distribution functions appear: $G_{2/3}(x, Q^2)$ $[G_{1/3}(x, Q^2)]$ for quarks or antiquarks of fractional charge $\pm 2/3$ $[\pm 1/3]$ and $G_g(x, Q^2)$ for gluons. We neglect b and t quarks but include charmed quarks in the photon (identifying $D_c^\pi(z)$ to $D_s^\pi(z)$). Leading log expressions for these G's have been parametrized by Nicolaidis [21]. $G_{2/3}$ and $G_{1/3}$ are remarkably hard: this is responsible for the expected large order of magnitude of high energy high p_T cross-sections and also for the specific shape of the angular distribution peaked in the forward direction. The gluon content of the photon is important at small x and at very high energy it will provide a large amount of the cross-section (so that we disagree with calculations at very high energy given in [9] where it is neglected). There are many terms in the sum of (4); let us write explicitly the contribution to $\Delta^\pi(\mathbf{p})$ under the form:

$$\Delta^\pi(\mathbf{p}) = \frac{1}{\pi}\int dx_a\, dx_b\, dz\,[D_u^{\pi^+}(z) - D_u^{\pi^-}(z)]\hat{s} \cdot \Sigma\,\delta(\hat{s} + \hat{t} + \hat{u})/z^2 \tag{5}$$

with

$$\begin{aligned}\Sigma = {} & [\sigma_1 G_g(x_a, Q^2) + 4\sigma_2 G_{2/3}(x_a, Q^2) \\ & + 4\sigma_2 G_{1/3}(x_a, Q^2)][G_{u/p}(x_b, Q^2) - G_{d/p}(x_b, Q^2)] \\ & + \sigma_3[G_{2/3}(x_a, Q^2) G_{u/p}(x_b, Q^2) - G_{1/3}(x_a, Q^2) \\ & \cdot G_{d/p}(x_b, Q^2)]\end{aligned} \tag{6}$$

where

$$\begin{aligned}\sigma_1 &= \frac{\pi\alpha_s^2(Q^2)}{\hat{s}^2}\left(-\frac{4}{9}\frac{\hat{t}^2 + \hat{s}^2}{\hat{t}\hat{s}} + \frac{\hat{t}^2 + \hat{s}^2}{\hat{u}^2}\right) \\ \sigma_2 &= \frac{\pi\alpha_s^2(Q^2)}{\hat{s}^2}\frac{4}{9}\frac{\hat{s}^2 + \hat{t}^2}{\hat{u}^2} \\ \sigma_3 &= \frac{\pi\alpha_s^2(Q^2)}{\hat{s}^2}\left(-\frac{8}{27}\frac{\hat{s}^2}{\hat{u}\hat{t}} - \frac{8}{27}\frac{\hat{t}^2}{\hat{s}\hat{u}} + \frac{8}{27}\frac{\hat{u}^2}{\hat{s}\hat{t}}\right)\end{aligned} \tag{7}$$

σ_1 is straightforwardly the contribution of the $qg \to qg$ subprocess σ_2 and σ_3 are the result of all properly symmetrized contributions of the type $q_i q_j \to q_i q_j$ (and $q \leftrightarrow \bar{q}$); all interference terms have been put in σ_3. Apart from this latter contribution, which is small, the integrand in (5) is proportional to $G_{u/p}(x_b) - G_{d/p}(x_b)$, since the photon is not coupled directly to the charge of the constituents in the proton. In absence of the small interference terms, the anomalous photon structure function contribution to $\Delta^\pi(\mathbf{p})$ would vanish when measured on an isoscalar target. This is to be contrasted with the expression of the direct coupling term where the u quark contribution is enhanced by the square charge factor, so that taking the difference is indeed a way of diminishing the anomalous photon contribution, keeping a large fraction of the direct coupling and thus a measurable number for Δ^π. This is an interesting feature as it allows to isolate the QCD Compton effect.

In formulae (4) and (5) the initial parton transverse momenta have been neglected. We shall comment on the importance of this effect in Sect. III when dealing with the comparison of predictions and data.

II. VDM Estimate of the Hadron-Like Photon Contribution

In order to estimate the hadron-like photon contribution, we use the VDM analogy between the photon and the vector mesons as already done by many authors [7, 9, 12]. We shall deal, here, with the contribution to the one-particle inclusive spectrum. There are actually two possible ways to proceed which are described in turn:

a) the VDM is used to identify the hadron-like part of the photon structure function with the vector meson structure function. We write, as usual, the quark content of the photon as

$$\gamma = g\left(\frac{2}{3}u\bar{u} + \frac{1}{3}d\bar{d} + \ldots\right) = \frac{g}{\sqrt{2}}\left(\rho + \frac{1}{3}\omega + \ldots\right) \tag{8}$$

We neglect the contribution of heavier resonances like $\rho', \phi, \psi \ldots$ which have smaller couplings to the photons and retain only ρ and ω with $g^2/2 = 4\pi\alpha/f_\rho^2 = \alpha/2.2$. From (8) one relates the momentum distributions of u and d quarks inside the photon and inside $u\bar{u}$ or $d\bar{d}$. These are supposed to be identical to the u quark momentum distribution inside the π^+ so that[1]:

$$u^\gamma(x) = \frac{4}{9}g^2 u^{\pi^+}(x) = 4d^\gamma(x) = \bar{u}^\gamma(x) = 4\bar{d}^\gamma(x) \tag{9}$$

For u^{π^+} we take the following form in agreement with data of μ pair production in $\pi^- p$ collisions for $x > 0.25$ [22]

$$u^{\pi^+}(x) = 0.5(1-x)/x \tag{10}$$

We parametrize the gluon distribution by:

$$g^\gamma(x) = \tfrac{5}{9}g^2 2(1-x)^3/x \tag{11}$$

in agreement with counting rules and assuming gluons take 50% of the momentum of either $u\bar{u}$ or $d\bar{d}$. These expressions of the quark and gluon distribution functions in the hadron-like photon are then used to calculate the corresponding inclusive spectrum along the same line as in *Ib*. In this approximative estimate of the hadron-like component of the photon, we neglect the Q^2-dependence of the structure functions in formulae (10) and (11).

b) A direct phenomenological estimate of the hadron-like photon contribution to $E d\sigma(\gamma p \to \pi X)/d\mathbf{p}$ uses VDM under the form:

$$E\frac{d\sigma}{d\mathbf{p}}(\gamma p \to \pi X) = \sum_V \frac{4\pi\alpha}{f_V^2} E\frac{d\sigma}{d\mathbf{p}}(Vp \to \pi X) \tag{12}$$

We restrict to the ρ for a detailed estimate since in this case, writing as usual $d\sigma(\rho^0 p \to \pi X) = \frac{1}{2}(d\sigma(\pi^+ p \to \pi X) + d\sigma(\pi^- p \to \pi X))$ we may rely on experimentally measured cross-sections. We shall multiply the final result by an overall factor ≈ 1.1 to include the ω (neglecting interference terms and heavier vector mesons). Focusing on π^+ production, we express $E\frac{d\sigma}{d\mathbf{p}}(\rho p \to \pi^+ X)$ in terms of $E\frac{d\sigma}{d\mathbf{p}}(\pi^+ p \to \pi^0 X)$ which has been measured at 90° [23]. It is convenient to define the following cross-sections ratios:

$$r_1 = d\sigma(\pi^+ p \to \pi^+ X)/d\sigma(\pi^+ p \to \pi^- X)$$
$$r_2 = d\sigma(\pi^+ p \to \pi^0 X)/d\sigma(\pi^- p \to \pi^\circ X)$$
$$r_3 = d\sigma(\pi^- p \to \pi^- X)/d\sigma(\pi^- p \to \pi^\circ X)$$

Then

$$E\frac{d\sigma}{d\mathbf{p}}(\rho p \to \pi^+ X) = (r_1/(1+r_1) + 1/r_2 - r_3/2r_2)$$
$$E\frac{d\sigma}{d\mathbf{p}}(\pi^+ p \to \pi^\circ X) \tag{14}$$

r_2 and r_3 may be calculated from the data of [23, 24] and depend very little on energy. They are found to be close to 1 at 90°: $r_2 \cong 0.95$; $r_3 \cong 1.1$. r_1 is not experimentally known but may be inferred from the analogous ratio for proton [25]: $r_1 \cong 1.7$ at 90° and $x_T \cong 0.4$. Similarly

$$E\frac{d\sigma}{d\mathbf{p}}(\rho p \to \pi^- X) = (r_2/(1+r_1) + r_3/2)$$
$$\cdot E\frac{d\sigma}{d\mathbf{p}}(\pi^- p \to \pi^\circ X) \tag{15}$$

1 We disagree by a factor 2 with the u^γ definition of [9]

As a consequence, the cross-section difference Δ^π receives a contribution:

$$\Delta^\pi(\mathbf{p}) = \frac{4\pi\alpha}{f_\rho^2}\left(\frac{r_1-1}{r_1+1}+\frac{1}{r_2}-\frac{r_3}{r_2}\right)E\frac{d\sigma}{d\mathbf{p}}(\pi^+ p \to \pi^\circ X) \tag{16}$$

With the above values for r_1, r_2, r_3, this is estimated at 90° to be of the order of 15% of the corresponding hadron-like contribution to $E\frac{d\sigma}{d\mathbf{p}}(\gamma p \to \pi^+ X)$. In the forward direction this ratio should be even smaller since in this region the mean charge is that of the photon.

The advantage of this phenomenological estimate, compared to the first method is that it does not rely on QCD to calculate the hard vector meson–hadron collision. We know indeed that, in the moderate p_T region, QCD has to be supplemented by a phenomenological treatment of constituent transverse motion in order to obtain agreement with the data [16, 26, 27]. Without playing this game, which appears to be very arbitrary [28, 29] one has therefore no chance to evaluate propertly the $\rho p \to \pi X$ cross-section. Thus, as will be shown in the next section, it is not surprising to find that the phenomenological estimate yields a much higher result than the theoretical one, in the moderate p_T region; the ratio is of the order of the enhancement factor due to constituent transverse motion, encountered in the same p_T and energy domain in proton–proton collisions. On the other hand, the theoretical estimate will be useful for correlations which are only little affected by constituent transverse motion [28, 30],

III Comparison with Data and Predictions for Next-to-Come Experiments

a) Comparison with Data

Data are already available in the energy range $45 \leqq E_\gamma^{\text{Lab}} \leqq 70$ GeV for π^+ and π^- photoproduction [14].

—Let us first comment on π^+ photoproduction. One sees from Fig. 2, which shows the rapidity distribution $\frac{d\sigma}{dy} = \int_{p_T=2} d\mathbf{p}_T \frac{d\sigma}{dy d\mathbf{p}_T}$, that the direct coupling contribution is much larger than the anomalous photon structure function one. The striking feature is the importance of the phenomenological VDM estimate for the hadron-like photon background which appears to represent the main bulk of the cross section. On the other hand, the theoretical VDM contribution is very small (a factor 30 smaller than the phenomenological VDM estimate at $y = 0$). As indicated in the previous section, this is to be understood as the sign of the importance of the constituent transverse motion, in this p_T range (mean $p_T \cong 2.3$ GeV), non mentioning the possibility of higher twist/CIM terms [31]. Correlatively we

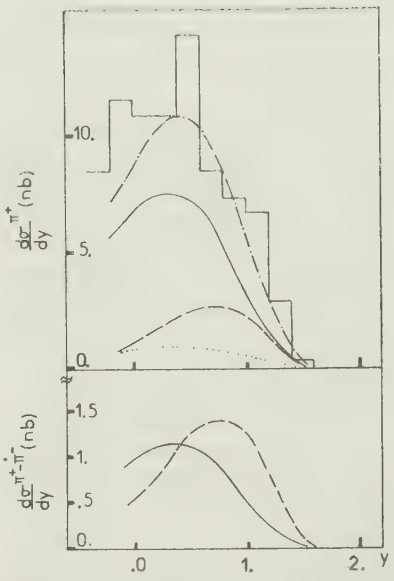

Fig. 2. The contribution of the various photon components to $d\sigma^{\pi^+}/dy$ (upper figure) and $d\sigma^{\pi^+-\pi^-}/dy$ (lower figure) for 45 GeV $\leqq E^\gamma \leqq$ 70 GeV and $p_T \geqq 2$ GeV/c: the direct coupling term (dashed line), the anomalous term (dotted line) and the phenomenological VDM term (full line). The dash-dotted is the sum of the various components. Data are from [14].

expect that some enhancement factor should also be applied to the QCD anomalous photon structure function calculation. This factor is certainly smaller than in hadron–hadron collisions, since resulting only from gluon bremsstrahlung. To summarize, even if the direct coupling term is little sensitive [8] in this p_T and energy domain to the parton transverse momentum, the other components: anomalous and hadron-like photon structure function contributions are too poorly predicted by the theory for allowing a meaningful comparison with experiment. Notice however that within uncertainties of the phenomenological estimate of the hadron-like photon background, the agreement with experimental data is altogether obtained.

– The situation is however more favorable for Δ^π. As mentioned in Sect. I, both the anomalous and hadron-like contributions are minimized in the cross section difference compared to the direct coupling term. In Fig. 2, we draw the phenomenological VDM estimate for the hadron-like background which we obtain from the corresponding contribution to $\gamma p \to \pi^+ X$ by multiplying by 0.15, as discussed in Sect. II. There we also indicated, however, that such a procedure yields an overestimate for $y > 0$. We are thus left with a situation where the direct coupling term is the dominant contribution so that it is meaningful to compare it to the data. We show $\frac{d\sigma}{dp_T^2}(\pi^+ - \pi^-)$ (integrated on y within the experimental acceptance, $\theta_{\text{lab}} < 15°$) on Fig. 3. The discrepancy in the region $p_T \geqq 2$ is consistent with

what we expect for the hadron-like background. We have also plotted $\frac{d\sigma}{dp_T^2}(\pi^+ - \pi^-)$ integrated in the region $y \geqq 0.5$ only. This cut presents the advantage of getting rid of most of the VDM background (and also contamination by spectator fragments of the proton). As may be expected, the agreement with corresponding data gets better and quite satisfactory.

To conclude this discussion on Δ^π, the lesson of the comparison with data is that in this p_T and energy domain Δ^π is a very interesting quantity to measure since it provides a meaningful test of the theory, in contrast with individual cross sections which are subject to uncertainties in the treatment of the hadron–like background and of the anomalous component. We shall see, when dealing with the higher energy and p_T range of the next to come experiments, that this is still true.

As a last point, let us comment on contamination of present data by K^+ and K^- due to lack of particle identification. Both positive and negative charged distributions get enhanced by $\approx 30\%$ (the equal status of π^- and K^- compared to π^+ and K^+ is due to the charge factor 4 associated with the u quark and to the relatively moderate value of $\langle z \rangle$ in the fragmentation function)

b) Predictions in the Intermediate Energy Domain

The next to come experiments [15] will have most of their statistics in the energy domain $E_\gamma^{\text{lab}} \sim 100$ GeV and it will be possible to explore values of p_T up to 5 GeV/c. In the region $p_T \geqq 3$ GeV/c, we expect that the hadron-like background be less important than previously and the more so with increasing p_T.

—Let us first examine the prediction for $E\frac{d\sigma}{d\mathbf{p}}$ ($\gamma p \to \pi^+ X$). We shall perform calculations for $p_T = 3$ GeV/c in order to keep a sizeable anomalous photon structure function contribution compared to the direct coupling terms. Both are shown on Fig. 4. For completeness, we indicate the amount of the anomalous photon structure function contribution provided by $qg \to qg$. Also shown is the VDM phenomenological estimate for the hadron-like background. Although relatively smaller than previously, it is still too large to allow a test of the theory. The theoretical VDM estimate is smaller by a factor 10 which is consistent with parton transverse motion enhancement factor encountered in the same p_T and energy domain in pp collisions. This indicates that the anomalous photon structure function contribution should be also enhanced somehow when considering parton transverse momentum due to gluon bremmstrahlung. In the same line of thought, the difference between theoretical and phenomenological VDM estimates leaves some room for the higher twist/CIM processes. To conclude, the situation is, as previously, such that it is very hard to compare the theoretical prediction to the data and especially to extract the anomalous component of the photon structure function as calculated in QCD.

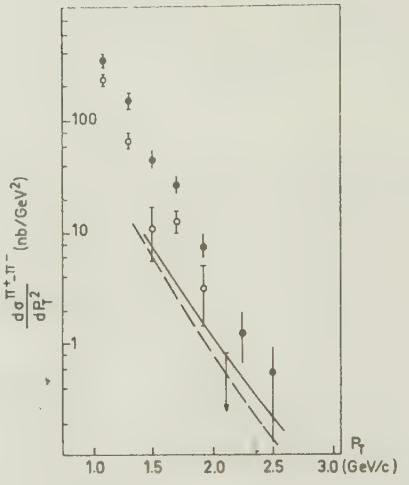

Fig. 3. The y-integrated cross-section differences $d\sigma^{\pi^+ - \pi^-}/dp_T^2$ for $\theta_{\text{Lab}} < 15°$ (full curve and full dots) and $y \geqq 0.5$ (dashed curve and open dots) and for 45 GeV $\leqq E' \leqq$ 70 GeV. Data are from [14]

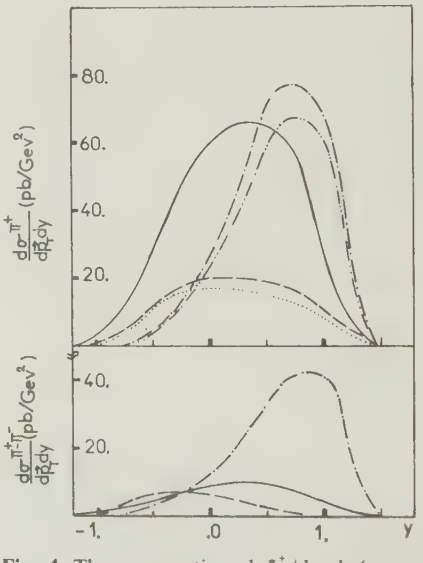

Fig. 4. The cross-sections $d\sigma^{\pi^+}/d\mathbf{p}_T dy$ (upper figure) and $d\sigma^{\pi^+ - \pi^-}/d\mathbf{p}_T dy$ (lower figure) for $p_T = 3$ GeV/c and $s = 200$ GeV^2. The direct coupling contribution: $\gamma q \to gq$ contribution (—..—..) and total (—.—.); the anomalous component contribution total (———) and neglecting the $qg \to qg$ subprocess (.....); the phenomenological VDM contribution (—)

– In contrast the situation is very favorable for a comparison of Δ^π with experiment and specifically a test of the theoretical prediction for the QCD Compton effect. On Fig. 4, we show that it provides the essential contribution to Δ^π which is a large fraction of the π^+ cross section. The anomalous component is small and vanishes completely in the

forward region,[2] and the same is true for the hadron-like background.

In what concerns the anomalous component of the photon structure function, in the p_T and energy domain of the next to come experiments, our conclusion is that it will be difficult to extract it from the data.

Is it, however, possible to find a way of getting rid of the hadron-like background or/and of the parton transverse momentum effects in order to strictly remain with the direct coupling and the anomalous components calculated in leading order QCD? A means to achieve this goal is to turn to symmetric pair correlations as will be discussed in Sect. V.

IV. Jet Studies

A fairly complete description of jet photoproduction has been given by Owens [7]. We shall not repeat his analysis here, but we want to develop some points which are interesting for our purpose: the identification and the experimental selection of the different components of the photon. We shall also discuss the possibility to observe gluon jets event by event.

The main point is that the final jets produced in the direct coupling reactions and in processes involving the structure function of the photon have a very different topology. The direct coupling results in two large p_T final jets and a backward low p_T jet made of proton fragments, whereas in the second case a fourth jet made of low p_T fragments of the photon is observed in the forward direction [14].

It is important to notice that the transverse momentum and the rapidities of the large angle jets of the 3-jet events have to verify a kinematical constraint. The double jet inclusive cross section is indeed given by

$$\frac{d\sigma}{d\mathbf{p}_T dy_1 dy_2} = \frac{2}{\pi} \sum_{a,b,c} x_b G_{b/p}(x_b) \frac{d\hat{\sigma}}{d\hat{t}}(\gamma b \to cd)$$

$$\cdot \delta(2 - x_T(e^{y_1} + e^{y_2})) \tag{17}$$

where $(\mathbf{p}_T, y_1)$ and $(-\mathbf{p}_T, y_2)$ are the transverse momenta and rapidities of the jets.

Thus inspection of the jet structure supplemented by the use of the 3-jet topology kinematical constraint, should allow one to separate the direct coupling events from the other ones. The interesting consequence of this selection is that we can now compare data and theory within each subset of events independently. Let us illustrate this point by studying the possibility to observe, event by event, a gluon jet.

The jet cross section is, in the direct coupling case,

$$E\frac{d\sigma}{d\mathbf{p}} = \frac{1}{\pi} \sum_{b,c,d} x_b G_{b/p}(x_b, Q^2) \frac{2}{2 - x_T e^y} \frac{d\hat{\sigma}}{d\hat{t}}(\gamma b \to cd) \tag{18}$$

2 In formula (7), σ_1 contributes little and σ_2 disappears like $1/\hat{u}^2$ for large y

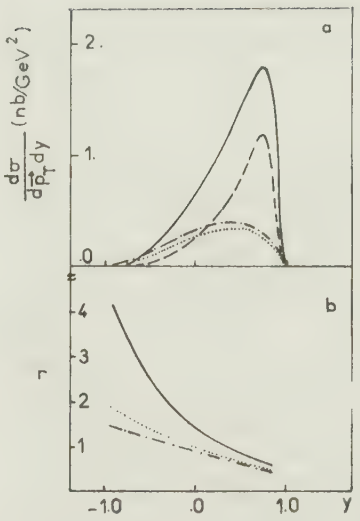

Fig. 5. a The various contributions to the jet cross-section at $p_T = 4\,\text{GeV}/c$ and $s = 200\,\text{GeV}^2$; direct coupling contribution: gluon and quark jets (—) and quark jets only (— — —); anomalous component contribution: gluon and quark jets (—.—.—.—.) and quark jets only (.....) **b** The gluon jet to quark jet ratio: direct coupling and anomalous component contributions (—.—.—), and direct coupling only (—) ((....,..) with the gluon distribution of [30])

with $x_b = x_T e^{-y}/(2 - x_T e^y)$. For the reaction involving the photon structure function, we have

$$E\frac{d\sigma}{d\mathbf{p}} = \frac{1}{\pi} \sum_{a,b,c,d} \int dx_a G_{a/\gamma}(x_a, Q^2) G_{b/p}(x_b, Q^2)$$

$$\cdot \frac{2x_a x_b}{2x_a - x_T e^y} \frac{d\hat{\sigma}}{d\hat{t}}(ab \to cd) \tag{19}$$

with $x_b = x_a x_T e^{-y}/(2x_a - x_T e^y)$

The situation in the next-to-come experiment energy domain ($s \cong 200\,\text{GeV}^2$) is interesting. In Fig. 5a, we show the different contributions to the jet cross section for a jet of $4\,\text{GeV}/c$ transverse momentum. One may observe that the direct coupling terms are dominant for positive rapidity and of the order of the anomalous photon component at negative rapidity. This picture is certainly blurred by the hadron-like background. But we lack experimental data at the corresponding energy and p_T range on jet production in πp collisions in order to evaluate it as in Sect. IIb. Although we expect a relatively smaller VDM contribution (due to a smaller parton transverse motion enhancement factor in jet than in particle production), it should certainly again forbid comparison with experiment. In Fig. 5b, we show the ratio of the expected yields of gluon jet to quark jets.

When considering both 3-jet and 4-jet events, this ratio is of order 1 (it should not be much affected by the hadron-like background); thus we have no possibility to observe a pure sample of gluon jets.

The situation looks better when focusing on the 3-jet events; gluon jets now dominate over quark jets for negative rapidity. Thus it is possible to observe gluon jets on an event by event basis; the yield should be sufficient to study gluon jet properties.

This conclusion is, however, obtained with a particular choice of the gluon distribution in the proton. We do not have yet any direct experimental information on the shape of this function (although its normalization is fairly well-known from sum rules). The Owens–Reya parametrization we have used may be considered as a mean choice among recently proposed functions [17, 30]. For softer choices [17] our results essentially remain unchanged but in the case of harder distributions, as that of ref [30] which decreases as $(1-x)^3$ at $Q_0^2 = 5\ \mathrm{GeV}^2$, they are drastically different. Indeed, the x region probed by the direct coupling term in the explored kinematical region ranges from about 0.4 to 1. This explains that the harder distribution yields a much more important $\gamma g \to q\bar{q}$ contribution, thus decreasing appreciably the ratio gluon jet/quark jet, as shown in Fig. 5b. This, in turn, amplifies the need of a direct determination of the gluon content of the proton; we will show in a forthcoming paper [32] that it may be given by the study of correlations in photoproduction.

V. Symmetric Pair Correlations

In this section we consider the problem of observing the contribution of the anomalous part of the photon. Two obstacles must be overcome before reaching our goal; in a first step we must isolate the photon structure function contribution, and then disentangle the anomalous component from the hadron-like one. We have seen in the preceeding section how it should be possible, on the ground of direct coupling kinematics, to isolate the sample of 4 jet events; we now turn to the second point.

To what concerns the one-particle inclusive cross-section we have shown in Sect. III that it is impossible to safely evaluate and subtract the hadron-like component in order to isolate the anomalous contribution.

Fortunately the situation is much more favorable when looking at two-particle correlations. In this case, by triggering on a symmetric pair of hadrons (hadrons with the same transverse momentum, but in opposite azimuthal hemispheres) one considerably reduces the parton transverse motion effect [30], and the contribution of possible Higher Twist/CIM [31] terms (due to the vanishing of $D(z)$ when $z \to 1$). In the case of hadronic collisions good fits to FNAL and ISR data [33, 34] were obtained by Baier et al., within the QCD approach [30].

In the photoproduction of symmetric pairs, the above considerations lead to the following interesting results. First, on the ground of results of Sect. III we expect the anomalous contribution to be higher than the VDM one, since the parton transverse momentum is now negligible. Correlatively, theoretical predictions (for both the anomalous and the hadron-like parts) are much less model dependent (in the medium p_T range) than the corresponding ones for single inclusive cross-sections. Let us make these points explicit by calculating the double inclusive cross-section:

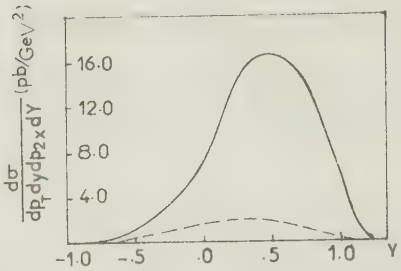

Fig. 6. The double inclusive cross-section $d\sigma/dp_T dy dp_{2x} dY$ as a function of Y for $y = 0$, $p_T = p_{2x} = 3$ GeV/c and $s = 200\ \mathrm{GeV}^2$ anomalous component contribution (—) and VDM contribution (— — —)

$$\frac{d\sigma}{dp_T dy dp_{2x} dY} = 2\pi \sum_{a,b,c,d} \int \frac{dz_1}{z_1} x_a G_{a/\gamma}(x_a, Q^2) x_b \cdot G_{b/p}(x_b, Q^2) \frac{1}{\pi} \frac{d\hat{\sigma}}{d\hat{t}}(ab \to cd) D_c(z_1) D_d(z_2) \tag{20}$$

with

$$x_a = \frac{x_T}{2z_1}(e^y + e^Y)$$

$$x_b = \frac{x_T}{2z_1}(e^{-y} + e^{-Y})$$

$$z_2 = \frac{|p_{2x}|}{p_T} z_1$$

The cross-section has been integrated over p_{2y}, the away hadron momentum component perpendicular to the scattering plane. The different building blocks of (20) have already been discussed in Sects. I and II; Y is the rapidity of the away hadron. In Fig. 6 we show the results of the calculations done for $s = 200\ \mathrm{GeV}^2$, $p_T = p_{2x} = 3\ \mathrm{GeV}/c$, $y = 0$, for charged pions.

We find that the anomalous contribution now dominates over the VDM one by an order of magnitude. This is an interesting result in view of the uncertainties associated with the VDM approach (unknown structure functions of the vector mesons and neglect of heavier vector mesons). Changing the VDM predictions by a factor two would not alter our conclusion that the anomalous component is quite observable. Notice that the dominating subprocess is the $qq \to qq$ scattering (q means either quark or antiquark). The subprocess $qg \to qg$ contributes about 3% and the others are negligible.

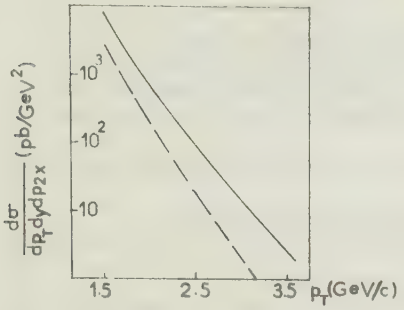

Fig. 7. The double inclusive cross-section $d\sigma/dp_T dy dp_{2x}$ (integrated over Y) anomalous component contribution (—) and VDM contribution (– – – –)

The p_T dependence of the cross-section (integrated over Y) is shown in Fig. 7. For $p_T \cong 2$ GeV/c, i.e. in a region where the background due to the low p_T photon and proton fragments may already be negligible, the cross-section is fairly large.

VI. Very High Energy Estimates

The future of photoproduction experiments relies mostly on very high energy e–p colliding machines. The Tristan project in Japan and the European projects at Hamburg and/or Cern plan center-of-mass energies of the order 100 GeV. We investigate in this section the interest of such almost real photon experiments as QCD tests. We shall show that they mostly probe the gluon content of incident particles. Moreover, the three and four gluon couplings specific of the non-abelian nature of QCD yield the main bulk of the cross-section, which is an almost unique fact in high energy physics [4]. Since luminosities at so high energy are likely to be low, we restrict on large p_T jet production. The drawback of this choice is the unprecise experimental jet definition.

High energy medium p_T events ($x_T \cong 0.1$) mostly probe the small x content of incident particles. In the photon case, in particular, gluons are predominant. We thus expect to probe this way the gluon content of the photon; moreover, the three gluon coupling specific of the non-abelian nature of the theory plays a very important role in gq scattering, the $gg \to gg$ subprocess being entirely due, to this order in α_s, to 3 and 4 gluon couplings. In Fig. 8 the jet inclusive cross-section at $y = 0$ is plotted as a function of the jet transverse momentum. Some of its components are shown. The $gg \to gg$ subprocess yields a significant amount of the cross-section but the gq scatterring amplitude dominates for all (reasonable) values of p_T. For this latter subprocess the 3 gluon coupling terms contribute about 90% of the cross-section. Also shown is the cross-section one would obtain if 3 and 4 gluon couplings were put equal to zero. At large enough p_T, since most of the uncertainties relative to the magnitude of the cross-section (effect of parton

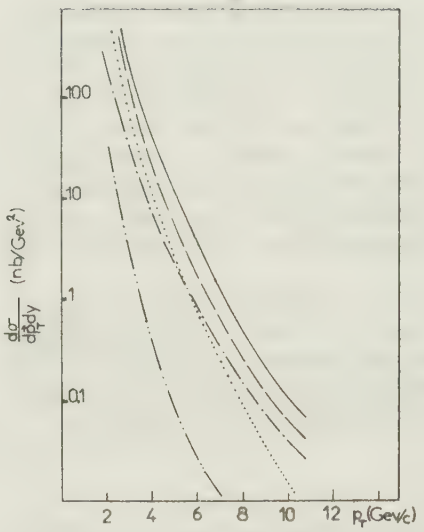

Fig. 8. The jet cross-section at very high energy (—): $\sqrt{s} = 100$ GeV and $y = 0$; various contributions shown are $qg \to qg$(– – – –), $gg \to gg$(...) and $gg \to q\bar{q}$ (—..—.), the cross-section obtained by putting to zero the 3 and 4 gluon couplings (—.—.)

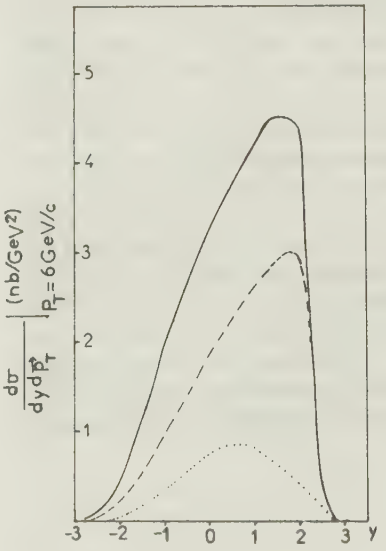

Fig. 9. The rapidity distribution of the jet cross-section at $\sqrt{s} = 100$ GeV and $p_T = 6$ GeV/c. Total (—)$gg \to gg$(...) and $qg \to qg$ (– – – –) contributions are shown

transverse motion, next to leading terms, mismatch of background and genuine jet particles) are expected to die away, we thus handle a very clear test of the non-abelian nature of the underlying theory.

In these energies and transverse momenta regions and in the light of our results at lower energy, one can safely ignore the hadron-like part of the structure function of the photon. Direct coupling terms only contribute about 1% of the cross-section.

The rapidity distribution at $p_T = 6$ GeV/c is shown in fig. 9. As expected the $gg \to gg$ contribution is

almost symmetric. The input used here for the gluon structure function in the proton [18] has a somewhat similar shape as the QCD calculated gluon in the photon. The qg scattering subprocess is very different since quarks have much harder distribution in the photon than in a hadron, yielding a rapidity distribution peaked in the direction of the incident photon. Because of the dominance of $qg \to qg$ and $gg \to gg$ subprocesses, as discussed above, gluon jets dominate the final state.

In conclusion, let us stress that very high energy photoproduction provides tests of QCD which are different from those at lower energy. It mostly allows to measure the strength of the 3 and 4 gluon couplings specific of the non-abelian nature of the theory.

VII. Conclusion

We have investigated in detail various tests of QCD in large p_T photoproduction. We have shown that it is possible to study separately the direct photon coupling by measuring cross-section differences. On the other hand, a careful investigation of the possibility of measuring the photon structure function at presently accessible energies has been carried out. We have shown that the hadron-like background is very important in single particle cross-sections and forbids to extract the anomalous photon structure function. We have proposed a way to perform this task which is to measure symmetric pair correlations. Furthermore, we have also studied reactions at very high energy and emphasized that they should provide a direct test of the non-abelian nature of the theory. The present analysis has been carried in the leading log approximation. The various tests, which we propose to perform, remain valid and feasible if next-to-leading corrections are incorporated. These may be eventually quite large and should be calculated when accurate experimental data become available.

Acknowledgements. We acknowledge useful discussions with M. Gorski, F. Richard and D. Treille and thank them for communication of the *WA*4 collaboration results prior to publication.

References

1. H. Fritzsch, P. Minkowski: Phys. Lett. **69B**, 316 (1977)
2. C.H. Llewellyn–Smith: Phys. Lett. **79B**, 83 (1978)
3. Tu Tung Sheng, Wu Chi Min: Nucl. Phys. **B156**, 493 (1979)
4. E. Gotsman, D. Silverman, A. Soni: Phys. Rev. **D20**, 2220 (1979)
   A. Soni: Slac Pub 2398 (1979) and Irvine preprint 79–45 (1979)
5. T. Chandramohan Phys. Lett. **88B** (1979) 163.
6. K. Ishida, T. Kobayashi, T. Yoshino: KEK preprint 79–14 (1979)
7. J. Owens: Phys. Rev. **D21**, 54 (1980)
8. M. Fontannaz, A. Mantrach, B. Pire, D. Schiff: Phys. Lett **89B**, 263 (1980)
9. I. Kang, C.H. Llewellyn–Smith: Oxford preprint 62/79 (1979)
10. K. Iguchi, A. Niegawa, Y. Uranishi: Osaka City University preprint OCU-61 (1979)
11. M. Fontannaz, A. Mantrach, B. Pire, D. Schiff: Ecole Polytechnique preprint A381–0380 (1980) to be published in Phys. Lett. B
12. E. Witten: Nucl. Phys. **B120**, 189 (1977)
13. R. DeWitt et al.: Phys. Rev. **D19**, 2046 (1979), **D20**, 1751 (E) (1979)
    W. Frazer, J. Gunion: Phys. Rev. **D20**, 147 (1979)
14. WA4 collaboration preliminary results. We thank M. Gorski and F. Richard for communication of their results prior to publication. These results are quoted in details in M. Fontannaz, Proceedings of the XV Rencontre de Moriond, 1980 to be published, ed. J. Tran Thanh Van
15. Na14 experiment of the CERN–London–Orsay–Saclay–Southampton collaboration. Wide band beam and tagged photon beam FNAL facilities
16. R. Feynman, R. Field, G. Fox: Phys. Rev. **D18**, 3320 (1978)
17. A. Buras, K. Gaemers: Nucl. Phys. **B132**, 249 (1978)
18. J. Owens, E. Reya: Phys. Rev. **D17**, 3003 (1978)
19. R. Field, R. Feynman: Phys. Rev. **D15**, 2590 (1977)
20. B. Combridge, J. Kripfganz, J. Ranft: Phys. Lett. **70B**, 234 (1977)
21. A. Nicolaidis: Nucl. Phys. **B163**, 156 (1980)
22. C.B. Newman et al.: Phys. Rev. Lett. **42**, 951 (1979)
    J. Badier et al.: Phys. Lett. **88B**, 145 (1979)
23. G. Donaldson et al.: Phys. Lett. **73B**, 375 (1978)
24. H.J. Frish et al.: Phys. Rev. Lett. **44**, 511 (1980)
25. D. Antreasyan et al.: Phys. Rev. Lett. **38**, 112 (1977)
26. A. Contogouris, R. Gaskell, S. Papadopoulos: Phys. Rev. **D17**, 2314 (1978)
27. J. Owens, J. Kimel: Phys. Rev. **D18**, 3313 (1978)
28. M. Fontannaz, D. Schiff, Nucl. Phys. **B132**, 457 (1978)
29. R. Horgan, P. Sharbach: Phys. Lett. **81B**, 215 (1979)
30. R. Baier, J. Engels, B. Petersson: Z. Phys. **C2**, 265 (1979)
31. D. Sivers, R. Blankenbecler, S. Brodsky: Phys. Rep. **23C**, 1 (1976)
32. M. Fontannaz, A. Mantrach, B. Pire, D. Schiff: Orsay preprint LPTHE 80/21 (1980)
33. H. Jöstlein et al.: Phys. Rev. Lett. **42**, 146 (1979)
34. M. Jacob: High p_T and Jets. Proceedings of the International Conference on High Energy Physics, Geneva 1979

HOW TO EXTRACT THE GLUON FRAGMENTATION FUNCTION FROM LARGE $p_\perp$ PHOTOPRODUCTION

M. FONTANNAZ [a], A. MANTRACH [a,1], B. PIRE [b] and D. SCHIFF [a]
[a] *LPTHE [2], Université Paris Sud Orsay, 91405 Orsay, France*
[b] *CPT [3], Ecole Polytechnique, 91128 Palaiseau Cedex, France*

Received 21 March 1980

A clear determination of the gluon fragmentation function $D_g^h(z, Q^2)$ is accessible in near to come large $p_\perp$ photoproduction experiments. This is done by analyzing differences of double inclusive cross sections. The scale invariance breaking effect is shown to be measurable.

The observation of gluon jets and of their properties is crucial for the verification of perturbative quantum chromodynamics ideas. The three jet structures discovered in e^+e^- annihilation have been a very beautiful confirmation of the existence of gluons. It is, however, difficult to go further in this reaction and to study the gluon properties. On the other hand, large $p_\perp$ photoproduction has the very interesting feature of producing gluons at the Born term level through the QCD Compton effect $\gamma q \to qg$ [1]. We have shown in a preceding paper [2] that this reaction provides a very clear test of QCD and allows a direct experimental approach of the QCD Compton cross section. The purpose of this letter goes further and aims to show that large $p_\perp$ photoproduction provides a determination of the gluon fragmentation function $D_g^h(z, Q^2)$ which is very clean and accessible to the next to come experiments [‡1].

Let us briefly recall the basic features of the QCD description of large $p_\perp$ photoproduction. In fig. 1 we show the contributing graphs: direct coupling processes (figs. 1a,b) and the photon structure function [3] terms (fig. 1c). The trick for picking up only the contribution of subprocess 1a, cancelling those of 1b and minimizing those of 1c, consists in taking the difference $\Delta^{h_1 h_2}$ of the double inclusive cross sections,

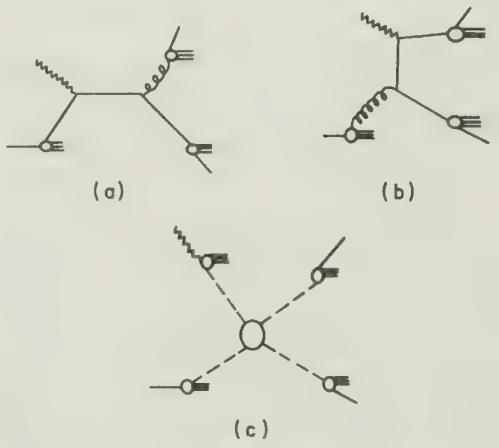

Fig. 1. The graphs contributing to large $p_\perp$ photoproduction: (a), (b) direct coupling terms; (c) photon structure function terms. In this last graph dashed lines represent quarks or gluons.

$$\Delta^{h_1 h_2} = \frac{E_1 E_2 \, d\sigma^{(2)}(\gamma p \to h_1^+ h_2 X)}{dp_1 \, dp_2} - \frac{E_1 E_2 \, d\sigma^{(2)}(\gamma p \to h_1^- h_2 X)}{dp_1 \, dp_2}, \quad (1)$$

[1] On leave from LPT, Faculté des Sciences de Rabat, Morocco.
[2] Laboratoire associé au CNRS.
[3] Groupe de Recherche du CNRS.
[‡1] NA 14 experiment of the CERN–London(Imp.Coll.)–Orsay(LAL)–Saclay–Southampton collaboration and wide band beam and tagged photon beam FNAL facilities. These experiments will have $s \approx 200$ GeV^2 and a yield of 5–50 particles/pb is expected in the CERN experiment.

where $h_1^{\pm}$ are the positively and negatively charged triggers at large $p_{\perp 1}$ and h_2 a hadron observed in the hemisphere away from the trigger; h_2 is either neutral or represents the sum $h_2^+ + h_2^-$. Then it is clear that of the direct coupling terms only the subprocess $\gamma q \to qg$ contributes to $\Delta^{h_1 h_2}$; moreover the particle h_1 may only come from the quark fragmentation; this means that in the away hemisphere one observes gluon fragments only.

In addition to selecting the subprocess $\gamma q \to qg$, the differences $\Delta^{h_1 h_2}$ present many interesting features that were described in a preceding letter [2]; let us briefly recall them:

(i) All terms which enter the theoretical prediction are well known (the distributions of valence quarks in the proton and the fragmentation functions of the u and d quarks are well determined from experiment).

(ii) The u quark contribution is strongly enhanced by the QED coupling, compared to that of the d quark; therefore, the cross section difference is a large fraction of the cross section itself.

(iii) Taking the difference $\Delta^{h_1 h_2}$ reduces the contributions due to the anomalous and VDM components of the photon structure function [3] to a negligible background (at $s \approx 200\ \mathrm{GeV}^2$, $p_{\perp 1} \gtrsim 3\ \mathrm{GeV}/c$).

Postponing to the end of this letter a more complete discussion of the background, let us now present some quantitative results for the direct coupling term. We consider the case where h_1 and h_2 are pions ($h_2 = \pi^+ + \pi^-$); the inclusion of kaons is straightforward. The cross section difference is written, with the usual notations (we have integrated over the p_2 component perpendicular to the scattering plane; p_{2x} is the component perpendicular to the beam axis in the scattering plane) as

$$\frac{\mathrm{d}\sigma^{\Delta}}{\mathrm{d}\boldsymbol{p}_{\perp 1}\,\mathrm{d}y_1\,\mathrm{d}p_{2x}\,\mathrm{d}y_2} = \frac{x}{p_{\perp 1}}\left[\tfrac{4}{9}G_u^{\mathrm{val}}(x,Q^2) - \tfrac{1}{9}G_d^{\mathrm{val}}(x,Q^2)\right] \times \left[D_u^{\pi^+}(z_1,Q^2) - D_u^{\pi^-}(z_1,Q^2)\right] \times \frac{1}{\pi}\frac{\mathrm{d}\hat{\sigma}}{\mathrm{d}\hat{t}}\left[D_g^{\pi^+}(z_2,Q^2) + D_g^{\pi^-}(z_2,Q^2)\right], \tag{2}$$

with

$$\frac{1}{\pi}\frac{\mathrm{d}\hat{\sigma}}{\mathrm{d}\hat{t}} = \tfrac{8}{3}\alpha\alpha_s(Q^2)\,\frac{1}{\hat{s}^2}\left(\frac{\hat{s}}{-\hat{u}} + \frac{-\hat{u}}{\hat{s}}\right),$$

$$z_1 = p_{\perp 1}(\mathrm{e}^{y_1} + \mathrm{e}^{y_2})/\sqrt{s}, \qquad z_2 = |p_{2x}|(\mathrm{e}^{y_1} + \mathrm{e}^{y_2})/\sqrt{s}, \qquad x = \mathrm{e}^{-y_1 - y_2}. \tag{3}$$

The Mandelstam invariant $\hat{u}$ is the square of the momentum transfer between the gluon and the incident quark and $\hat{s} = xs$ where $\sqrt{s}$ is the γ–p c.m. energy. For $\alpha_s(Q^2)$ we take the canonical value $12\pi/[25 \times \log(Q^2/0.25)]$. The leading logarithm approach used here does not specify the expression of Q^2. We use that of ref. [4]: $Q^2 = 2\hat{s}\hat{t}\hat{u}/(\hat{s}^2 + \hat{t}^2 + \hat{u}^2)$. Notice that we have not taken into account the incident quark Fermi motion. It is indeed known that double inclusive cross sections are little sensitive to its effects [5,6]. Moreover we have shown in ref. [2] that already at the one particle level the Fermi motion is negligible as soon as $p_{\perp} > 2.5\ \mathrm{GeV}/c$ contrary to the case of hadron–hadron collisions. We have also neglected the hadron transverse momentum with respect to the away jet axis. The magnitude of this spread is unknown. If it is large, it might show up in a kinematical scale breaking of the fragmentation function for relatively small $p_{\perp 1}$. Such an effect has been studied in hadronic reactions by Alonso et al. [7]. This should be kept in mind when analyzing data.

Expression (2) exhibits a remarkable feature: the subprocess kinematics are completely fixed by observing $\boldsymbol{p}_{\perp 1}, y_1, p_{2x}$ and y_2. No integration is needed; the extraction of $D_g^h(z, Q^2)$ is thus straightforward. In order to get $D_g^h(z, Q^2)$ from experiment, we make use of the peculiar direct coupling kinematics by defining a cross section at fixed $\sqrt{s}/(\mathrm{e}^{y_1} + \mathrm{e}^{y_2})$ which is the outgoing jet transverse momentum $p_{\perp}^{\mathrm{jet}}$:

$$\frac{\mathrm{d}\sigma^{\Delta}}{\mathrm{d}z_2\,\mathrm{d}p_{\perp}^{\mathrm{jet}}} = \int_{p_{\perp 1}^{\min}} \mathrm{d}\boldsymbol{p}_{\perp 1} \int \mathrm{d}p_{2x}\,\delta\left(z_2 - \frac{|p_{2x}|}{p_{\perp}^{\mathrm{jet}}}\right) \times \int_{y_1^{\min}}^{y_1^{\max}} \mathrm{d}y_1\,\mathrm{d}y_2\,\delta\left(p_{\perp}^{\mathrm{jet}} - \frac{\sqrt{s}}{\mathrm{e}^{y_1} + \mathrm{e}^{y_2}}\right) \times \frac{\mathrm{d}\sigma^{\Delta}}{\mathrm{d}\boldsymbol{p}_{\perp 1}\,\mathrm{d}y_1\,\mathrm{d}p_{2x}\,\mathrm{d}y_2}, \tag{4}$$

which can be written as

$$\frac{d\sigma^{\Delta}}{dz_2\, dp_\perp^{jet}} = D_g^{h_2}(z_2, \bar{Q}^2) \times d(p_{\perp 1}^{min}, p_\perp^{jet}, s, y_1^{min}, y_1^{max}), \quad (5)$$

with

$$d = 2\pi\sqrt{s} \int_{z_1^{min}}^{1} dz_1 \int_{y_1^{min}}^{y_1^{max}} dy_1\, e^{-y_2} D_u^{\pi^+ - \pi^-}(z_1, Q^2) \times x[\tfrac{4}{9} G_u^{val}(x, Q^2) - \tfrac{1}{9} G_d^{val}(x, Q^2)] \frac{1}{\pi} \frac{d\hat{\sigma}}{d\hat{t}}, \quad (6)$$

where $e^{y_2} = \sqrt{s}/p_\perp^{jet} - e^{y_1}$ and $z_2 = |p_{2x}|/p_\perp^{jet}$. In expression (4) we integrate over a y_1 range fixed by theoretical or experimental considerations.

The interest of eq. (5) comes from the fact that in the y_1 range where the cross section is important, Q^2 is nearly constant depending only on the value of $p_\perp^{jet}$ [‡2]. Therefore the gluon fragmentation function may safely be factored out. With the definition of ref. [4] for Q^2, we find $\bar{Q}^2 \approx \frac{4}{3}(p_\perp^{jet})^2$.

In order to show that $d\sigma^{\Delta}/dz_2\, dp_\perp^{jet}$ is fairly large and thus should allow a precise measurement of $D_g(z, Q^2)$, we perform the calculations at $s = 200$ GeV^2 with the proton structure functions of ref. [8], the quark fragmentation functions of ref. [9] (without scale breaking in agreement with e^+e^- data) and the gluon fragmentation function $D_g^h(z, Q^2)$ of ref. [4].

We integrate over the range $y_1 > 0$ where the direct coupling term is peaked and fix $p_{\perp 1}^{min} = 2$ GeV/c. The results are shown in fig. 2. The use of a different parametrization [6] for $D_g^h(z, Q^2)$ gives quite different results as shown in fig. 2.

The factorized form (4) allows us to go further and define the ratio

$$r_1(z_2, z_2', \bar{Q}^2) = \frac{d\sigma^{\Delta}/dz_2\, dp_\perp^{jet}}{d\sigma^{\Delta}/dz_2'\, dp_\perp^{jet}} = \frac{D_g^h(z_2, \bar{Q}^2)}{D_g^h(z_2', \bar{Q}^2)}, \quad (7)$$

in which many of the experimental and theoretical uncertainties cancel; then the z_2 dependence at fixed $\bar{Q}^2$ may be investigated very clearly. The Q^2 dependence may be studied by means of the double ratio

$$r_2 = \frac{r_1(z_2, z_2', \bar{Q}^2)}{r_1(z_2, z_2', \bar{Q}'^2)} = \frac{D_g(z_2, \bar{Q}^2)/D_g(z_2', \bar{Q}^2)}{D_g(z_2, \bar{Q}'^2)/D_g(z_2', \bar{Q}'^2)}. \quad (8)$$

Using the parametrization of ref. [5] we show in fig. 3 that we get a quite observable effect when fixing $\bar{Q}^2 = 10$ GeV^2, $z_2 = 0.2$ (a value at which D_g is almost Q^2 independent) and $z_2' = 0.8$; this large effect is intimately related to the QCD three gluon coupling [10] and provides a stringent test of this latter. A more standard approach consists in taking moments of eq. (5), the ratio of which are directly given in terms of experimental data:

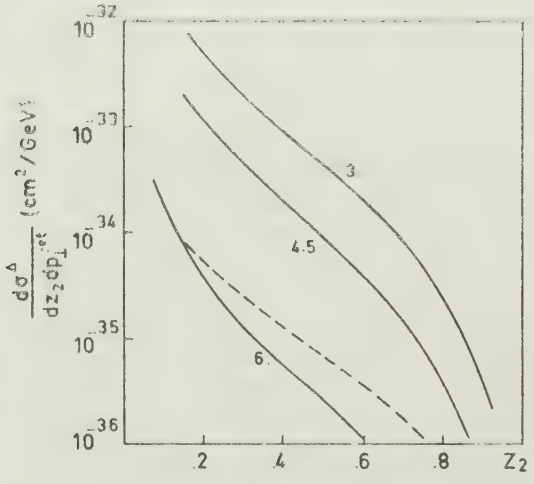

Fig. 2. The differential cross section $d\sigma^{\Delta}/dz_2\, dp_\perp^{jet}$. Full (dashed) curves correspond to the gluon fragmentation function of ref. [5] ([7]). Curves are labelled with the value of $p_\perp^{jet}$.

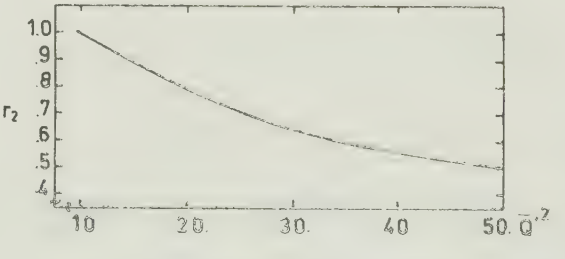

Fig. 3. The expected scaling violation as measured by the double ratio r_2 defined in the text for $z_2 = 0.2$, $z_2' = 0.8$ and $\bar{Q}^2 = 10$ GeV^2.

[‡2] This statement is true for a very large class of definitions of Q^2 due to the sharp peaking in y_1 of the cross section.

$$\frac{M_g^n(\bar{Q}^2)}{M_g^m(\bar{Q}^2)} = \frac{\int_0^1 dz_2\, z_2^{n-1}\, d\sigma^{\Delta}/dz_2\, dp_1^{jet}}{\int_0^1 dz_2\, z_2^{m-1}\, d\sigma^{\Delta}/dz_2\, dp_1^{jet}}. \quad (9)$$

Let us now comment on the background. Before the collision, the photon may, briefly speaking, transform in an almost collinear $q\bar{q}$ pair subsequently renormalized by the strong (QCD) interaction [3] or in a vector boson. Then large angle scattering takes place between gluons and/or quarks exactly as in hadron–hadron collisions. In hadron–hadron reactions, it was found that the incident parton Fermi motion does not strongly modify the double (toward–away) inclusive cross section [5,6]. We shall therefore neglect it in our estimate. Neglecting also the VDM contribution which is much smaller (see Kang and Llewellyn-Smith [1]) than the anomalous one, we estimated the contribution of this latter and found that it represents roughly 10–20% of the direct coupling one. This small background may again be experimentally reduced by using veto-counters forbidding forward jets. Another source of background is the presence of proton fragments; they may obscure the measurement of $D_g^h(z, Q^2)$ at small values of z and must be subtracted. It should be possible, by inspection of the y_2 behaviour of $d\sigma^{\Delta}/dp_{\perp 1}\, dy_1\, dp_{2x}\, dy_2$ to disentangle their contribution – a flat curve – from that of the gluon jet – a marked peak, the position of which can be fixed by the trigger rapidity.

To conclude, we have indicated a clear way to extract the gluon fragmentation function: orders of magnitude are such that it is measurable as is also the scaling violation effect. Of course, one should keep in mind that in a second step it will be necessary to bypass the leading logarithm approximation and calculate the next to leading terms.

We acknowledge useful discussions with F. Gorski and F. Richard.

References

[1] H. Fritzsch and P. Minkowski, Phys. Lett. 69B (1977) 316;
Tu Tung-Sheng and Wu Chi-Min, Nucl. Phys. B156 (1979) 493;
Tu Tung-Sheng, Nucl. Phys. B161 (1979) 417;
J. Owens, Phys. Rev. D21 (1980) 54;
I. Kang and C. Llewellyn-Smith, Oxford preprint 62/79;
E. Gotsman, D. Silverman and A. Soni, Phys. Rev. D20 (1979) 2220.
[2] M. Fontannaz, A. Mantrach, B. Pire and D. Schiff, Phys. Lett. 89B (1980) 26.
[3] E. Witten, Nucl. Phys. B120 (1977) 189;
C. Llewellyn-Smith, Phys. Lett. 79B (1978) 83;
R. De Witt et al., Phys. Rev. D19 (1979) 2046;
W. Frazer and J. Gunion, Phys. Rev. D20 (1979) 147.
[4] R. Feynman, R. Field and G. Fox, Phys. Rev. D18 (1978) 3320.
[5] M. Fontannaz and D. Schiff, Nucl. Phys. B132 (1978) 457.
[6] R. Baier, J. Engels and B. Petersson, Z. Phys. C2 (1979) 265.
[7] J.L. Alonso, A. Cruz, G. Ringland and R. Roberts, Nucl. Phys. B157 (1979) 498.
[8] A. Buras and K. Gaemers, Nucl. Phys. B132 (1978) 249.
[9] R. Field and R. Feynman, Nucl. Phys. B136 (1978) 1.
[10] K. Koller, T. Walsh and P. Zerwas, Phys. Lett. 82B (1979) 263.

Z. Physik C, Particles and Fields 6, 357–364 (1980)

Zeitschrift für Physik C Particles and Fields
© by Springer-Verlag 1980

Gluon Physics in Large $p_\perp$ Photoproduction

M. Fontannaz[1], A. Mantrach[1*], B. Pire[2], and D. Schiff[1]

1 Laboratoire de Physique Théorique et Hautes Energies, Université Paris-Sud Orsay, Bâtiment 211, F-91405 Orsay Cedex, France
2 Centre de Physique, Théorique, École Polytechnique, F-91128 Palaiseau Cedex, France

Received 7 July 1980

Abstract. Large $p_\perp$ photoproduction turns out to be a beautiful laboratory for gluon physics. The gluon properties namely the distribution function inside the proton and the fragmentation function may be studied by measuring two particle correlations. It is also possible to extract the anomalous photon structure function. The orders of magnitude encountered for the various cross sections are shown to be measurable by the present generation of photoproduction experiments.

Introduction

As already pointed out [1–4], large $p_\perp$ photoproduction is a very good place to test the validity of perturbative QCD. The point-like coupling of the photon to charged partons results in completely calculable amplitudes assuming the proton structure functions are known from deep inelastic experiments; these amplitudes are reliable provided one is in the hard scattering regime, $(p_\perp^2 \gg M^2)$. It is moreover remarkable that the lowest order graphs which describe the hard subprocesses involve gluons and therefore comparison between theory and experiment allows detailed studies of the gluon properties. In this respect, large $p_\perp$ photoproduction may be viewed as a laboratory to study gluon physics.

The way the photon interacts with the proton may be described under two categories:

1) The *direct coupling* terms of Fig. 1a, b: the Compton and fusion graphs.

2) The *photon structure function* [5] contribution represented on Fig. 2 which describes the interaction of the partons in the photon with partons inside the proton. The photon structure function is usually described as being made of two parts: the *anomalous* component which is completely calculable in QCD and dominates at large Q^2 over the *hadron-like*-component. This last one may be estimated in the framework of the vector dominance model and contributes as a background to the other parts which are in principle completely described by the theory.

In an earlier paper [4] we discussed in detail how these various components might be disentangled. In particular, we showed under which conditions the background might be sufficiently suppressed in order not to spoil the QCD predictions.

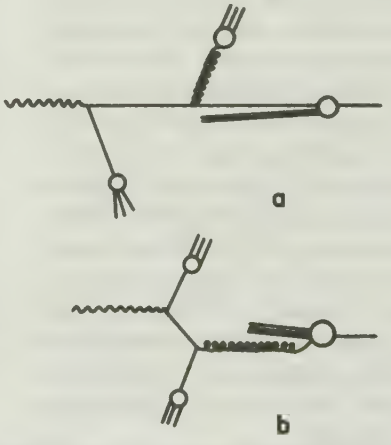

Fig. 1a and b. The direct coupling graphs a Compton, b fusion

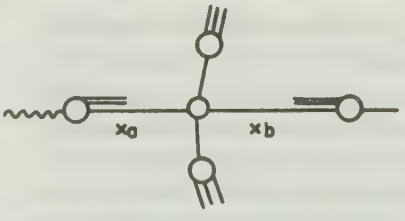

Fig. 2. The photon structure function contribution

* On leave from L.P.T., Faculté des Sciences de Rabat, Maroc
** Laboratoire associé au C.N.R.S.
*** Equipe de Recherche associée au C.N.R.S.

0170-9739/80/0006/0357/$01.60

In this paper we address ourselves to a complete study of gluon physics in large $p_\perp$ photoproduction. We will show that the direct coupling terms may be separated in a way which allows to study the gluon fragmentation function and the gluon distribution in the proton. Large p_T photoproduction indeed appears as one of the best places where to measure this latter. On the other hand, it is possible to isolate the anomalous photon term and thus study the parton content of the photon. A detailed discussion of the background will be given in each case. We shall work in the energy and p_T domain of the coming CERN-SPS and FNAL' experiments [6], that is $s \simeq 200\,\mathrm{GeV}^2$ and $p_T \lesssim 5\,\mathrm{GeV}/c$.

Let us outline the content of this paper. In Sect. I, we discuss the possibility to isolate and observe the various contributions to the cross-sections. In Sect. II, we focus on the measurement of $D_g^h(z, Q^2)$ whereas Sect. III deals with the gluon content of the proton. Section IV is a brief comment about the study of the quark and gluon content of the photon. Section V is the conclusion.

I. Observing the Photon Components

In this section, we recall the results of [4] in which the possibility to observe the different photon components is studied in detail; we have shown that various tricks such as cross-section differences, symmetric pairs correlations, kinematical constraints must be used in order to disentangle the contributions of the photon components and to isolate them. Let us briefly describe these results which are the starting point of this paper.

We begin by the separation of 3 jet events, corresponding to Fig. 1a, b, from 4 jet events (Fig. 2) in which a fourth forward jet made of the photon fragments can be observed. These two types of events have a very different jet topology; moreover, it is important to notice that the 3 jet events have to verify the following kinematical constraint

$$p_\perp(e^{y_1} + e^{y_2})/\sqrt{s} = 1\,, \tag{1}$$

where $p_\perp$, y_1, and y_2 are respectively the transverse momentum and the rapidities of the two large $p_\perp$ jets; $\sqrt{s}$ is the energy of the reaction in the overall CMS. Thus inspection of the jet structure, supplemented by the use of the 3 jet topology kinematical constraint (1), should allow one to separate the direct coupling events from the other ones. The interesting consequence of this selection is that we can now compare data and theory within each subset of events independently.

The 4-jet sample is populated by the contribution of the anomalous and of the hadron-like component of the photon. The one particle inclusive cross-section is dominated, as shown in [4], by the hadron-like component which hides the anomalous one. This dominance of the hadron-like part is explainable by the parton Fermi motion enhancement effect. However, when symmetric pairs are observed (two hadrons with the same $p_\perp$, but in opposite azimuthal hemispheres), the Fermi motion effect is considerably reduced and the anomalous component of the photon now dominates. Thus there is a possibility to isolate this component, which opens the way to interesting experimental tests of perturbative QCD (Sect. IV).

The method described above for disentangling 3 jet from 4 jet events evidently requires sophisticated experiments observing jets and measuring most particle momenta. However it is possible to isolate the 3 jet event contributions by simply taking cross-section difference [2]. For instance, for the one particle inclusive cross-section, taking the difference

$$E d\Delta^\pi/d\mathbf{p} = E d\sigma(\gamma p \to \pi^+ X)/d\mathbf{p} - E d\sigma(\gamma p \to \pi^- X)/d\mathbf{p} \tag{2}$$

enhances the 3 jet contributions compared to the 4 jet contributions, as shown in detail in [4]. This comes from the photon direct coupling to the quark charge which considerably enhances the u-quark jets (thus the π^+ production) compared to the d-quark jets; this effect is not present for the graphs of Fig. 2.

Let us end this section by noting that cross-section differences also allow, within the 3 jet sample, to disentangle the QCD. Compton contribution from the fusion one. We define the double inclusive cross-section

$$\frac{d\Delta^{\pi,h}}{d\mathbf{p}_{\perp 1} dy_1 dp_{2x} dy_2} = \frac{d\sigma(\gamma p \to \pi^+ h X)}{d\mathbf{p}_{\perp 1} dy_1 dp_{2x} dy_2} - \frac{d\sigma(\gamma p \to \pi^- h X)}{d\mathbf{p}_{\perp 1} dy_1 dp_{2x} dy_2}\,, \tag{3}$$

where the hadron h of momentum $\mathbf{p}_2$ is measured in the hemisphere away from the trigger π^+ or π^- (with transverse momentum $\mathbf{p}_{\perp 1}$ and rapidity y_1).

When $h = \pi^\pm$, it may be written:

$$\begin{aligned}
&\frac{d\Delta^{\pi,\pi^\pm}}{d\mathbf{p}_{\perp 1} dy_1 dp_{2x} dy_2} \\
&= \frac{x}{p_{\perp 1}} \left(\tfrac{4}{9} G_u^{\mathrm{val}}(x, Q^2) - \tfrac{1}{9} G_d^{\mathrm{val}}(x, Q^2)\right) D_u^{\pi^+ - \pi^-}(z_1, Q^2) \\
&\quad \cdot D_g^{\pi^\pm}(z_2, Q^2) \frac{1}{\pi} \frac{d\hat{\sigma}^C}{d\hat{t}} \mp \frac{x}{p_{\perp 1}} G_g(x, Q^2) \\
&\quad \cdot \tfrac{5}{9} D_u^{\pi^+ - \pi^-}(z_1, Q^2) D_u^{\pi^+ - \pi^-}(z_2, Q^2) \frac{1}{\pi} \frac{d\hat{\sigma}^F}{d\hat{t}}
\end{aligned} \tag{4}$$

with

$$x = e^{-(y_1 + y_2)}$$

$$z_1 = p_{\perp 1}(e^{y_1} + e^{y_2})/\sqrt{s}$$

$$z_2 = p_{2x}(e^{y_1} + e^{y_2})/\sqrt{s}\,.$$

In (4), we have integrated over the component p_{2y} perpendicular to the scattering plane and used the notation $D_q^{\pi^+-\pi^-}(z,Q^2)=D_q^{\pi^+}(z,Q^2)-D_q^{\pi^-}(z,Q^2)$. The subprocess cross-sections are given by:

$$\frac{1}{\pi}\frac{d\hat{\sigma}^C}{d\hat{t}}=\frac{8}{3}\frac{\alpha\alpha_s(Q^2)}{\hat{s}^2}\left(\frac{\hat{s}}{-\hat{u}}+\frac{-\hat{u}}{\hat{s}}\right)$$
$$\frac{1}{\pi}\frac{d\hat{\sigma}^F}{d\hat{t}}=\frac{\alpha\alpha_s(Q^2)}{\hat{s}^2}\left(\frac{\hat{u}}{\hat{t}}+\frac{\hat{t}}{\hat{u}}\right) \tag{5}$$

with $\alpha_s(Q^2)=(12\pi/25)/\log(Q^2/\Lambda^2)$ and

$$\hat{s}=xs$$
$$\hat{t}=-xse^{y_1}/(e^{y_1}+e^{y_2}) \tag{6}$$
$$\hat{u}=-se^{-y_1}/(e^{y_1}+e^{y_2}).$$

We use the definition [7]

$$Q^2=2\hat{s}\hat{t}\hat{u}/(\hat{s}^2+\hat{t}^2+\hat{u}^2) \tag{7}$$

and $\Lambda=500$ MeV. It is now clear, from (4), that the sum

$$\frac{d\Delta^{\pi,\pi^++\pi^-}}{d\mathbf{p}_{\perp 1}dy_1dp_{2x}dy_2}=\frac{d\Delta^{\pi,\pi^+}}{d\mathbf{p}_{\perp 1}dy_1dp_{2x}dy_2}+\frac{d\Delta^{\pi,\pi^-}}{d\mathbf{p}_{\perp 1}dy_1dp_{2x}dy_2} \tag{8}$$

allows a direct determination of the gluon fragmentation function $D_g(z,Q^2)$, whereas the difference

$$\frac{d\Delta^{\pi,\pi^--\pi^+}}{d\mathbf{p}_{\perp 1}dy_1dp_{2x}dy_2}=\frac{d\Delta^{\pi,\pi^-}}{d\mathbf{p}_{\perp 1}dy_1dp_{2x}dy_2}-\frac{d\Delta^{\pi,\pi^+}}{d\mathbf{p}_{\perp 1}dy_1dp_{2x}dy_2} \tag{9}$$

allows the measurement of the gluon distribution within the proton $G_g(x,Q^2)$.

II. The Fragmentation Function of the Gluon

As shown in the previous section, the fragmentation function of the gluons is directly accessible through the cross-section combination:

$$\frac{d\Delta^{\pi,\pi^++\pi^-}}{d\mathbf{p}_{\perp 1}dy_1dp_{2x}dy_2}=\frac{x}{p_{\perp 1}}\left(\tfrac{4}{9}G_u^{\mathrm{val}}(x,Q^2)-\tfrac{1}{9}G_d^{\mathrm{val}}(x,Q^2)\right)$$
$$\cdot D_u^{\pi^+-\pi^-}(z_1,Q^2)D_g^{\pi^++\pi^-}(z_2,Q^2)\frac{1}{\pi}\frac{d\hat{\sigma}^C}{d\hat{t}}. \tag{10}$$

This determination of D_g turns out to be very clear [3]: a) The building blocks entering (10) are well-known: only the valence quark distributions are needed. b) No integration is involved in (10) and the variables z_2 and Q^2 are fixed by the momenta $\mathbf{p}_1$ and $\mathbf{p}_2$ of the observed hadrons. c) The Fermi motion of the incident partons has a negligible effect. A possible background may come from the 4-jet events, if these latter have not been discarded as described in Sect. I. However, we are going to show that such a background is rather small.

In order to study the gluon fragmentation function, it is useful to define

$$\frac{d\Delta^{\pi,\pi^++\pi^-}}{d\mathbf{p}_{\perp 1}dy_1dp_{\perp\,\mathrm{jet}}dt_2}=\frac{\sqrt{s}}{p_{\perp\,\mathrm{jet}}}\frac{1}{e^{y_2}}\frac{d\Delta^{\pi,\pi^++\pi^-}}{d\mathbf{p}_{\perp 1}dy_1dp_{2x}dy_2}, \tag{11}$$

where

$$p_{\perp\,\mathrm{jet}}=\sqrt{s}/(e^{y_1}+e^{y_2})$$
$$z_2=p_{2x}/p_{\perp\,\mathrm{jet}}. \tag{12}$$

The quantity $p_{\perp\,\mathrm{jet}}$ is nothing else than the quark or gluon jet transverse momentum. Such a variable is useful in that it fixes almost completely the value of Q^2 which depends very weakly on y_1 in the region where the cross-section is non negligible. For instance, with our choice (7) for Q^2, we have $Q^2\simeq\frac{4}{3}(p_{\perp\,\mathrm{jet}})^2$.

The contribution of the anomalous component of the photon is given by

$$\frac{d\Delta^{\pi,\pi^++\pi^-}}{d\mathbf{p}_{\perp 1}dy_1dp_{\perp\,\mathrm{jet}}dz_2}$$
$$=\frac{\sqrt{s}}{p_{\perp\,\mathrm{jet}}}\frac{1}{e^{y_2}}\frac{1}{p_{\perp 1}}\frac{1}{s^2}\int\frac{dz_1}{z_1}D_u^{\pi^+-\pi^-}(z_1,Q^2)\alpha_s^2(Q^2)$$
$$\cdot\{[(u_\gamma(x_a,Q^2)(1+c(\tilde{z}_2))+d_\gamma(x_a,Q^2)(1+s(\tilde{z}_2)))$$
$$\cdot(G_u^{\mathrm{val}}(x_b,Q^2)-G_d^{\mathrm{val}}(x_b,Q^2))2|A_1|^2$$
$$+(u_\gamma(x_a,Q^2)G_u^{\mathrm{val}}(x_b,Q^2)-d_\gamma(x_a,Q^2)G_d^{\mathrm{val}}(x_b,Q^2))I]$$
$$\cdot D_u^{\pi^++\pi^-}(\tilde{z}_2,Q^2)+g_\gamma(x_a,Q^2)$$
$$\cdot(G_u^{\mathrm{val}}(x_b,Q^2)-G_d^{\mathrm{val}}(x_b,Q^2))$$
$$|A_2|^2D_g^{\pi^++\pi^-}(\tilde{z}_2,Q^2)\}/x_ax_b, \tag{13}$$

where

$$|A_1|^2=\tfrac{4}{9}(\hat{s}^2+\hat{u}^2)/\hat{t}^2$$
$$|A_2|^2=(\hat{u}^2+\hat{s}^2)/\hat{t}^2-4(\hat{u}^2+\hat{s}^2)/9\hat{u}\hat{s} \tag{14}$$
$$I=-8(s^3+\hat{u}^3-\hat{t}^3)/27\hat{s}\hat{t}\hat{u}.$$

We have the following kinematical relations

$$x_a=x_{\perp 1}(e^{y_1}+e^{y_2})/2z_1 \qquad \hat{s}=x_ax_bs$$
$$x_b=x_{\perp 1}(e^{-y_1}+e^{-y_2})/2z_1 \qquad \hat{t}=-x_bx_{\perp 1}se^{y_1}/2z_1 \tag{15}$$
$$\tilde{z}_2=z_1|p_{2x}|/p_{\perp 1} \qquad \hat{u}=-x_ax_{\perp 1}se^{-y_1}/2z_1$$
$$x_{\perp 1}=2p_{\perp 1}/\sqrt{s}.$$

In expression (13), u_γ, d_γ, and g_γ are the distribution functions within the photon of quarks of charge 2/3,

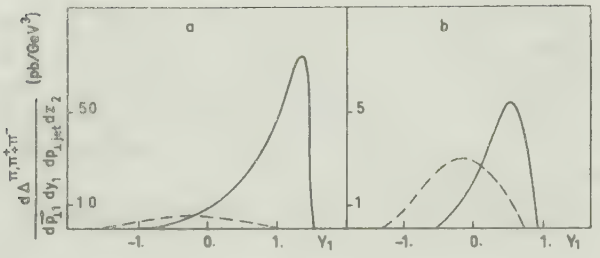

Fig. 3a and b. The double inclusive cross-section $d\Delta^{\pi,\pi^+ +\pi^-}/dp_{\perp 1}dy_1dp_{\perp \text{jet}}dz_2$ for $s=200\ \text{GeV}^2$, $p_{\perp 1}=2.5\ \text{GeV}/c$, $z_2=0.4$ and **a** $p_{\perp \text{jet}}=3\ \text{GeV}/c$, **b** $p_{\perp \text{jet}}=5\ \text{GeV}/c$. The Compton graph contribution (—) and the anomalous photon contribution (– – –)

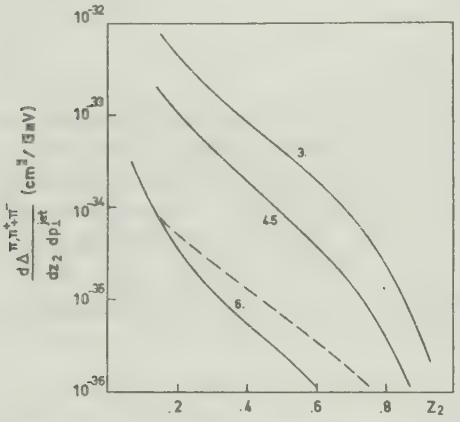

Fig. 4. The differential cross-section $d\Delta^{\pi,\pi^+ +\pi^-}/dz_2dp_{\perp \text{jet}}$. Full and dashed curves correspond to the parametrizations of [16, 12] respectively for the gluon distribution function. Curves are labelled with the value of $p_{\perp \text{jet}}$

1/3 and of the gluons. We use here the parametrization of [8]: for the distributions G_g^{val}, we use the parametrization of Buras and Gaemers [9] and for the quark fragmentation functions, the expressions of Field and Feynman [10] (without scale breaking in agreement with e^+e^- data). $c(\tilde{z}_2)$ and $s(\tilde{z}_2)$ in (13) mean $D_c^{\pi^+ +\pi^-}(\tilde{z}_2)/D_u^{\pi^+ +\pi^-}(\tilde{z}_2)$ and $D_s^{\pi^+ +\pi^-}(\tilde{z}_2)/D_u^{\pi^+ +\pi^-}(\tilde{z}_2)$; we take $c(\tilde{z}_2)=s(\tilde{z}_2)$. For $D_g(\tilde{z}_2, Q^2)$ we use the parametrization of [7]. Notice also that we have not taken into account the Fermi motion of the incident parton in (13); we know indeed that the Fermi motion effect is small in double inclusive cross-sections [11].

The results of our calculations (done for $E^\gamma_{\text{Lab}}=100\ \text{GeV}$, as everywhere in this paper) are shown in Fig. 3. We see that the direct coupling term dominates over the anomalous one for $p_{\perp \text{jet}} \lesssim 5\ \text{GeV}/c$, provided we choose $y_1 \gtrsim 0$. On the other hand, we have not considered the VDM background, since we already know from [4] that it is smaller in double inclusive cross-sections than the anomalous component contribution. We conclude from these calculations that the direct coupling contribution to $d\Delta^{\pi,\pi^+ +\pi^-}/d\mathbf{p}_{\perp 1}dy_1dp_{\perp \text{jet}}dz_2$ is quite observable, for $p_{\perp \text{jet}}$ not too large, even if the 4-jet events have not been discarded.

To extract $D_g(z, Q^2)$ from (10), we integrate over y_1 and $\mathbf{p}_{\perp 1}$ defining

$$\frac{d\Delta^{\pi,\pi^+ +\pi^-}}{dz_2dp_{\perp \text{jet}}} = D_g(z_2, \bar{Q}_2)d(p_{\perp 1}^{\min}, y_1^{\min}, y_1^{\max}, p_{\perp \text{jet}}, s) \tag{16}$$

with

$$d = 2\pi\sqrt{s}\int_{z_1^{\min}}^{1} dz_1 \int_{y_1^{\min}}^{y_1^{\max}} dy_1 e^{-y_2} D_u^{\pi^+ -\pi^-}(z_1, Q^2)$$
$$\times\left(\tfrac{4}{9}G_u^{\text{val}}(x, Q^2) - \tfrac{1}{9}G_d^{\text{val}}(x, Q^2)\right)\frac{1}{\pi}\frac{d\hat{\sigma}^C}{d\hat{t}} \tag{17}$$

and $\bar{Q}^2 \simeq 4(p_{\perp \text{jet}})^2/3$.

This cross-section is fairly large and should be quite observable, as shown in Fig. 4. These results are obtained by integrating over $y_1>0$ and taking $p_{\perp 1}^{\min}=2\ \text{GeV}/c$. We show also in Fig. 4 the curve obtained with another parametrization of the gluon fragmentation function [12]. The results are very different, which emphasizes the sensitivity of this approach for measuring $D_g(z, Q^2)$.

The factorized form (16) allows us to go further and to define ratios in which many of the experimental and theoretical uncertainties cancel. By defining

$$r_1(z_2, z_2', \bar{Q}^2) = \frac{d\Delta^{\pi,\pi^+ +\pi^-}/dz_2dp_{\perp \text{jet}}}{d\Delta^{\pi,\pi^+ +\pi^-}/dz_2'dp_{\perp \text{jet}}} = \frac{D_g^{\pi^+ +\pi^-}(z_2, \bar{Q}^2)}{D_g^{\pi^+ +\pi^-}(z_2', \bar{Q}^2)} \tag{18}$$

the z_2 dependence of $D_g(z_2, Q^2)$ at fixed Q^2 may be investigated very clearly. Similarly the ratio

$$r_2 = \frac{r_1(z_2, z_2', \bar{Q}^2)}{r_1(z_2, z_2', \bar{Q}'^2)} = \frac{D_g(z_2, \bar{Q}^2)}{D_g(z_2, \bar{Q}'^2)} \Big/ \frac{D_g(z_2', \bar{Q}^2)}{D_g(z_2', Q'^2)} \tag{19}$$

allows the observation of scale breaking effect, as explicitly shown in [3].

To end this section, let us comment on two effects which could obscure the measurement of $D_g(z_2, Q^2)$. One effect comes from the transverse spread of the final hadrons in the gluon jet. In that case, the measured value $z_2^m = |p_{2x}|/p_{\perp \text{jet}}$ does not coincide with the definition $z_2 = \dfrac{\mathbf{p}_2 \cdot \mathbf{p}_{\text{jet}}}{\mathbf{p}_{\text{jet}}^2}$ and a bias is thus introduced in the measurement of $D_g(z_2, Q^2)$. It is however possible to get rid of this effect, extensively studied in [13] for hadron-hadron collisions, if the jet axis is experimentally determined, which allows to use the true definition of z_2.

A second effect comes from the background due to the proton low $p_\perp$ fragments in the backward direction; the fragments may be confused with gluon jet

fragments at low p_{2x}. We estimate this background by the approximation

$$\frac{d\Delta^{\pi,\pi^+ +\pi^-}}{d\mathbf{p}_{\perp 1}dy_1dp_{2x}dy_2} = \frac{dN^{\pi^+ +\pi^-}}{dp_{2x}dy_2}\frac{d\sigma^\pi}{d\mathbf{p}_{\perp 1}dy_1}, \tag{20}$$

where $dN^{\pi^+ +\pi^-}/d\mathbf{p}_{\perp 2}dy_2$ describes the spectator diquark fragmentation [14, 15]

$$\begin{aligned} dN^{\pi^+ +\pi^-}/d\mathbf{p}_{\perp 2}dy_2 &= \frac{A}{\pi}e^{-Ap_{\perp 2}^2}x_2 D_{qq}^{\pi^+ +\pi^-}(x_2) \\ x_2 D_{qq}^{\pi^+ +\pi^-}(x_2) &= [(1-x_2)^3+(1-x_2)^5]/2 \\ x_2 &\simeq 2p_{\perp 2}\mathrm{sh}y_2/\sqrt{s} \\ dN^{\pi^+ +\pi^-}/dp_{2x}dy_2 &= \int dp_{2y}dN^{\pi^+ +\pi^-}/d\mathbf{p}_{\perp 2}dy_2 \end{aligned} \tag{21}$$

For A we take the value $A=6$ which gives $\langle p_{\perp 2}\rangle \simeq 360$ MeV/c. The results of our calculations are shown[1] in Fig. 5a and b. The diquark background is negligible, even for $p_{2x}=300$ MeV/c. Moreover, it contributes only for negative values of y_2, whereas the signal is important for positive y_2.

This approximate treatment of the background is very crude in the $y_2 \simeq 0$ region. A better description of the background would be obtained by following the approach developed in [15]; in that approach, the hadrons are considered as fragments of a string which stretches between colored charges, and a satisfying description of the $y_2 \simeq 0$ region can be obtained. We do not however expect [15] the relative value of the signal over the background to be changed.

III. The Gluon Content of the Proton

In this section, we turn to the possibility to measure the gluon distribution within the proton in photoproduction experiment. The cross-section difference

$$\frac{d\Delta^{\pi,\pi^- -\pi^+}}{d\mathbf{p}_{\perp 1}dy_1dp_{2x}dy_2} = \frac{2x}{p_{\perp 1}}G_g(x,Q^2)\frac{1}{\pi}\frac{d\hat{\sigma}^F}{d\hat{t}}\frac{5}{9} \cdot D_u^{\pi^+ -\pi^-}(z_1,Q^2)D_u^{\pi^+ -\pi^-}(z_2,Q^2) \tag{22}$$

is directly proportional to the gluon distribution $G_g(x,Q^2)$ and the variables x and Q^2 are fixed by the rapidities y_1 and y_2 of the observed π's. Thus we have a way to directly observe the gluon content of the proton; the cross-section differences must, of course, be sizeable and not small compared to various backgrounds. We are going to show that this measurement is indeed possible.

1 The peculiar shape of the Compton curves near the upper value of y_2 is due to the behaviour of the fragmentation function $D_u^{\pi^+ -\pi^-}(z_1)$ when $z_1 = p_{\perp 1}(e^{y_1}+e^{y_2})/\sqrt{s}$ goes to 1; in the Field-Feynman parametrization which we use here this difference does not vanish at $z_1 = 1$

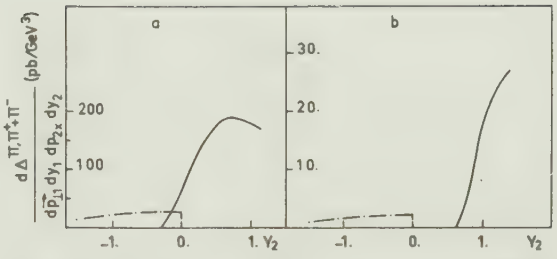

Fig. 5a and b. Comparison of the Compton graph contribution (–) to the double inclusive cross-section $d\Delta^{\pi,\pi^+ +\pi^-}/d\mathbf{p}_{\perp 1}dy_1dp_{2x}dy_2$ with the corresponding background due to low $p_\perp$ proton fragments ($s=200\,\mathrm{GeV}^2$, $p_{\perp 1}=3$ GeV/c, $p_{2x}=0.3$ GeV/c and **a** $y_1=0.5$; **b** $y_1=-0.5$)

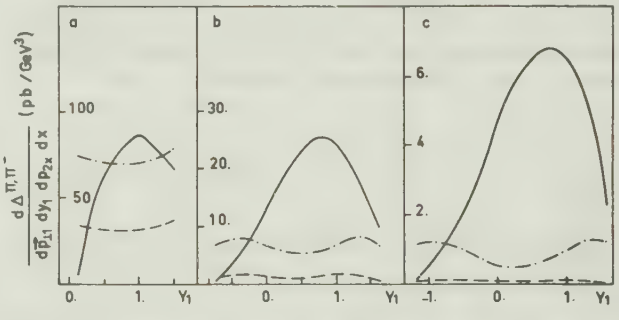

Fig. 6a–c. Comparison between the Compton graph (–) and the fusion graph contributions to the double inclusive cross-section $d\Delta^{\pi,\pi^-}/d\mathbf{p}_{\perp 1}dy_1dp_{2x}dx$. The dashed and dash-dotted lines correspond to the fusion graph evaluated with the parametrization of [16, 12] respectively for the gluon distribution function. ($s=200\,\mathrm{GeV}^2$, $p_{\perp 1}=2$ GeV/c, $p_{2x}=1$ GeV/c and **a** $x=0.2$, **b** $x=0.4$, **c** $x=0.6$)

Let us begin by estimating the relative magnitude of the Compton and fusion contributions, using two somewhat extreme parametrizations of $G_g(x,Q^2)$ [12, 16]. As the cross-section differences (4), read:

$$\frac{d\Delta^{\pi,\pi^\pm}}{d\mathbf{p}_{\perp 1}dy_1dp_{2x}dy_2} = \frac{d\Delta^{\pi,\pi^+}(\text{Compton})}{d\mathbf{p}_{\perp 1}dy_1dp_{2x}dy_2} \mp \frac{d\Delta^{\pi,\pi^-}(\text{fusion})}{d\mathbf{p}_{\perp 1}dy_1dp_{2x}dy_2} \tag{23}$$

a necessary condition to observe $G_g(x,Q^2)$ is that $d\Delta^{\pi,\pi^-}$ (fusion) is not too small compared to $d\Delta^{\pi,\pi^+}$ (Compton). It is useful to let the x variable appear through

$$\frac{d\Delta^{\pi,\pi^+}}{d\mathbf{p}_{\perp 1}dy_1dp_{2x}dx} = \int dy_2\,\delta(x-e^{-y_1-y_2})\frac{d\Delta^{\pi,\pi^+}}{d\mathbf{p}_{\perp 1}dy_1dp_{2x}dy_2}. \tag{24}$$

The dependence of this cross-section on $p_{\perp 1}$ and p_{2x}, through the quark and gluon fragmentation functions, is trivial and of no interest here; we fix $p_{\perp 1}=2.5$ GeV/c and $p_{2x}=1$ GeV/c. The Compton and fusion cross-sections are shown (see footnote 1) in Fig. 6a–c as functions of y_1 for $x=0.2$, 0.4, and 0.6. We have used the quark structure and fragmentation functions de-

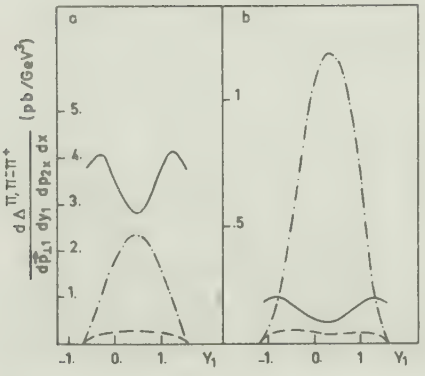

Fig. 7a and b. The double inclusive cross-section $d\Delta^{\pi,\pi^- - \pi^+}/d\mathbf{p}_{\perp 1}dy_1dp_{2x}dx$ for $s=200\,\text{GeV}^2$, $p_{\perp 1}=2.5\,\text{GeV}/c$, $p_{2x}=1\,\text{GeV}/c$ and **a** $x=0.4$, **b** $x=0.6$. The fusion graph contribution (–) is compared to the anomalous photon contribution (–·–·–). The dashed curve is the anomalous photon contribution with the condition $x_a>0.9$

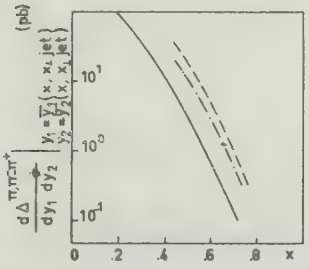

Fig. 8. The differential cross-section $d\Delta^{\pi,\pi^- - \pi^+}/dy_1dy_2$ ($s=200\,\text{GeV}^2$, $p_{\perp 1}^{\min}=2\,\text{GeV}/c$, $p_{2x}^{\min}=1\,\text{GeV}/c$) as a function of x for 2 values of $p_{\perp\text{jet}}$: $p_{\perp\text{jet}}=2.5\,\text{GeV}/c$ (–) and $p_{\perp\text{jet}}=4.5\,\text{GeV}/c$ (–·–). The dashed curve is obtained for $p_{\perp\text{jet}}=4.5\,\text{GeV}/c$, with no scaling violation in the gluon distribution function when Q^2 is held fixed $Q^2=Q_0^2=7.33\,\text{GeV}^2$

fined in the preceeding section and two different parametrizations for the gluon distribution within the proton, that of [16] and that of [12]. We see that the contribution of the fusion term may be sizable for x up to 0.6.

We already know that taking cross-section differences enhances the ratio of the 3 jet signal to the 4 jet one. However, the 4 jet events may still produce an appreciable background in some kinematical regions. Let us, for instance, study the contribution of the anomalous component of the photon to the difference $d\Delta^{\pi,\pi^- - \pi^+}/d\mathbf{p}_{\perp 1}dy_1dp_{2x}dx$ and see how it compares to the direct coupling contribution. The results of our calculations, done with the gluon distribution of [16] are shown (see footnote 1) in Fig. 7a and b. We see that for the higher value the background due to the anomalous component of the photon may be large.

We have however, in Sect. II, shown that it was possible to completely eliminate the 4 jet event background. Another and maybe simpler way to discard the 4 jet events consists in putting a forward veto counter allowing to discard events with a forward jet. Thus eliminating events with forward jets carrying more than 10% of the incident photon momentum [this amounts to require the variable x_a of the photon constituent (Fig. 2) be bigger than 0.9], we considerably reduce the anomalous component contribution as shown in Fig. 7.

Thus our conclusion is that, as long as $x\lesssim 0.6$, the fusion term can be safely isolated.

In order to extract the gluon distribution function, it is useful to define the cross-section (22) as function of x and Q^2, where Q^2 is a given expression of s, e^{y_1} and e^{y_2}. With our choice (7) for Q^2, it is simpler to introduce as in Sect. III, the variable

$$p_{\perp\text{jet}}=\sqrt{s}/(e^{y_1}+e^{y_2}).$$

The value of Q^2 is now essentially fixed by $p_{\perp\text{jet}}$ and varies very little with x for $0.1<x<0.8$; we found, within 20%, that $Q^2\simeq 4p_{\perp\text{jet}}^2/3-1$. Integrating (22) over $p_{\perp 1}$ and p_{2x}, and expressing the result as a function of x and

$$x_{\perp\text{jet}}=2p_{\perp\text{jet}}/\sqrt{s},$$

we get the simple form:

$$\left.\frac{d\Delta^{\pi,\pi^- - \pi^+}}{dy_1dy_2}\right|_{\substack{y_1=\bar{y}_1(x,x_{\perp\text{jet}})\\ y_2=\bar{y}_2(x,x_{\perp\text{jet}})}}=\frac{20\pi\alpha}{9s}\left(1-\frac{x_{\perp\text{jet}}^2}{2x}\right)$$
$$\cdot\alpha_s(Q^2)\mathfrak{D}_u^{\pi^+ - \pi^-}(z_1^{\min},Q^2)\mathfrak{D}_u^{\pi^+ - \pi^-}(z_2^{\min},Q^2)G_g(x,Q^2), \tag{25}$$

where we have defined

$$\mathfrak{D}_q^h(z_1^{\min},Q^2)=\int_{z_1^{\min}}^{} dz_1 D_q^h(z_1,Q^2). \tag{26}$$

In (25), the values of the rapidities are connected with x and $x_{\perp\text{jet}}$ by the relation

$$\bar{y}_{\frac{1}{2}}=\ln\{1/x_{\perp\text{jet}}\pm(1/x_{\perp\text{jet}}^2-1/x)^{1/2}\}. \tag{27}$$

Notice that expression (25) is invariant under the substitution $y_1\to y_2$.

In Fig. 8, we show the cross-sections

$$d\Delta^{\pi,\pi^- - \pi^+}/dy_1dy_2$$

as function of x and $p_{\perp\text{jet}}$ for

$$p_{\perp 1}^{\min}=2\,\text{GeV}/c,\quad p_{2x}^{\min}=1\,\text{GeV}/c$$

and the structure function of [16]. These cross-sections are fairly large for x up to about 0.5 and should allow a direct measure of $G(x,Q^2)$. The Q^2 evolution of $G(x,Q^2)$ is related to the variation of $d\Delta^{\pi,\pi^- - \pi^+}/dy_1dy_2$ with $p_{\perp\text{jet}}$ as written in (25). For illustration we also plot in Fig. 8 the value obtained for $d\Delta^{\pi,\pi^- - \pi^+}/dy_1dy_2$ when the scaling violation in $G(x,Q^2)$ is frozen by taking

$$Q^2(p_{\perp\text{jet}})=Q^2(2.5)=7.33\,GeV^2.$$

We find that scaling violation effects are relatively small and should thus be difficult to detect.

Of course these results strongly depend on the parametrization of $G_g(x, Q^2)$. To see the effect of another choice for $G_g(x, Q^2)$, we present in Fig. 9, results for the cross-section

$$\frac{d\Delta^{\pi,\pi^- - \pi^+}}{dx} = \int dy_1 dy_2 \delta(x - e^{-y_1 - y_2}) \cdot \int_{p_{\perp 1}^{\min}} d\mathbf{p}_{\perp 1} \int_{p_{\perp 2}^{\min}} d\mathbf{p}_{\perp 2} \frac{d\Delta^{\pi,\pi^- - \pi^+}}{d\mathbf{p}_{\perp 1} dy_1 dp_{2x} dy_2} \quad (28)$$

with $p_{\perp 1}^{\min} = 2.0\,\text{GeV}/c$, $p_{2x}^{\min} = 1\,\text{GeV}/c$ and $-1 < y_1 < 2$. The great difference between the curves obtained with the parametrizations of [12, 16] is the effect of the current ignorance of the gluon distribution within the proton and a good illustration of the method we propose to measure it.

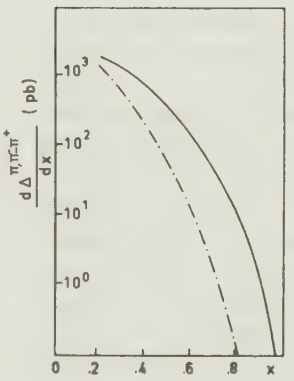

Fig. 9. The differential cross-section $d\Delta^{\pi,\pi^- - \pi^+}/dx$ for $s = 200\,\text{GeV}^2$, $p_{\perp 1}^{\min} = 2\,\text{GeV}/c$, $p_{2x}^{\min} = 1\,\text{GeV}/c$, y_1 integrated between -1 and 2. Comparison between the parametrization of [16] (–·–) and [12] (–) for the gluon distribution function

IV. Quark and Gluon Content of the Photon

We already indicated in [4] how it is possible to isolate the contribution of the anomalous photon component in the 4-jet event sample. This is done by measuring symmetric pair correlations which are found to be fairly large for $E_{\text{Lab}}^{\gamma} = 100\,\text{GeV}$ and $p_\perp = 2.5\,\text{GeV}/c$. In this case the dominant subprocess is the $qq \to qq$ scattering, and $qg \to qg$ contributes only 3% which means that this measurement will not yield information on the gluon content of the photon.

In order to obtain this, we propose to measure the difference of opposite side double inclusive cross-sections:

$$\frac{d\Delta^g}{dp_{\perp 1} dy_1 dp_{2x} dy_2} = \frac{d\sigma(\gamma p \to \gamma \pi^+ X)}{dp_{\perp 1} dy_1 dp_{2x} dy_2} - \frac{d\sigma(\gamma p \to \gamma \pi^- X)}{dp_{\perp 1} dy_1 dp_{2x} dy_2},$$

where the photon and the pions are detected at large $p_\perp$ in opposite hemispheres with rapidity y_1 and y_2 and transverse momenta $p_{\perp 1}$ and p_{2x} respectively. It is straightforward to see (Fig. 10) that only the gluon content of the photon contributes to the difference. This difference is written under the simple expression

$$\frac{d\Delta^g}{dp_{\perp 1} dy_1 dp_{2x} dy_2} = \frac{2}{3} \frac{\pi \alpha \alpha_s(Q^2)}{\hat{s}^2} x_a g_\gamma(x_a, Q^2) \cdot \left[\frac{4}{9} x_b G_u(x_b, Q^2) - \frac{1}{9} x_b G_d(x_b, Q^2)\right] \cdot D_u^{\pi^+ - \pi^-}(z_2) \left(\frac{\hat{s}}{-\hat{t}} + \frac{-\hat{t}}{\hat{s}}\right), \quad (30)$$

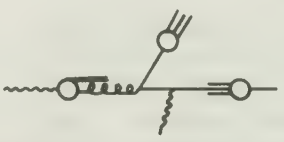

Fig. 10. The contribution of the gluon in the photon to the large $p_\perp$ photon inclusive production

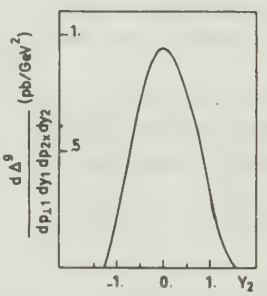

Fig. 11. The double inclusive cross-section $d\Delta^g/dp_{\perp 1} dy_1 dp_{2x} dy_2$ for $s = 200\,\text{GeV}^2$, $p_{\perp 1} = 2.5\,\text{GeV}/c$, $p_{2x} = 1.0\,\text{GeV}/c$ and $y_1 = 0$

where

$$x_a = x_{\perp 1}(e^{y_1} + e^{y_2})/2$$

$$x_b = x_{\perp 1}(e^{-y_1} + e^{-y_2})/2$$

$$z_2 = |p_{2x}|/p_{\perp 1}.$$

The results of the calculations done with the same ingredients as defined in previous section are shown in Fig. 11. They turn out to be very small ($E_{\text{lab}}^{\gamma} = 100\,\text{GeV}$, $p_{\perp 1} = 2.5\,\text{GeV}/c$, $p_{2x} = 1\,\text{GeV}/c$, and $y_1 = 0$). Thus the measurement of the gluon content of the photon would require very high statistics experiments.

V. Conclusion

We have shown in this paper how large $p_\perp$ photoproduction should in the near future reveal very interesting results on the gluon properties. The orders of

magnitude which come out of the calculations are all large enough to yield sufficient counting rates within the expected experimental luminosities.

Let us conclude by some remarks about the next steps in the study of gluon physics in photoproduction.

i) on the experimental side, very high energy photon beams (as the HERA project in Europe and the TRISTAN project in Japan) would allow the anomalous contribution to dominate much over the direct coupling and hadron-like terms. Moreover, as shown in [4] the processes contributing mainly are $qg \to qg$ and $gg \to gg$ provided $p_\perp$ is not too large (say $p_\perp < 10\,\text{GeV}/c$ for $\sqrt{s} \simeq 100\,\text{GeV}$).

ii) The use of polarized photon beams either on unpolarized targets [17] or on polarized ones [18] should provide new tests of QCD and more precisely of the vector nature of the gluon.

iii) On the theoretical side, a deeper understanding of the applicability of perturbative QCD is needed. The problem of next to leading terms which have been shown to yield a very significant correction to the leading log approximation [19] is as sharp in photoproduction as in other reactions. Some of the conclusions of this paper may well be invalidated if it turns out that these next to leading corrections completely destroy the simple picture of hard processes we have been used to.

We indeed are just at the beginning of the study of large $p_\perp$ photoproduction. The preliminary data of the WA4 collaboration at CERN show an encouraging trend. More data at higher energy will be available in the near future which should help the gluon properties to be better known.

Acknowledgements. We wish to thank M. Gorski and F. Richard for helpful discussions.

References

1. H.Fritzsch, P.Minkowski: Phys. Lett. **69**B, 316 (1977)
   C.H.Llewellyn-Smith: Phys. Lett. **79**B, 83 (1978)
   Tu Tung Sheng, Wu Chi Min: Nucl. Phys. B**156**, 493 (1979)
   J.Owens: Phys. Rev. D**21**, 54 (1980)
   K.Ishida, T.Kobayashi, T.Yoshino: KEK preprint 79–14 (1979)
   I.Kang, C.H.Llewellyn-Smith: Nucl. Phys. B**166**, 413 (1980)
2. M.Fontannaz, A.Mantrach, B.Pire, D.Schiff: Phys. Lett. **89**B, 263 (1980)
3. M.Fontannaz, A.Mantrach, B.Pire, D.Schiff: Phys. Lett. **94**B, 509 (1980)
4. M.Fontannaz, A.Mantrach, B.Pire, D.Schiff: Z. Phys. C **6**, 241 (1980)
5. E.Witten: Nucl. Phys. B**120**, 189 (1977)
   C.H.Llewellyn-Smith: Phys. Lett. **79**B, 83 (1978)
   R.DeWitt et al.: Phys. Rev. D**19**, 2046 (1979); D**20**, 1751(E) (1979)
   W.Frazer, J.Gunion: Phys. Rev. D**20**, 147 (1979)
6. NA14 experiment of the CERN–London–Orsay–Saclay–Southampton collaboration. Wide band beam and tagged photon beam FNAL facilities
7. R.Feynman, R.Field, G.Fox: Phys. Rev. D**18**, 3320 (1978)
8. A.Nicolaïdis: Nucl. Phys. B**163**, 156 (1980)
9. A.Buras, K.Gaemers: Nucl. Phys. B**132**, 249 (1978)
10. R.Field, R.Feynman: Nucl. Phys. B**136**, 1 (1978)
11. M.Fontannaz, D.Schiff: Nucl. Phys. B**132**, 457 (1978)
12. R.Baier, J.Engels, B.Petersson: Z. Phys. C **2**, 265 (1979)
13. J.L.Alonso, A.Cruz, G.Ringland, R.Roberts: Nucl. Phys. B**157**, 498 (1979)
14. M.Fontannaz, B.Pire, D.Schiff: Phys. Lett. **77**B, 315 (1978)
15. M.Fontannaz, B.Pire, D.Schiff: Nucl. Phys. B**162**, 317 (1980)
16. J.Owens, E.Reya: Phys. Rev. D**17**, 3003 (1978)
17. B.Petersson, B.Pire: Phys. Lett. **95**B, 119 (1980)
18. M.Fontannaz, B.Pire, D.Schiff: Ecole Polytechnique preprint A416 (1980)
19. J.Abad, B.Humpert: Phys. Lett. **78**B, 627 (1978); **80**B, 433(E) (1979)
    G.Altarelli, R.Ellis, G.Martinelli: Nucl. Phys. B**143**, 521 (1978); B**157**, 461 (1979)
    J.Kubar-André, F.Paige: Phys. Rev. D**19**, 221 (1979)
    W.Bardeen, A.Buras: Phys. Rev. D**20**, 166 (1979)
    D.Duke, J.Owens: FSU preprint HEP 802401 (1980)

CHAPITRE II

La radiation des gluons et la montée de la section efficace totale hadronique inélastique.

COMMISSARIAT A L'ENERGIE ATOMIQUE

DIVISION DE LA PHYSIQUE

SERVICE DE PHYSIQUE THEORIQUE

QCD AND THE RISE OF HADRONIC TOTAL CROSS SECTIONS

by

G. Cohen-Tannoudji, A. Mantrach*, H. Navelet, R. Peschanski

*LPTHE Université Paris Sud 91405 Orsay France
on leave from LPT Faculté des Sciences de Rabat (Maroc)

CEN-SACLAY – 91191 GIF-sur-YVETTE CEDEX – FRANCE

ABSTRACT

We have computed the sum of all multi parton production cross sections induced by one hard gluon exchange in the leading logarithm approximation of QCD for high energy hadronic collisions. The rise of hadronic total cross sections is explained by the excess of the rise of parton multiplicities with respect to the decrease of each individual cross section. We have shown that this rise is very sensitive to only one free parameter, namely the mass of the constituent quark, but not to other non perturbative effects. With a reasonable value of 350 MeV, we have obtained a rise of 15 mb between ISR and collider energies.

To be submitted for publication to
"Physical Review D"

SPh.T/70
October 1982

I. INTRODUCTION

It is now a rather well established fact that the observables of hadronic multiple production exhibit similar behaviour both in purely hadronic reactions and in hard lepton-hadron reactions at least at moderate values of Q^2. For instance, the increase of multiplicities and average transverse momentum, long range correlations have been observed in high energy hadronic reactions as well as in e^+e^- annihilation [1]. Since QCD is the theoretical framework used to describe these behaviours in hard lepton-hadron reactions, the observed similarities suggests that perturbative QCD may be a good tool to explain some features of purely hadronic reactions.

In the present paper we answer the question of the relevance of QCD to describe hadronic total cross sections, Indeed we show by means of a quantitative estimate that the gluon radiation induced in hard parton collisions may be responsible for the rise of hadronic total cross sections. We discuss the theoretical significance of this result.

We exclude from the domain of application of perturbative QCD the constant component of total cross sections, which is obviously related to non perturbative effects. We concentrate on the rise of the total cross sections, and the problem is to explain a rise of order of about 15 mb from ISR to $p\bar{p}$ collider energies, by means of small cross sections typical of hard processes.

We obtain this effect thanks to the increase of the number of gluons radiated by bremsstrahlung[2][3]. Qualitatively, the higher the transfer momentum, the lower the individual parton cross section but the higher the multiplicity of partons. Indeed, it has been observed that the rise of hadronic total cross sections is connected with an increase of multiplicities faster than logarithmic. This increase is related to the increase of the height of the central plateau, where gluons and sea quarks are supposed to be dominant. On the other hand large P_T inclusive cross sections increase very rapidly with energy, for instance at P_T = 10 GeV $E\frac{d\sigma}{d^3p}$ increases by orders of magnitude from ISR to collider [4] energies. It has also been observed, in calorimeter experiments [5], that the cross section to deposit

a large transverse energy is large and is built up by events involving large multiplicities. On a more theoretical ground L.V. Gribov et al [6] have shown that the cross section of the production of high P_T hadrons in the pionization region may be much larger than the one expected in commonly used parametrizations.

II. TOTAL CROSS SECTION OF VALONS [7] IN THE LEADING LOGARITHM APPROXIMATION

1) Valons and the additive quark model

In order to study hadronic total cross sections we have to proceed in two steps.

In a first step one extracts from the incoming hadrons the so called constituent quarks or valons by means of a non perturbative Q^2 independent distribution.

One then applies QCD to describe the interaction of these valons. This separation is necessary since QCD in the leading logarithm approximation in the axial or planar gauges applies only for inclusive distribution of partons inside a parton and not inside a hadron. On the other hand this two step procedure guarantees that one obtains the results of the so called additive quark model which are known to agree with data.

Let A and B be the incoming hadrons and $\dot{q}_A$ and $\dot{q}_B$ their valons. By constituent quarks or valons we mean valence quarks (or antiquarks in the case of an antiproton) accompanied by sea quarks and gluons, carrying the whole momentum of the incoming hadron and interacting independently.

Valons are characterized by their rest mass m_q (expected to be of the order of one third of the nucleon mass) and by a Q^2 independent probability distribution :

$$\psi_{A\to\dot{q}_A}(z)$$

which is constrained by

$$\int_o^1 \psi_{A\to\dot{q}_A}(z)\, dz = 3 \quad \text{for a proton or an antiproton} \qquad (1)$$

(conservation of the number of valence quarks ; note that we do not

distinguish u and d quarks) and by

$$\int_0^1 z\, \psi_{A\to\dot{q}_A}(z)\, dz = 1 \qquad (2)$$

(energy momentum conservation).

With the help of the ψ distributions we write the hadron total cross section in terms of the valon total cross section as :

$$\sigma_{AB}^{tot}(s) = \int_{\frac{2m_q}{\sqrt{s}}}^1 dz_a \int_{\frac{2m_q}{\sqrt{s}}}^1 dz_b\, \psi_{A\to\dot{q}_A}(z_a)\, \psi_{B\to\dot{q}_B}(z_b)\, \sigma_{\dot{q}_A\dot{q}_B}^{tot}(z_a z_b s) \qquad (3)$$

which simply expresses that valons interact independently.

In a first step we shall study the valon total cross section by means of QCD, afterwards we shall show that the hadronic total cross section is not very sensitive to the peculiar form of the ψ distributions.

2. One gluon exchange contribution to the valon cross section

High $P_\perp$ events in hadron-hadron collisions are reasonably well described by perturbative QCD [8]. At the parton level they correspond to the exchange of a gluon with large invariant squared mass or virtualness (of modulus $\hat{t}$) between quarks or gluons carrying a large fraction of the hadron longitudinal momenta. These events are characterized by a jet like structure.

But, let us consider the same one-gluon-exchange contribution without a large $P_\perp$ trigger. Now, gluon radiation due to the bremsstrahlung of the valons may be important. From the infrared properties of perturbative QCD, one expects a rather large accumulation of events corresponding to small relative longitudinal momenta and intermediate $\hat{t}$ values (say $\hat{t}$ of order of a few GeV^2) which contributes to the central plateau of hadronic multiplicity distributions. Experimental data on large transverse energy inclusive cross sections confirm this expectation [5].

The contribution to the valon total cross section from one gluon exchange between partons (see Fig.1) is obtained by summation over all

final state configurations. One obtains

$$\tilde{\sigma} \equiv \sigma^{tot}_{\dot{q}_A \dot{q}_B}(\tilde{s}) = \sum_{a,b} \iiint_{\Delta} d\hat{t}\, dx_a\, dx_b \frac{d\sigma}{d\hat{t}}(ab \to ab)\, \mathcal{D}^a_{\dot{q}_A}(x_a,\hat{t})\, \mathcal{D}^b_{\dot{q}_B}(x_b,\hat{t}) \quad (4)$$

The integration domain Δ will be discussed later on. $\tilde{s} = z_a z_b s$ (see Eq.3) is the c.m squared energy of the valon reaction, $\mathcal{D}^a_{\dot{q}_A}(x_a,\hat{t})$ (resp. $\mathcal{D}^b_{\dot{q}_B}(x_b,\hat{t})$) is the probability of finding parton a in valon $\dot{q}_A$ (resp. b in $\dot{q}_B$) with the fraction x_a (resp x_b) of the incident valon momentum, with a resolution scale $\hat{t}$, $\frac{d\sigma}{d\hat{t}}(ab \to ab)$[9] is the differential cross section in the one gluon exchange approximation

$$\frac{d\sigma}{d\hat{t}}(ab \to ab) = \frac{\pi}{2}\alpha_s(\hat{t}^2)\frac{1}{\hat{t}^2}\left\{\left[C_2\,\delta_{aq} + N_c\delta_{ag}\right]\left[C_2\,\delta_{bq} + N_c\,\delta_{bg}\right] + O\left(\frac{\hat{t}}{\hat{s}}\right)\right\} \quad (5)$$

The Kronecker δ symbols select the vertices with quarks or antiquarks (a,b=q) and gluons (a,b=g). $\hat{s} = x_a x_b \tilde{s}$ is the cm squared energy in the parton collision. As usual we define

$$\alpha_s(\hat{t}) = \frac{1}{b \log \frac{\hat{t}}{\Lambda^2}} \quad \text{with } b = \frac{11N_c - 2N_f}{12\pi}$$

$C_2 = \frac{N_c^2 - 1}{2N_c}$ where $N_c = 3$ is the number of colors and $N_f = 4$ the number of flavors. Λ is the usual QCD scale, which is set at .1 GeV according to the theoretical expectations of Ref.[10] and in agreement with the current world average [11]. Note that only elastic (but for color) differential cross sections appear in (Eq.4) because we have neglected parton reactions involving quark exchange. The summation over colors in the final state has been performed in Eq.5. In terms of hadrons, the processes which we study are obviously inelastic since they involve one gluon exchange. Our calculation thus applies to the total inelastic cross section.

3. The domain of integration Δ

We rely on the leading logarithm approximation (LLA) of QCD which has been extensively studied by Y.L. Dokshitzer, D.I. Dyakonov and S.I. Troyan[2] (hereafter denoted as DDT) to determine the domain of integration Δ in Eq.4 and the parton structure functions $\mathcal{D}^a_{\dot{q}_A}$ and $\mathcal{D}^b_{\dot{q}_B}$.

DDT have shown that, in a planar gauge, at the LLA the contributions which dominate the process of Fig.1 are the ones corresponding to tree

diagrams which, in the modulus squared of the amplitude give rise to generalized ladder diagrams (namely ladder diagrams with vertex and propagator renormalizations) (see Fig.2).

The kinematics for which the process depicted in Fig.2 is dominant is characterized by the strong ordering of the moduli of the transfers of momentum (as in heavy lepton pair production) [2]

$$\begin{aligned} m_q^2 &<< \ldots t_A^{i+1} << t_A^i << \ldots \hat{t} \\ m_q^2 &<< \ldots t_B^{i+1} << t_B^i << \ldots \hat{t} \end{aligned} \tag{6}$$

On the other hand the subsequent relative longitudinal momenta are also ordered. To establish this property which is of crucial importance for our purpose we have first to consider the cascading of a time like parton of virtualness $Q^2 > 0$ down to a valon (see Fig.3).

At step i we have

$$P_\perp^2 = t_i z_i (1-z_i) - t_{i+1}(1-z_i) - m^2 z_i \tag{7}$$

where z_i is the relative energy of parton i+1 with respect to parton i. Because of the strong ordering of the virtualness (see Eq.6), the condition that $P_\perp^2$ is positive, implies that

$$z_i > \frac{t_{i+1}}{t_i} \tag{8}$$

Repeating this reasoning step by step we obtain that z, the relative energy of the final valon is bounded by

$$z > \frac{m_q^2}{Q^2} \tag{9}$$

The process depicted in Fig.2 involves space like partons, but the Gribov Lipatov reciprocity relation [12] holds in the LLA and condition (9) provides us with a first constraint for the domain Δ :

$$x_a > \frac{m_q^2}{\hat{t}} \quad , \quad x_b > \frac{m_q^2}{\hat{t}} \tag{10}$$

the second one is given by

$$\hat{t} < \hat{s} = x_a x_b \tilde{s} \tag{11}$$

which reflects the kinematics of two body reactions at the parton level. The integration domain Δ is simpler in terms of rapidity like variables :

$$\begin{aligned} y_{a,b} &= \log \frac{1}{x_{a,b}} \\ \eta &= \log \frac{\hat{t}}{m_q^2} \\ \eta_s &= \log \frac{\tilde{s}}{m_q^2} \end{aligned} \tag{12}$$

$0 \leq \eta \leq \eta_s$; y_a, $y_b \in \Delta_y(\eta)$ where $\Delta_y(\eta)$ is defined as follows ; it turns out that in order to make Eq.10 and 11 compatible one has three cases as shown in Fig.4.

$$\text{i)} \quad 0 \leq \eta \leq \frac{\eta_s}{3} \quad (m_q^2 \leq \hat{t} \leq m_q^{4/3} \tilde{s}^{1/3}) \qquad \Delta_y = \{0 \leq y_{a,b} \leq \eta\}$$

$$\text{ii)} \quad \frac{\eta_s}{3} \leq \eta \leq \frac{\eta_s}{2} \quad (m_q^{4/3} \tilde{s}^{1/3} \leq \hat{t} \leq m_q \tilde{s}^{1/2}) \qquad \Delta_y = \{0 \leq y_{a,b} \leq \eta\} \cap \{y_a + y_b \leq \eta_s - \eta\} \tag{13}$$

$$\text{iii)} \quad \frac{\eta_s}{2} \leq \eta \leq \eta_s \quad (m_q \tilde{s}^{1/2} \leq \hat{t} \leq \tilde{s}) \qquad \Delta_y = \{y_a + y_b < \eta_s - \eta\}$$

4. Valon structure functions

It is well known that sea quark and gluon structure functions are more singular than x^{-1} near x=0, which leads to multiplicities which increase more than logarithmically with energy. This is due to an essential singularity in the moment space near j=1. DDT have shown that this effect reflects in the following small x behaviour of gluon and sea quark structure functions :

$$\begin{aligned} x\, \mathcal{D}_q^g(x,\hat{t}) &\propto I_1(v)/v \\ x\, \mathcal{D}_q^{q_S}(x,\hat{t}) &\propto I_2(v)/v^2 \end{aligned} \tag{14}$$

where $v = (16N_c \xi \log \frac{1}{x})^{1/2}$, I_1 and I_2 are the modified Bessel functions which behave for large v as $\frac{\exp(v)}{\sqrt{2\pi v}}$ and

$$\xi = \int_{\mu^2}^{\hat{t}} \frac{dQ^2}{Q^2} \frac{\alpha_s(Q^2)}{4\pi} = \frac{1}{4\pi b} \log \frac{\alpha_s(\mu^2)}{\alpha_s(\hat{t})}$$

$$= \frac{1}{4\pi b} \log \frac{\log \frac{\hat{t}}{\Lambda^2}}{\log \frac{\mu^2}{\Lambda^2}} \qquad (15)$$

The parameter μ controls the way how ξ and thus the gluon and sea quark multiplicities vary with $\hat{t}$. DDT have determined μ by demanding a realistic value for the fraction of momentum carried by gluons in a nucleon at $Q^2 \simeq 2.5$ GeV^2. They have obtained this way $\mu = .15$ GeV for $\Lambda = .1$ GeV. Now according to Eq.15 ξ vanishes at $\sqrt{\hat{t}} = \mu$, which is too small to be interpreted as the mass of the valon. Nevertheless for our quantitative calculations we have used the DDT parametrization with $\mu = .15$ GeV but we have allowed the mass of the valon (that is the scale at which ξ should vanish) to be different from μ by means of a slight modification of ξ, namely

$$\xi = \frac{1}{4\pi b} \log \frac{\log \frac{\hat{t}-m_q^2+\mu^2}{\Lambda^2}}{\log \frac{\mu^2}{\Lambda^2}} \qquad (16)$$

This ansatz does not affect at all the structure functions at the Q^2 values which are relevant for the rise of total cross sections ($\hat{t} \gg m_q^2 - \mu^2$).

The LLA applies for small values of x [13] provided that

$$1 \ll \log \frac{1}{x} \lesssim \log \frac{\hat{t}}{\Lambda^2} \qquad (17)$$

In our calculations $x_{a,b} > \frac{m_q^2}{\hat{t}}$ (region i) in Eq.13), and provided that $\frac{1}{\pi} \alpha_s(m_q^2)$ is small i.e. $\frac{m_q^2}{\Lambda^2} \gg 1$ Eq.(17) is satisfied and the LLA applies. As will be shown below $\frac{m_q^2}{\Lambda^2}$ turns out to be of order 10 which yields $\frac{1}{\pi} \alpha_s(m_q^2) \sim .2$.

5. Factorizable approximation

From Eq.(4), (5) and (14) we can discuss qualitatively the contributions of sea quarks and gluons in the valon total cross section. In Eq.(4) the parton differential cross section favors small values of $\hat{t}$ (see Eq.5). But, because of the domain of integration defined in (Eq.13) and because of the behaviour of structure functions near x=0 (see Eq.14) the parton multiplicities favor large values of $\hat{t}$. We thus expect that the maximum valon total cross section is obtained for intermediate $\hat{t}$.

From Eq.14 we see that the integrand in Eq.4 is maximum when both y_a and y_b are large. In region i) the integrals in y_a and y_b are factorized which simplified the calculations. By replacing regions ii) and iii) by the domain Δ'_y (see Fig.4)

$$\Delta'_y \left\{ y_{a,b} \leq \frac{\eta_s - \eta}{2} \right\} \tag{18}$$

we obtain the best factorizable approximation to the contribution of the integral in regions ii) and iii). In any case this factorizable approximation provides us with a lower bound for the effect we are studying.

6. Truncated multiplicites

Let us consider truncated parton multiplicities in valons, which are nothing but the parton multiplicities in valons obtained in the LLA, namely

$$n^p(\eta) = \begin{cases} \displaystyle\int_0^{\eta} \mathcal{D}_q^p(y,\eta)\,dy & \text{for } \eta \leq \frac{\eta_s}{3} \\ \displaystyle\int_0^{\frac{\eta_s - \eta}{2}} \mathcal{D}_q^p(y,\eta)\,dy & \text{for } \eta > \frac{\eta_s}{3} \end{cases} \tag{19}$$

where p = v for valence quark, S for sea quarks and g for gluons. These multiplicities are truncated because the y integrals are performed in the domain Δ'_y.

In terms of these truncated multiplicites, equation (4) becomes :

$$\tilde{\sigma} = \frac{\pi}{2m_q^2} \int_o^{\eta_s} d\eta \, [C_2(n^v(\eta) + n^S(\eta)) + N_c \, \eta^g(\eta)]^2 \, e^{-\eta} \, \frac{1}{b^2\left(\eta + \log \frac{m_q^2}{\Lambda^2}\right)^2} \quad (20)$$

For valence quark we have approximated the truncated multiplicity by the full multiplicity which is finite : $n^v(\eta) = 1$. For gluon and sea quarks the truncated multiplicities are obtained from Eq.14 and the normalization is fixed by means of the second moments. This yields to

$$n^g(\eta) = \lambda_g [I_o[(16N_c\xi\bar{\eta})^{1/2}]-1] \quad (21)$$

$$n^S(\eta) = \lambda_S \left[\frac{I_1[(16N_c\xi\bar{\eta})^{1/2}]}{(16N_c\xi\bar{\eta})^{1/2}} - \frac{1}{2}\right] \quad (22)$$

where

$$\bar{\eta} = \begin{cases} \eta & \eta \leq \frac{\eta_s}{3} \\ \frac{\eta_s - \eta}{2} & \eta > \frac{\eta_s}{3} \end{cases} \quad (23)$$

$$\lambda_g = \frac{4C_2 \exp[-4N_c\xi]}{4C_2+N_f} \quad \frac{1-\exp[-\frac{2}{3}(4C_2+N_f)\xi]}{1-\exp[-4N_c\xi]} \quad (24)$$

$$\lambda_S = \frac{8N_c\xi\left\{\frac{N_f}{4C_2+N_f} - \exp\left[-\frac{8}{3}C_2\xi\right] + \frac{4C_2}{4C_2+N_f}\exp\left[-\frac{2}{3}\xi[4C_2+N_f]\right]\right\}}{\exp[4N_c\xi] - 1 - 4N_c\xi} \quad (25)$$

It is possible now to understand qualitatively the origin of the rise of total cross sections. From the asymptotic behaviour of modified Bessel function one can evaluate the behaviour of the integrand in Eq.20 as a function of η. Neglecting the slow variation of ξ (which behaves like $\log \eta$) we obtain for the gluon-gluon contribution to the integrand

$$I_{gg} \sim e^{-\eta+2\sqrt{16N_c\xi\eta}} \quad \text{in region i, ie} \quad \eta \leq \frac{\eta_s}{3} \quad (26)$$

and

$$I_{gg} \sim e^{-\eta+2\sqrt{16N_c\xi(\frac{\eta_s-\eta}{2})}} \quad \text{in region ii and iii, ie} \quad \eta > \frac{\eta_s}{3} \tag{27}$$

It appears that mostly region i) contributes to the rise of total cross section because there exists a region in which the integrand is increasing, whereas the behaviour of the integrand in Eq.27 is continously decreasing. Indeed we rewrite Eq.26 as

$$I_{gg} \sim e^{-(\sqrt{\eta}-\sqrt{16N_c\xi})^2}$$

which is a gaussian centered at

$$\eta = 16N_c\xi \tag{28}$$

which corresponds to a very large value of η. With ξ, as defined in Eq.16, one can solve Eq.28. For $m_q^2 \sim .125\ GeV^2$ we find that the logarithmic derivative of the cross section is positive (increasing integrand in region i), for $\eta_s \lesssim 56$ i.e. $\tilde{s} \lesssim 10^{23}\ GeV^2$. We thus see that for the rise of the cross section the most important region is the upper end of region i), i.e. $\eta \simeq \frac{\eta_s}{3}$ ($\hat{t} \sim m_q^{4/3}\ \tilde{s}^{1/3}$). The approximations to calculate the contributions of region ii) and iii) are furthermore justified by the fact that the integrand is decreasing there.

III THE RISE OF THE NN TOTAL INELASTIC CROSS SECTION, A QUANTITATIVE ESTIMATE

To evaluate hadron cross sections from the knowledge of valon total cross sections one needs to know the non perturbative distributions $\psi_{A\to q_A}(z_a)$ and $\psi_{B\to q_B}(z_b)$ which appear in Eq.3, However the valon total cross section depends on z_a and z_b only through the upper bound in Eq.4 $\tilde{s} = z_a z_b s$, and it turns out that the valon total cross section is a slowly rising function of the energy. As a consequence the hadron total cross section does not depend very much on the specific form of the ψ distributions. Provided that these distributions obey the constraints 1) and 2), a good approximation of the nucleon-nucleon (or

nucleon antinucleon) cross section is given by

$$\sigma_{NN}(s) \simeq 9\, \sigma_{q\dot{q}}^{tot}\left(\frac{s}{9}\right) \tag{29}$$

which is nothing but the result obtained from the additive quark model using the quark kinematics.

We have performed a quantitative estimate of the QCD contributions to the nucleon-nucleon total inelastic cross section. We have used the approximations discussed both in section II (one gluon exchange approximation, factorization of the truncated multiplicities obtained in the LLA) and in Eq.29. The parameters are Λ, μ and m_q. Λ and μ have been fixed at 100 MeV and 150 MeV respectively in agreement with the current world average for Λ [11] and the DDT estimate for μ [2]. The only free parameter for our estimate is m_q, the mass of the valon. For the validity of the LLA one needs that $\frac{m_q^2}{\Lambda^2} >> 1$, and a reasonable expectation is that m_q is around one third of the nucleon-mass. Our quantitative estimate is shown in Fig.5. It is remarkable that with $m_q \sim 350$ MeV we obtain a rise of the cross section from ISR energy to the collider energy of about 15 mb, in agreement with data [14]. Surprisingly we even obtain a rough agreement (see Fig.6) with the absolute normalisation of the total inelastic cross section. To be more specific about the question of the rise of the cross section we have introduced a new scale Q_T^2 of the order of one GeV^2 which separates the soft region from the hard one in which perturbative QCD safely applies. In Eq.4 we cut the $d\hat{t}$ integral into two pieces

$$\int_{m_q^2}^{\tilde{s}} d\hat{t} = \int_{m_q^2}^{Q_T^2} d\hat{t} + \int_{Q_T^2}^{\tilde{s}} d\hat{t} \tag{30}$$

The first piece contributes a constant a part from a kinematical rise. Indeed as soon as $\frac{\eta_s}{3} > \mathrm{Log}\,\frac{Q_T^2}{m_q^2}$ i.e. $\tilde{s} \simeq \frac{s}{9} \gtrsim 20\, Q_T^2$, the contribution of the first piece in Eq.30 to the total cross section is energy independant. On the contrary the reasoning about the energy variation of the integrand displayed in section II applies for the second piece in Eq.30. So it is the hard region which is responsible for the rise of the cross

section. In Fig.6 we show the separation of σ_{NN}^{in} into two pieces according to Eq.30 for a few values of Q_T^2.

We find that for $Q_T^2 = 1.50\ (GeV)^2$ the constant contribution of the soft region is around 31 mb.

IV. DISCUSSION

We thus see that with the standard leading logarithm approximation, with a natural value for the only free parameter one is able to obtain not only the rise of the total inelastic cross section but also its absolute normalization. To discuss this result we try in this concluding section to answer three questions about the theoretical meaning of our calculation.

i) Does this model for the cross section obey the Froissart bound ? We have already discussed in section II the asymptotic behaviour of the integrand in Eq.20. From this discussion it turns out that at ultra asymptotic energies, the integrand (see Eq.26) begin to decrease, which means that the cross section finally flattens out. For instance we reach the value of 1 barn at about 10^{30} GeV^2 (see Fig.7). It thus appears that s-channel unitarity is not violated although it has not been taken into account explicitly.

ii) How hard are the parton processes responsible for the rise of the total cross sections ? To answer this question we have computed the average value of $\hat{t}$, (see Fig.8). $<\hat{t}>$ is the average squared transverse momentum of partons.

From Fig.8 we notice at first that the average value of $\hat{t}$ is indeed rather moderate and slowly varying with respect to s. The asymptotic law of variation is, as expected proportional to $s^{1/3}$ corresponding to the maximum of the integrand (see Eq.26). Note that this asymptotic form is valid only above $\sqrt{s} \sim 100$ GeV $\hat{t} \sim .04\ s^{1/3}$.

At the collider energy we find for $<\hat{t}>$ about 3 GeV^2. Assuming 2 or 3 hadrons per parton this value is not incompatible with the average transverse momentum of hadron which has been measured ($<P_\perp> \sim 500$ MeV). Which means that the main bulk of inelastic events can be described by

means of our model.

iii) How the proposed model compare with theoretical expectations based on Pomeron calculus ? To answer this question we rely on the scheme of correspondence between QCD and dual Pomeron calculus developped in Ref.[15]. According to this approach there exists a transition scale at which the leading logarithm approximation of QCD and the dual topological unitarization (DTU) scheme can be applied simultaneously. This transition scale of a few GeV^2 corresponds to the so called preconfinement transition. If we interpret Q_T^2 as this transition scale the soft component would be associated with the contribution of the "bare Pomeron" (lowest topology in DTU) and the hard component would be associated with the sum of all multipomeron corrections to this "bare Pomeron".

In view of this discussion we conclude that perturbative QCD, at the leading logarithm approximation may provide a quantitative theoretical description of the main bulk of inelastic cross sections at high energy. Indeed further tests are needed to draw a more affirmative conclusion.

A first test would be to describe, by means of our dynamical model, the inclusive cross section to produce one hadron at large $P_\perp$. It is well known that, for not too large trigger transverse momentum, it is necessary to take into account the effect of gluon bremsstrahlung. In this respect, it is interesting to note that the recent calculations [4], which take into account these bremsstrahlung effects, lead to a very decent agreement with ISR and collider data down to $P_\perp \sim 1$ GeV/c.

The best test would be to apply our model to the description of large transverse energy cross section. We are currently investigating this extension of our model.

One of us A.M. would like to thank the kind hospitality enjoyed at Saclay to complete this work. We acknowledge R. Lacaze for a careful reading of the manuscript and S. Pokorski, A. Capella and Tran Thanh Van for interesting discussions.

REFERENCES

[1] See for instance P. Renton Rapporteur's talk, Proceedings of the XIII International symposium on multiparticle dynamics (82)

[2] Yu. L. Dokshitzer, D.I. Dyakonov and S.I. Troyan, Physics Reports 58, 270 (1980)

[3] A. Basseto, M. Ciafaloni, G. Marchesini, NP B163, 477 (1980)

[4] G. Arnison et al, UA1 Collaboration Preprints CERN EP/82-120 and CERN EP/82-125

[5] A. Clark, UA2 Collaboration ; A. Norton, UA1 Collaboration presented to the XXI International Conference on High Energy Physics Paris (1982)

[6] L.V. Gribov, E.M. Levin and M.G. Ryskin, Phys. Lett. 100B, 173 (1981)

[7] R.C. Hwa, Proceedings of the Europhysics study conference Erice (Italy) 1981 Edited by RT Van de Walle

[8] D. Sivers, R. Blankenbecler and S. Brodsky, Phys. Rep. 23C (1976)

[9] R.P. Feynman, R.D. Field and G.C. Fox, Phys. Rev. D18, 3320 (1978)

[10] M.A. Shifman, A.I. Vainshtein and V.I. Zakharov, Nucl. Phys. B147, 385, 448, 519 (1979)

[11] F. Eisele Rapporteur's talk Proceedings of the XXI International Conference on High Energy Physics Paris (1982)

[12] V.N. Gribov, L.N. Lipatov, Sov. J. Phys. 15, 438 and 675 (1972)

[13] Yu. L. Dokshitzer, JETP 46, 641 (1977)

[14] M. Haguenauer, UA4 Collaboration presented to the XXI International Conference on High Energy Physics Paris (1982)

[15] M. Bishari, G. Cohen-Tannoudji, H. Navelet and R. Peschanski, Z. Phys. C Particles and Fields 14, 7 and 197 (1982)

FIGURE CAPTIONS

Fig.1 : Valon Valon total cross section ; $\hat{t}$ is the virtualness of the gluon exchanged between parton a and b.

Fig.2 : Dominant contributions of valon-valon cross section in the planar gauge at the LLA.
2a Typical tree diagram in the amplitude
2b Typical generalized ladder diagram in the cross section.

Fig.3 : Cascading of a time like virtual partons.

Fig.4 : The integration domain Δy (shaded area). Dotted lines are the limit of the domain leading to the factorizable approximation.

Fig.5 : $\frac{\Delta\sigma}{\Delta \ell n\ s}$ the solid line is our prediction for m_q = 350 MeV
Data are from UA4 [14].

Fig.6 : The N-N total inelastic cross section as a function of energy. In dotted line, the constant contribution corresponding to 2 different value of Q_T^2. Data are from UA4 [14].

Fig.7 : Behaviour of the total inelastic cross section at ultra asymptotic energies.

Fig.8 : Average value of the maximum virtualness of the exchanged gluon. The solid curve represents our calculation, and the dots the $s^{1/3}$ behaviour predicted asymptotically by the model.

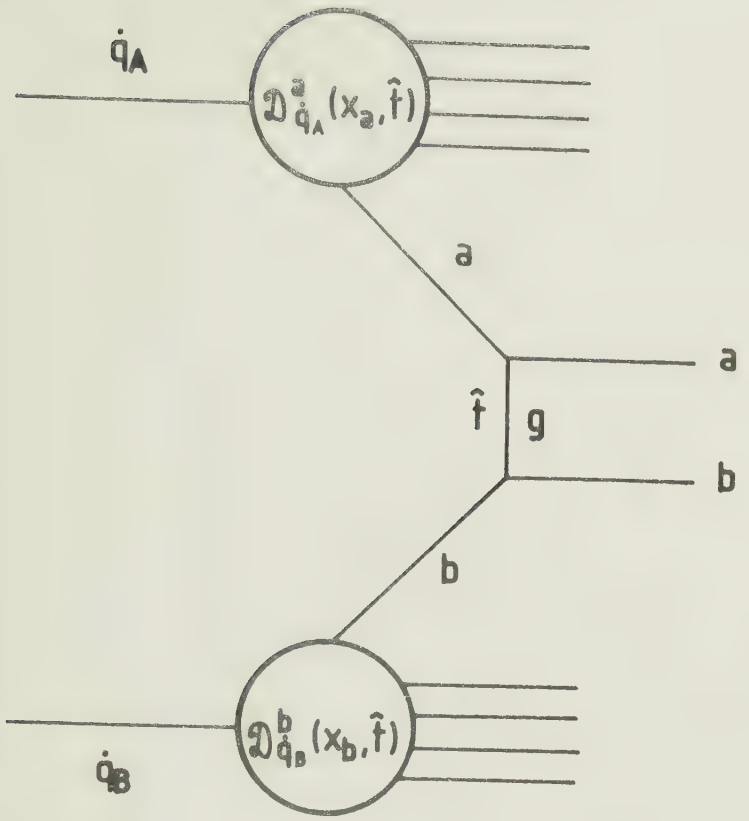
$\dot{q}_A$
$\mathcal{D}^a_{\dot{q}_A}(x_a,\hat{t})$
a
a
$\hat{t}$
g
b
b
$\mathcal{D}^b_{\dot{q}_B}(x_b,\hat{t})$
$\dot{q}_B$

FIG. 1

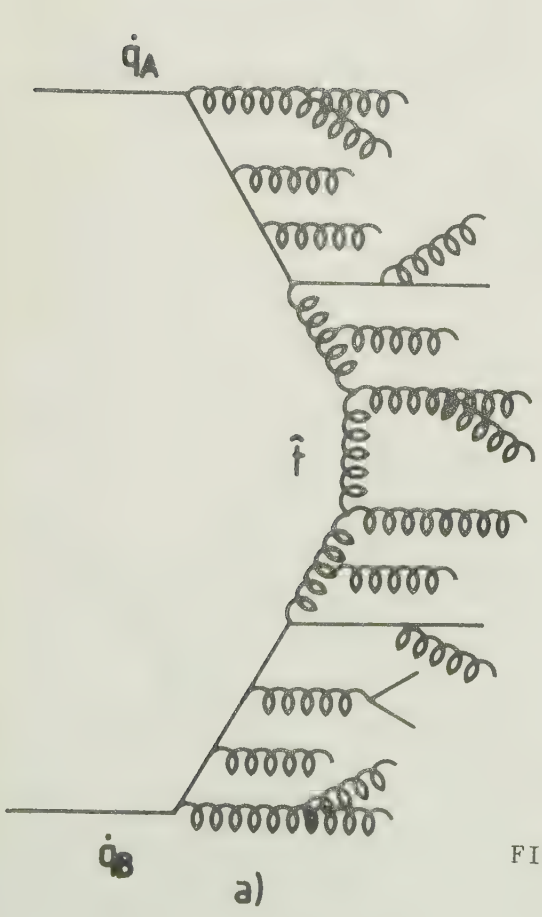
$\dot{q}_A$
$\hat{t}$
$\dot{q}_B$
a)

FIG. 2

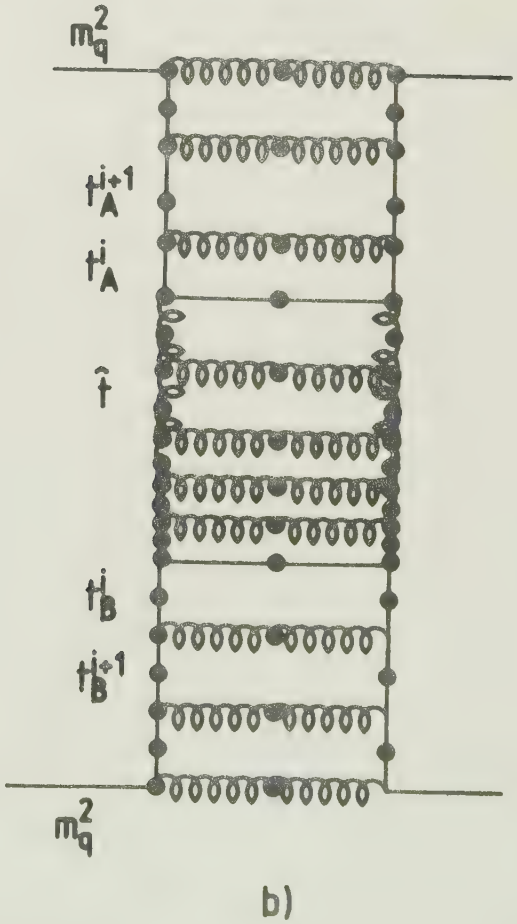
m_q^2
t_A^{i+1}
t_A^i
$\hat{t}$
t_B^i
t_B^{i+1}
m_q^2
b)

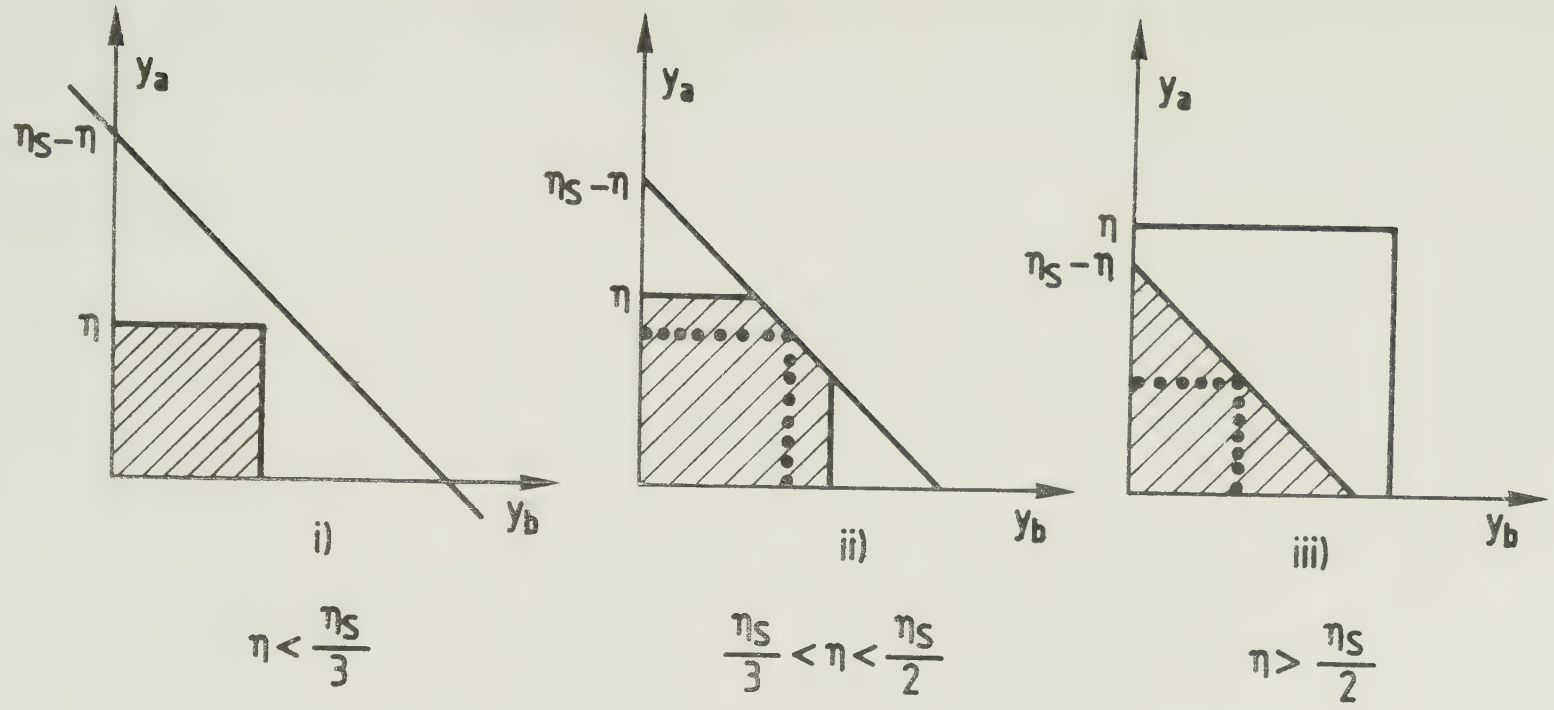
y_a
$\eta_S - \eta$
η
y_b
i)
$\eta < \frac{\eta_S}{3}$
y_a
$\eta_S - \eta$
η
y_b
ii)
$\frac{\eta_S}{3} < \eta < \frac{\eta_S}{2}$
y_a
η
$\eta_S - \eta$
y_b
iii)
$\eta > \frac{\eta_S}{2}$

FIG.3

Q^2
i
i+1
m^2

FIG.4

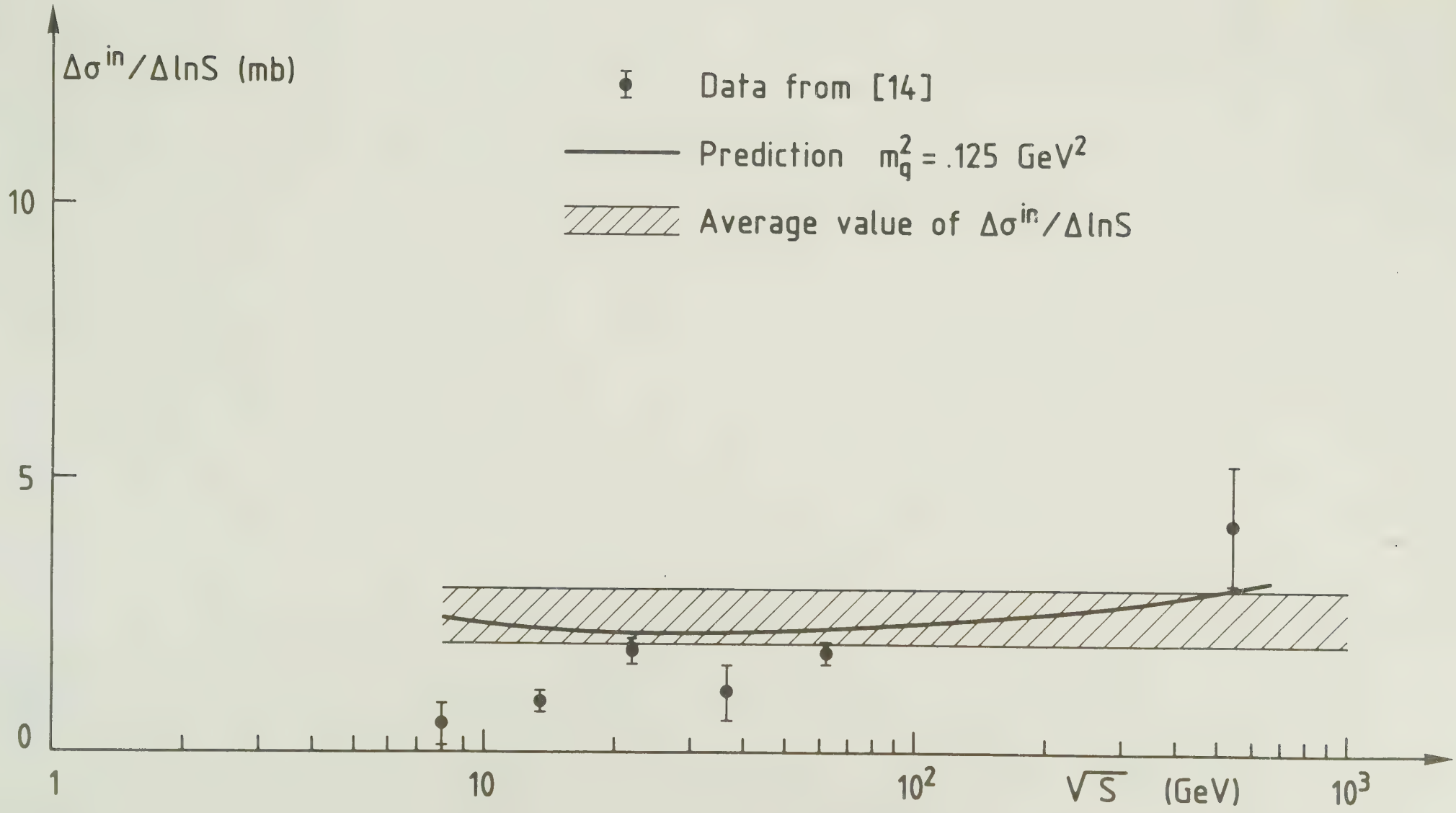
$\Delta\sigma^{in}/\Delta\ln S$ (mb)
Data from [14]
Prediction $m_q^2 = .125$ GeV^2
Average value of $\Delta\sigma^{in}/\Delta\ln S$
10
5
0
1
10
10^2
$\sqrt{S}$ (GeV)
10^3

FIG.5

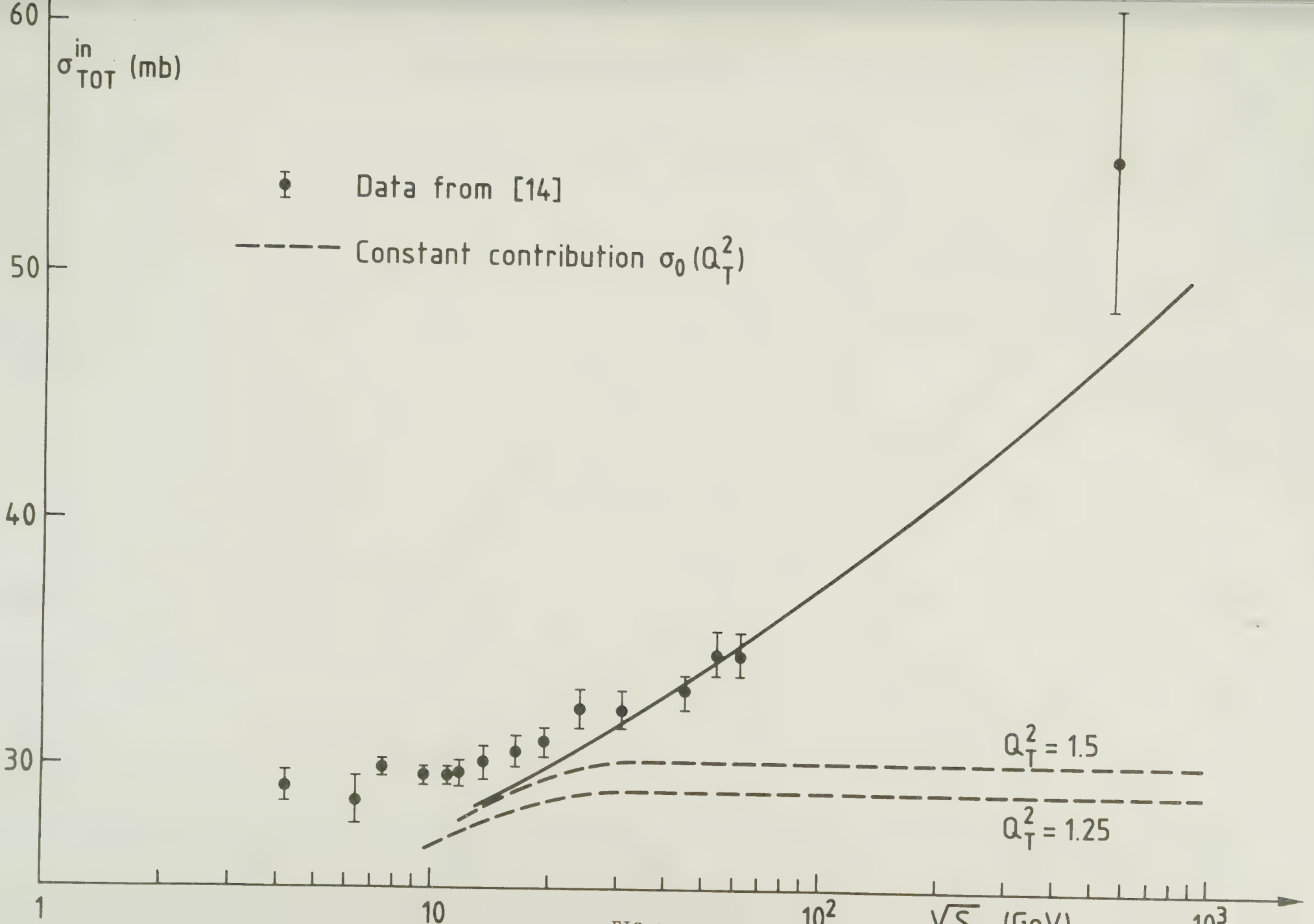
60
50
40
30
σ^{in}_{TOT} (mb)
Data from [14]
Constant contribution $\sigma_0(Q_T^2)$
$Q_T^2 = 1.5$
$Q_T^2 = 1.25$
1
10
10^2
10^3
$\sqrt{s}$ (GeV)

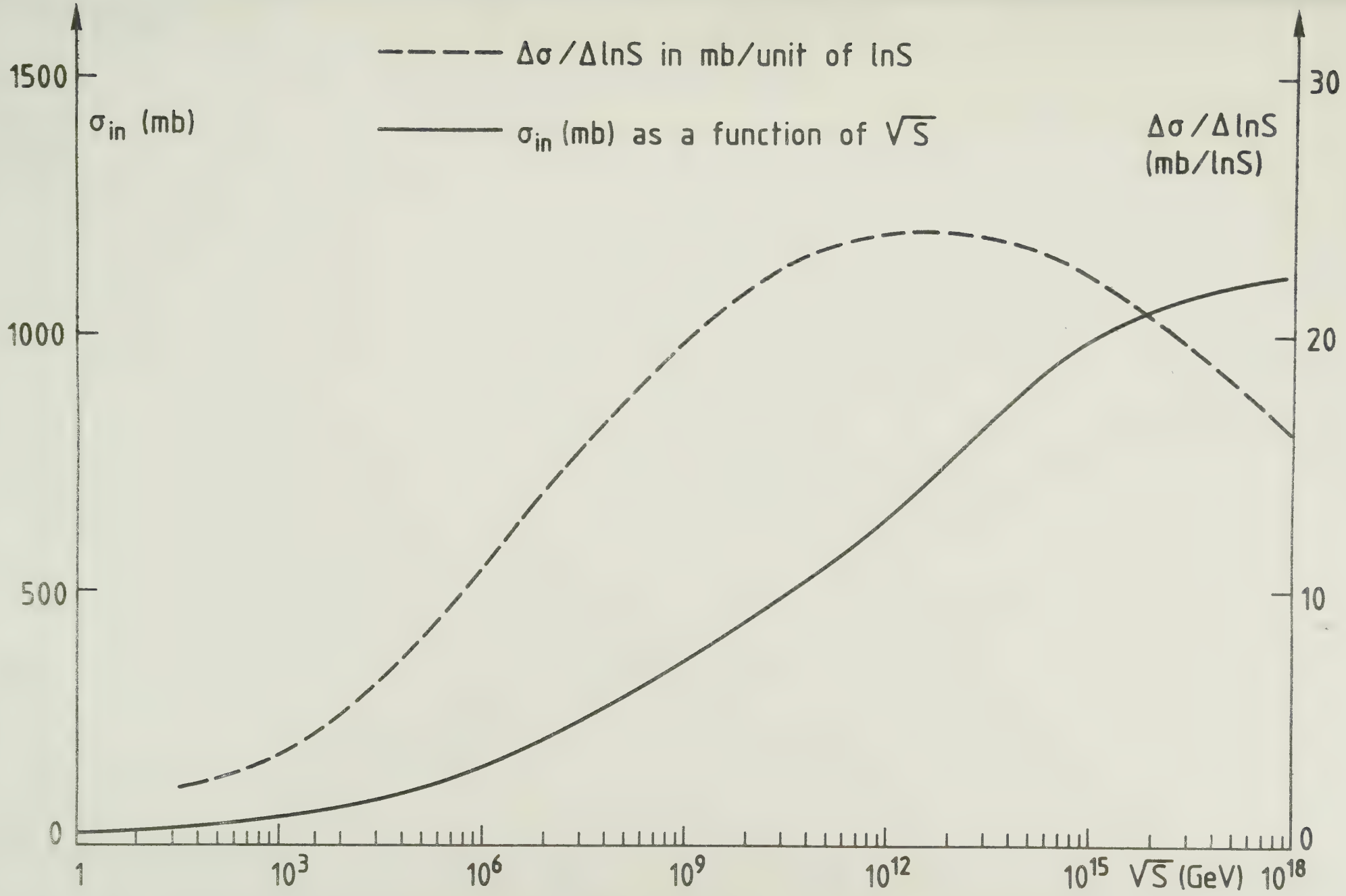
Δσ/ΔlnS in mb/unit of lnS
σin (mb) as a function of √S
σin (mb)
Δσ/ΔlnS (mb/lnS)
1500
1000
500
0
30
20
10
0
1
10^3
10^6
10^9
10^12
10^15
√S (GeV)
10^18

FIG.7

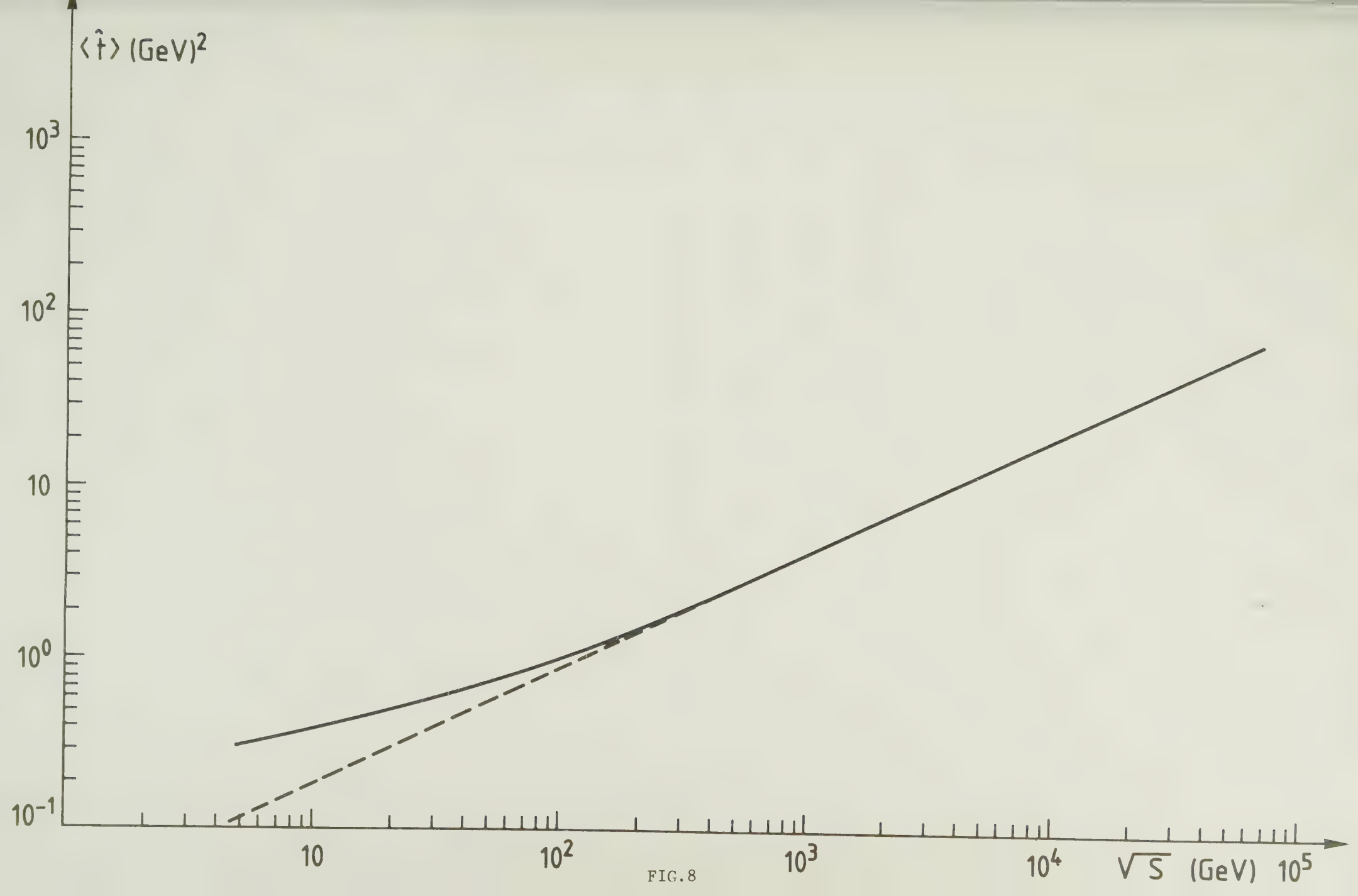
$\langle \hat{t} \rangle$ (GeV)^2
10^3
10^2
10
10^0
10^{-1}
10
10^2
10^3
10^4
$\sqrt{s}$ (GeV)
10^5

FIG.8

C H A P I T R E III

III QCD à l'approximation des logarithmes dominants et le modèle dual des partons.

III. 1. le préconfinement

III. 2. Confinement et développement topologique

III. 3. DTU et le modèle dual des partons

CHAPITRE III

III. 1. Le préconfinement.

Dans la réaction d'annihilation e^+e^- en hadrons, on sait que les graphes dominants à l'ALD, dans une jauge axiale, sont les graphes en arbres ordonnés, dans lesquels un quark de virtualité maximum Q, perd cette virtualité par l'émission successive de gluons et de paires $q\bar{q}$, presque colinéaires jusqu'à une virtualité minimum Q_T. (voir figure 1).

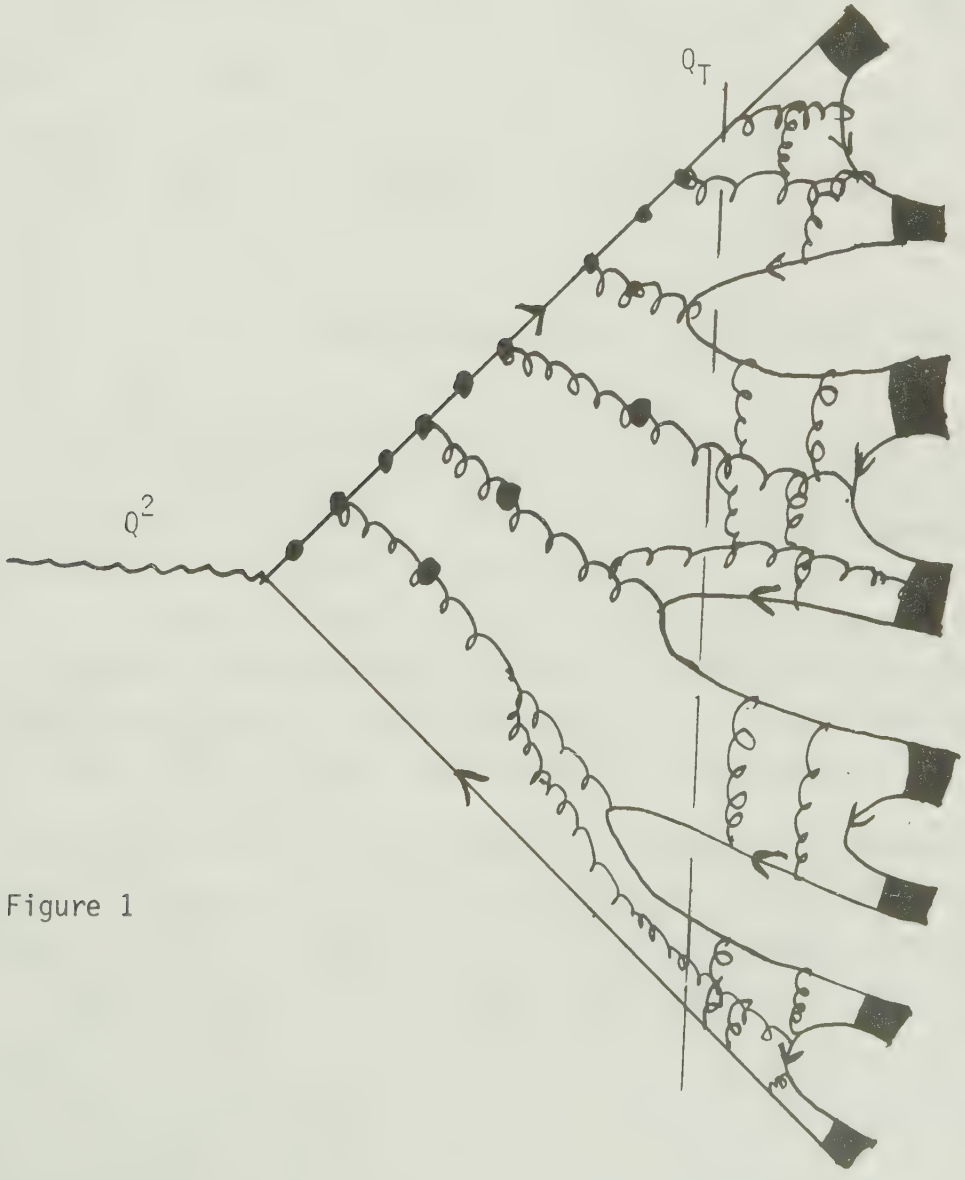

Figure 1

Si on regroupe les quanta produits dans cette cascade, en amas singulets de couleur de masse μ, on constate que le spectre de masse de ces amas est piqué au voisinage [1] de la virtualité minimum :

$$\frac{d\sigma}{d\mu} \alpha \left(\frac{\mu}{Q_T}\right)^{-\lambda}$$

où la puissance λ est indépendante de la virtualité initiale Q. Q_T apparait donc comme une virtualité de transition, appelée transition de préconfinement : les amas singulets de couleur de masse moyenne égale à Q_T peuvent être interprétés comme de véritables "pré-hadrons" dont l'évolution est gouvernée par QCD dans la région des couplages forts. La propriété de préconfinement est compatible avec l'hypothèse (que l'on doit toujours faire lorsque l'on utilise QCD) que les effets de confinement n'interfèrent pas avec les effets à petite distance : dans le cas présent, il s'agit de l'indépendance de λ par rapport à la virtualité initiale Q.

III. 2. Confinement et développement topologique.

A partir du préconfinement les effets des boucles deviennent importants et donc la topologie devient importante pour caractériser les diagrammes dominants. (La topologie n'a aucun intéret pour les diagrammes en arbres). Or le préconfinement "prépare", les préhadrons dans une topologie planaire (voir fig. 1).'t Hooft a proposé de réarranger le développement de QCD en un développement topologique permettant de formuler une conjecture précise à propos du confinement : il s'agit d'un développement en puissance[2] de $\frac{1}{N_c}$ (g^2N_c fixé) ou N_c est le nombre de couleurs,où chaque terme est caractérisé par ses propriétés topologiques (nombre de boucles internes de quarks, nombre de frontières, nombre de poignées). La conjecture de 't Hooft consiste à supposer que le confinement est déjà présent au niveau du terme

d'ordre le plus bas, c'est à dire le terme planaire, et qu'il n'est pas détruit par les corrections topologiques d'ordre plus élevé.

Selon cette conjecture QCD à la limite N_c grand, g^2N_c fixé tend vers une théorie dans laquelle les champs fondamentaux sont des hadrons singulets de couleurs, et cette théorie est complètement équivalente à QCD. A cause des propriétés de topologie on s'attend à ce que cette théorie de hadrons, équivalente à QCD, soit une théorie de cordes duales (c'est d'ailleurs ce qui a été démontré à deux dimensions).

III. 3. Le modèle dual des partons.

Le modèle dual des partons s'appuie sur la conjecture de 't Hooft et utilise l'unitarization topologique duale (DTU) (développement en puissance de $\frac{1}{N_f}$ à grand nombre de saveurs N_f, g^2N_f fixé)[3] pour tenter d'unitariser la théorie duale de corde supposée équivalente à QCD. Toutes les contraintes non linéaires sont concentrées au niveau planaire et les topologies supérieures sont calculables par des equations linéaires. L'interprétation partonique des topologies les plus basses de DTU est expliquée dans la ref. (4) pour les fonctions de fragmentation et dans la ref. (5) pour les fonctions de structure

En interprétant les fonctions de structure du modèle dual des partons comme les fonctions de structure à la transition du préconfinement et en utilisant les équations d'évolution de QCD au voisinage de cette transition nous avons élaboré une paramétrisation des fonctions de structure à tout x et tout Q^2. La dérivation de ce modèle et sa comparaison avec les données expérimentales est montrée dans les références (6) et (7).

REFERENCES

(1) D. Amati et G. Veneziano, Phys. Lett. 83B (1979) 87.

(2) G't Hooft, Nucl. Phys. B 72 (1974) 461.

(3) G. Veneziano, Phys. Lett. 52 B (1974) 220 ; Nucl. Phys. B 74 (1974) 365.

(4) A. El Hassouni, A. Mantrach, E.G. Oudrhiri-Safiani, Particles and Fields C9 (1981) 185.

(5) G. Cohen-Tannoudji, A. El Hassouni, J. Kalinowski and R. Peschanski Phys. Rev. D19 (1979) 3397.
G. Cohen-Tannoudji, A. El Hassouni, J. Kalinowski, O. Napoly and R. Peschanski, Phys. Rev. D21 (1980) 2699.
A. El Hassouni and O. Napoly, Phys. Rev. D23 (1981) 19.

(6) G. Cohen-Tannoudji, A. El Hassouni, A. Mantrach, E. G. Oudrhiri-Safiani, Particles and Fields C13 (1982) 219.

(7) G. Cohen-Tannoudji, A. Mantrach, E. G. Oudrhiri-Safiani, Particles and Fields C14 (1982) 171.

Z. Phys. C – Particles and Fields 9, 185–195 (1981)

Zeitschrift für Physik C Particles and Fields
© Springer-Verlag 1981

Dual Model for u, d, s, and c Quark Fragmentation Functions

A. El Hassouni[1]

D. PH. T., C.E.N. de Saclay – Orme des Merisiers, BP n° 2, F-91190 Gif-sur-Yvette, France

A. Mantrach[1]

L.P.T.H.E., Université de Paris-Sud Orsay, Laboratoire associé au C.N.R.S., Bâtiment 211, F-91405 Orsay, France

E. G. Oudrhiri-Safiani[1]

L.P.T.H.E., Université de Paris VII Tour 33, Laboratoiré associé au CNRS LA 280, 1er étage, 2, place Jussieu, F-75261 Paris Cedex 05, France

Received 5 February 1981

Abstract. In the dual topological unitarization scheme, we derive a model for the u, d, and s quark fragmentation into mesons by considering the parton interpretation of planar one particle inclusive cross sections. A good agreement with experiment is obtained. Relying on these results, we generalize the model in order to include the charm fragmentation functions into any meson and again get a nice agreement with data.

I. Introduction

It is well known that in hadron-hadron collisions the interaction extends over a region of space characterized by the Radius R of the hadrons (soft interactions), in contrast with e^+e^- annihilation, deep-inelastic, Drell-Yan and large $p_\perp$ processes where the interaction is point like (hard-scattering). However, the fact that in the two situations the mechanism of formation of the intermediate states is different, does not necessarily imply that hadron production is different or that the two distributions of final states cannot be related. In fact, several experiments [1] on hadron-hadron interactions mesuring physical observables of hard processes have exhibited many striking similarities, which may reflect a deep connection between the two a priori different situations.

At the level of a theory of hadronic physics, there are two main approaches, namely the S-matrix scheme known as the Dual Topological Unitarization [2] (DTU) and the popular Quantum Chromodynamics (QCD). The predictive power of each of these two approaches are restricted to their own applicability domains, which are limited and distinct. For instance, whereas for QCD perturbative field theory techniques can be applied to large transfer momentum processes (thanks to the factorization property of the long distance effects [3]), DTU provides one with a quantitative description of low $p_\perp$ physics where perturbative QCD do not apply. So, although they are distinct, the two domains are complementary. The authors of [4] have looked for connections between the two approaches, by means of the common features of their topological properties. They use the general result that the quark lines of duality diagrams can be interpreted as the quarks of a workable and predictive quark-parton model for soft hadronic reactions. They were led to establish the rules for this interpretation, which they call topological correspondence.

This topological correspondence was used in [5], for a complete study of the probability for finding a parton inside a hadron [the structure function $G(x)$]. In this paper, we focus on the probability for finding a hadron (we shall restrict ourselves to the meson sector) inside a jet of quark, i.e. the quark fragmentation function $D(Z)$ [6]. Altogether, these results ([5] and this paper) on scale invariant parton densities can be considered as providing an input, containing the non-perturbative long distance effects, for the Altarelli-Parisi Eqs. [7] which only reflect the balance of the parton fluxes [8] as they evoluate according to perturbative QCD.

In Sect. II, we recall the results of the topological correspondence for the planar one particle inclusive cross section, which fixe the behaviour near $Z=1$ of the fragmentation functions. We also give the normalization of these functions by means of an analogue of the Gribov-Lipatov relation [9] in the hadron sector and using the so-called f-dominance of the pomeron.

1 On leave of absence from the Laboratoire de Physique Théorique, Faculté des Sciences de Rabat, Av. Ibn Battota, BP n° 1014, Rabat, Maroc

0170-9739/81/0009/0185/$02.20

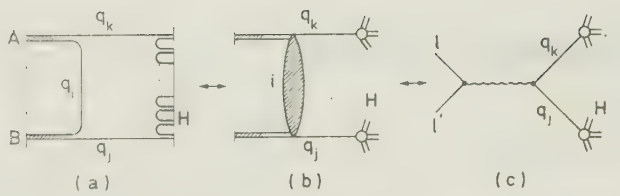

Fig. 1. Topological correspondence between one particle inclusive planar cross sections and $e^+e^-\to H+X$: **a)** The dual diagram; **b)** The parton interpretation of (a); **c)** The hard process giving rise to the same final distribution as **(b)**

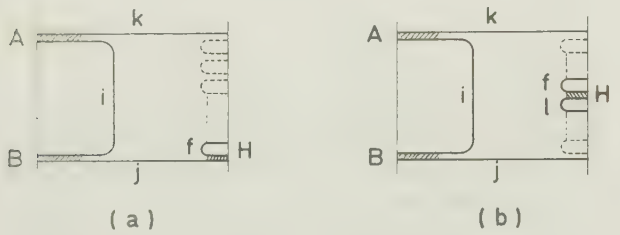

Fig. 2. The dual diagrams contributing to **a)** The direct fragmentation, H contains the quark j; **b)** The indirect fragmentation, H does not contain the quark j

In Sect. III, after a discussion on the nature of the mesons produced (pseudoscalars and vectors) and of the quarks involved (u, d, and s), we compute the effects of vector resonance decays into pseudoscalars. Next, applying quantum number sum rules for the various distributions introduced in Sects. II and III, we determine (Sect. IV), the behaviour near $Z=0$ of the direct part of fragmentation and, in the absence of experimental data, we compare our results on the differential charge distributions versus Z with those of Feynman-Field (FF) [10]. A good agreement is obtained. Finally, the absolute normalization of the complete fragmentation function is fixed by means of energy-momentum conservation. A comparison with experiments is given.

In Sect. V, relying on the previous encouraging results, we make the extension of our method to predict the charm fragmentation functions. Section VI is devoted to conclusions and outlooks.

II. Direct and Indirect Fragmentations

One of the quantitative consequences of the topological correspondence is that the quark fragmentation functions can be obtained through a parton interpretation of the one particle inclusive *planar* cross sections. In order to recall this point, we consider the process $A+B\to H+X$ where H lies in the fragmentation region of the incoming particle B. The planar part of this process is interpreted in two steps. The first one is a two-to-two process $A+B\to q_j+q_k$ at $t=0$, corresponding to the exchange of a wee valence quark. The second one consists in a hadronization process of the planar configuration of the partons q_j and q_k, expressed in terms of the usual quark fragmentation functions, as given by $e^+e^-\to q\bar{q}\to H+X$. With the notations of Fig. 1, one writes:

$$\varrho^{pl}(Z)=\frac{1}{\sigma^{pl}_{AB}(S)}\sum_{\vec{A}}\frac{d\sigma}{dZ}(B\to H)=ZD_{q_j\to H}(Z) \tag{1}$$

where Z is the longitudinal fraction carried by H of the momentum of B: $Z=P''_H/P_B$ and $\sigma^{pl}_{AB}(S)$ is the total planar cross section, given by:

$$\sigma^{pl}_{AB}(S)=g^2S^{\alpha_{ii}(0)-1}. \tag{2}$$

In terms of dual diagrams, and to the lowest order of DTU, there are two diagrams contributing to $\varrho^{pl}_{AB\to H}(Z)$, corresponding respectively to the cases where the particle H produced contains (Fig. 2a) or does not contain (Fig. 2b) the initial quark q_j. We shall refer to them as the direct and the indirect fragmentations respectively.

According to Mueller-Regge [11] analysis, the contributions of these diagrams are obtained by taking the discontinuity of the $3\to3$ forward amplitudes represented by the dual diagrams of Fig. 2. The triple Regge limit $\left(Z\simeq1,\frac{M^2}{S}\right)$ fixed yields their behaviour near $Z=1$, and within the so-called one dimensional bootstrap approximation [12], the results obtained in [5] are given by:

$$ZD^{\mathrm{dir}}_{q_j\to H}(Z)\underset{Z\alpha1}{\propto}(1-Z)^{\alpha_{ii}-2\bar{\alpha}_{if}},\quad\text{with}\quad H=(q_fq_f) \tag{3}$$

$$ZD^{\mathrm{ind}}_{q_j\to H}(Z)\underset{Z\alpha1}{\propto}(1-Z)^{\alpha_{ii}-2\bar{\alpha}^c_{if\,\bullet\,jl}}\quad\text{with}\quad H=(q_lq_f) \tag{4}$$

In these equations, $\bar{\alpha}$ and $\bar{\alpha}^c$ are averaged values respectively of the Regge pole and of the Regge cut, $\alpha(t)$ and $\alpha^c(t)$ trajectories. In Ref. [5], in addition to these behaviours near $Z=1$ for the direct and indirect fragmentation functions, a complete determination of the structure functions, based on the same DTU scheme has been given, leading to a reasonable agreement with experiments [13]. Let us now proceed to determine the fragmentation functions in a similar way. The method we use consists in calculating the behaviours near $Z=0$ and $Z=1$ and considering that the quark fragmentation functions are given by the product of the two behaviours appropriately normalized.

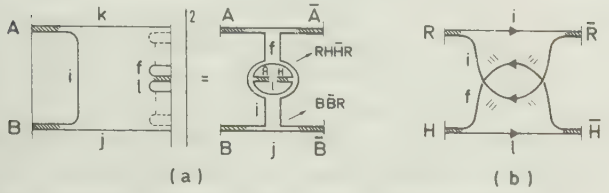

Fig. 3. The dual diagram for the indirect fragmentation: **a)** The two couplings which determine the normalization; **b)** The coupling $RH\bar{H}\bar{R}$ in the crossed channel

2.1. The Direct Fragmentation

The double Regge limit of a six point function represented by a given 3 to 3 duality diagram allows one to get the behaviour near $Z=0$ of the corresponding parton density. For the case of the quark fragmentation function, the double Regge limit of Fig. 2a is complicated, because one of the exchanged regg is not a simple Regge pole [14]. For this reason, we postpone the determination of the power behaviour $D^{\text{dir}}(Z)\simeq Z^n$ near $Z=0$ to a later section of this paper, where use will be made of sum rules given by quantum number conservation.

For structure functions, the momentum rule:

$$\int_0^1 G^{\text{val}}_{B\to q}(X)\,dX=1 \quad . \tag{5}$$

determines the absolute normalization of $G^{\text{val}}_{B\to q}(X)$, once its dependence on X is known. This way of fixing the normalization can be extended to the functions $D(Z)$. At the level of the triple Regge limit (of Fig. 3a of Ref. [5] and of Fig. 2a), we have established that the fragmentation function of a parton into a hadron behaves in the limit $Z\simeq 1$ exactly like the structure function of a hadron into a parton. Furthermore, all the coupling constants involved into the two cases are strictly identicals. Therefore, we assume that the dominant parts of the fragmentation function (the direct one) and of the structure function (the valence one) not only have the same behaviour near $X=1$ given by triple Regge limit, but also the same absolute normalization up to the usual factor of color 1/3 [15]. This argument suggests that the perturbative relation of Gribov-Lipatov [9], established at the LLA level may be extended to the hadronic sector. Then we write:

$$D^{\text{dir}}_{q_j\to H}(Z)=\frac{Z^{n_{jf}}(1-Z)^{1.5-\alpha_f}}{3\,B(1-\alpha_j,\,2.5-\alpha_f)}, \quad \text{with} \quad H=(q_jq_f) \tag{6}$$

This equation makes use of the result obtained in Ref. [5] within the one dimensional bootstrap model of Kwiecinski and Sakai [12], namely

$$\begin{aligned} &\alpha_{ii}-2\bar{\alpha}_{if}=1.5-\alpha_f \qquad \text{(a)} \\ &\alpha_{if}-\bar{\alpha}_{if}\ =0.75 \qquad\quad \text{(b)} \end{aligned} \tag{7}$$

2.2. The Indirect Fragmentation

In the same way as in the direct case the bootstrap calculations give the relation:

$$\alpha^c_{if\,\cdot\,jl}=\bar{\alpha}_{if}+\bar{\alpha}_{jl}-1$$

which implies:

$$\alpha_{ii}-2\bar{\alpha}^c_{if\,\cdot\,jl}=2(\alpha^c-\bar{\alpha}^c)+4(\alpha-\bar{\alpha})+2-\alpha_j-\alpha_l-\alpha_f \tag{8}$$

The slope of the Regge-Regge cut trajectory is known to be about a half of the normal Regge trajectory one. We expect that the shift $(\alpha^c-\bar{\alpha}^c)$ is also a half of the shift $(\alpha-\bar{\alpha})$ estimated to be of order 0.75 in the bootstrap model. We then obtain:

$$\alpha_{ii}-2\bar{\alpha}^c_{if\,\cdot\,jl}=5.75-\alpha_j-\alpha_l-\alpha_f\,. \tag{9}$$

The behaviour near $Z=0$ is simply given by the fact that there is a pomeron in the channel $B\bar{H}$, or that there exists no quark common to B and H, which leads to:

$$D^{\text{ind}}(Z)\underset{Z\alpha 0}{\propto}\frac{1}{Z}. \tag{10}$$

This means that the fragmentation function develop the plateau in rapidity observed experimentaly [16].

The height of the plateau depends on the absolute normalization of the indirect quark fragmentation function.

Thanks to the factorization property of the residues, the normalization is given by the product of the two couplings $(BR\bar{B})$ and $(\bar{R}H\bar{H}R)$. The first coupling does not depend on the auxiliary quark exchanged between the incident particles A and B. The second one, as can be seen by considering the t-channel of the subprocess $R+H\to X$ (see Fig. 3), can be written through the f-dominance property of the pomeron as:

$$(RH\bar{H}\bar{R})=\left(\frac{1}{1-\alpha_f}+\frac{1}{1-\alpha_l}\right)\lambda \tag{11}$$

The proportionality factor λ, which is universal (independent of f and l), can be included into the first coupling according to:

$$(BR\bar{B})\lambda=N_j \tag{12}$$

where N_j is a constant depending only on the initial quark, and to be determined. We shall come back to this factor N_j in Sect. IV. Combining the above results, we write:

$$D^{\text{ind}}_{q_j\to H}(Z)=N_j\left(\frac{1}{1-\alpha_f}+\frac{1}{1-\alpha_l}\right)\frac{1}{Z}\,(1-Z)^{5.75-\alpha_j-\alpha_l-\alpha_f} \tag{13}$$

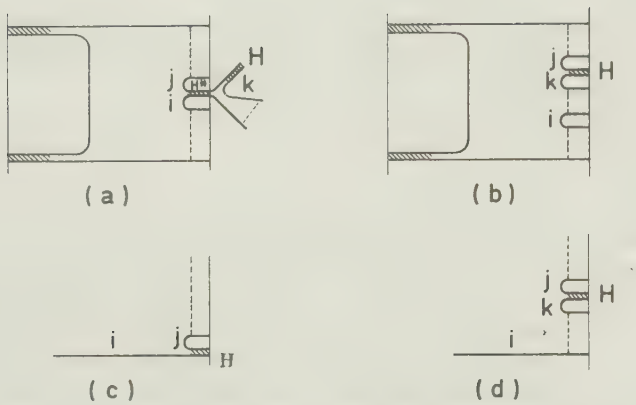

Fig. 4. The rearrangement **(4-b)** of the dual diagram for vector meson production and its decay $H^* \to H +$ anything **(4.a)**. Diagrams c and d exhibit the direct and the indirect fragmentation of i into $H^*(ij)$ and $H(jk)$ respectively

Table 1. The experimental branching ratios for 1^- vector meson decay pseudoscalars. We have used

$$\eta, \omega = \frac{u\bar{u}-d\bar{d}}{2} \sin\theta_{ps,v} + (s\bar{s})\cos\theta_{ps,v}$$

$$\eta', \phi = \frac{u\bar{u}-d\bar{d}}{2} \cos\theta_{ps,v} - (s\bar{s})\sin\theta_{ps,v}$$

with $\theta_{ps} = \frac{\pi}{4}$ and $\theta_v = \frac{\pi}{2}$

β	π^+	π^0	π^-	K^+	K^-	K^0	$\bar{K}^0$
ϱ^+	1	1	0	0	0	0	0
ϱ^0	1	0	1	0	0	0	0
ϱ^-	0	1	1	0	0	0	0
K^+	2/3	1/3	0	1/3	0	2/3	0
K^-	0	1/3	2/3	0	1/3	0	2/3
K^0	0	1/3	2/3	2/3	0	1/3	0
$\bar{K}^0$	2/3	1/3	0	0	2/3	0	1/3
ω	0.60	0.70	0.60	0	0	0	0
ϕ	0	0	0	0.48	0.48	0.35	0.35
η	0.18	0.80	0.18	0	0	0	0
η'	0.54	0.48	0.54	0	0	0	0

III. Resonance Contributions

At this point, let us make clear which particle H formulae (6) and (13) may be applied to. As we point it out in the introduction, our purpose is to determine the non perturbative part of the quark fragmentation functions, to be used as an input to Altarelli-Parisi equations. Since the perturbative corrections leading to scaling violations are small [the power of $(1-Z)$ gets an additional term proportional to $\ln\ln Q^2$], our parametrization should be taken as appropriate to describe jet phenomenology in a typical range of Q^2 between 10 and 100 GeV^2.

In this energy domain we neglect the small production of charmed particles, so that the flavors involved are only those of u, d, and s. Furthermore, we assum that only mesons belonging to the pseudoscalar none 0^- or to the vector nonet 1^- are substantially pro duced. Indeed, several hadron-hadron experiment [17] on hadron production, either at low or high $p_\perp$ show that in the considered range of energy, both th rates production of "$1^- + 0^-$" relative to the total and of "1^-" relative to "0^-" are of order 1.

3.1. Vector Decay Functions

With these hypotheses, we have to express how thes vector mesons fragment into pseudoscalar ones. L us consider a vector meson $H^*(ij)$ formed somewhe in the jet from a quark i by creation of a quark $H(jk)$ being a decay product of H^* as shown in Fig 4a. The properties of dual diagrams, allow us to re draw the diagram of Fig. 4a under the form of Fig. 4 Therefore, the productions from the quark i of H and H can be regarded respectively as a direct (Fig. 4c and an indirect (Fig. 4d) fragmentations. Hence, w write the indirect fragmentation of the quark i into H as the convolution product of the direct fragmentatio of i into H^* by the decay function $f_{H^*\to H}$ of H^* int H [18]:

$$D^{\text{ind}}_{i\to H}(Z) = \int_Z^1 D^{\text{dir}}_{i\to H^*}(Y)\, f_{H^*\to H}(Y/Z)\,\frac{dY}{Y}. \tag{14}$$

Since the decay mechanism does not contain any hig transfer momentum, the averaged trajectories $\bar{\alpha}$ appear ing in the behaviour near $Z=1$ for $D^{\text{dir}}_{i\to H^*}$ and $D^{\text{ind}}_{i\to}$ must be taken equal to α, i.e.:

$$D^{\text{dir}}_{i\to H^*}(Z) \underset{\alpha=\bar{\alpha}}{|} \underset{Z\alpha 1}{\propto} (1-Z)^{-\alpha_j} \tag{15a}$$

$$D^{\text{ind}}_{i\to H}(Z) \underset{\alpha=\bar{\alpha}}{|} \underset{Z\alpha 1}{\propto} (1-Z)^{2-\alpha_i-\alpha_j-\alpha_k}. \tag{15b}$$

On the other hand for a convolution as (14), in whic the function involved admit the parametrizatio $Z^n(1-Z)^m$, the powers m of $(1-Z)$ obey the follow ing relation:

$$m(D^{\text{ind}}_{i\to H}) = m(D^{\text{dir}}_{i\to H^*}) + m(f_{H^*\to H}) + 1 \tag{15c}$$

Combining Eqs. (14) and (15) yields:

$$f_{H^*\to H}(Z) \underset{Z\alpha 1}{\propto} (1-Z)^{1-\alpha_i-\alpha_k}.$$

The behaviour near $Z=0$ is also easy to get: on exactly repeats the argument changing the quark i int the quark j and Z into $(1-Z)$, and gets

$$f_{H^*\to H}(Z) \propto Z^{1-\alpha_j-\alpha_k}(1-Z)^{1-\alpha_i-\alpha_k}$$

which must be normalized according to the experi mental branching ratios of H^* into the possible deca channels. We write

$$f_{H^*\to H}(Z)=\beta_{H^*\to H}\frac{Z^{1-\alpha_j-\alpha_k}(1-Z)^{1-\alpha_i-\alpha_k}}{B(2-\alpha_j-\alpha_k,\,2-\alpha_i-\alpha_k)}. \tag{16}$$

The values of the quantities β are given in Table 1, where we assume that the mixing angles in the 1^- and 0^- configurations are equal to $\frac{\pi}{2}$ and $\frac{\pi}{4}$ respectively. We also allow the η and the η' states to decay.

3.2. Properties of $f_{H^*\to H}$

The last result (16) calls for the following remarks.

i) For the ordinary quarks (u, d), the decay of ϱ into $\pi_1\pi_2$ is given by a flat distribution since $\alpha_u=\alpha_d=\alpha_{f^0\text{meson}}=0.50$

$$f_{\varrho\to\pi_1}(Z)=\beta_{\varrho\to\pi}=1. \tag{17}$$

The second moment is just $\int_0^1 Z\cdot dZ=1/2$. The two pions equally share the momentum.

ii) Taking $\alpha_s=\alpha_{\phi\,\text{meson}}=0.17$, as given by a linear exchange degenerate trajectory passing through the $\phi(1.020)$ and $f'(1.515)$ states, the decay of K^* into $K\pi$ is given by

$$f_{K^*\to\pi}(Z)=\beta_{K^*\to\pi}\frac{(1-Z)^{0.33}}{0.75} \tag{18a}$$

$$f_{K^*\to K}(Z)=\beta_{K^*\to K}\frac{Z^{0.33}}{0.75} \tag{18b}$$

For $Z\simeq 1$ the K takes all the momentum of the K^*, leaving the pion almost at the rest. This is known as the leading effect, which must be accentuated for heavier particles like $D^*\to D\pi$ (the higher are the masses, the lower are the trajectories). Indeed the second moment of (18) gives: $\langle Z\rangle_K\simeq 0.6\,\beta_{K^*\to K}$ and $\langle Z\rangle\simeq 0.4\,\beta_{K^*\to\pi}$.

iii) In the case of $\phi\to KK$, the decay function is

$$f_{\phi\to K}(Z)=\beta_{\phi\to K}\frac{Z^{0.33}(1-Z)^{0.33}}{0.53}. \tag{19}$$

This function is symmetric under $Z\leftrightarrow 1-Z$ and

$$\langle Z\rangle_K=\langle Z\rangle_{\bar K}=0.50\,\beta_{\phi\to K}.$$

iv) Being non planar, the OZI [19] violating decays like $\phi\to\pi\pi$ are forbidden in our approximations. We set $\beta_{\phi\to\pi+\pi}=0$. As ϕ production is small anyway, this should not affect appreciably the π yield.

3.3. The Total Quark Fragmentation Function

The total quark fragmentation function into pseudoscalars contains in addition to the indirect (13) and direct (6) non resonating contributions, the direct and the indirect production of resonances which then decay into the observed mesons (π or K). Using the definitions

$$D^{r\,\text{dir}}_{q\to H}(Z)=\sum_{H^*}\int_Z^1 D^{\text{dir}}_{q\to qj}(Z)\,f_{qj\to qf}(Z/Y)\frac{dY}{Y},\quad H^*=(qj) \tag{20}$$

$$D^{r\,\text{ind}}_{q\to if}(Z)=\sum_{H^*}\int_Z^1 D^{\text{ind}}_{q\to ij}(Z)\,f_{ij\to if}(Z/Y)\frac{dY}{Y},\quad H^*=(ij) \tag{21}$$

for the contributions from the resonances, we have

$$D_{q\to H}(Z)=D^{\text{dir}}_{q\to H}(Z)+D^{\text{ind}}_{q\to H}(Z)+D^{r\,\text{dir}}_{q\to H}(Z)+D^{r\,\text{ind}}_{q\to H}(Z) \tag{22}$$

For resonance production, only the first two terms D^{dir} and D^{ind} subsist, since we have assumed that there are no resonances higher than those of the first 1^- nonet.

IV. The Quark Fragmentation Functions

4.1. Determination of n_{if} and N_q

In this section, we are going to determine the last two unknown parameters, which fix the behaviour near $Z=0$ of the direct contribution and the absolute normalization of the indirect one. This can be achieved by looking for quantities which do not contain both parameters. So are the sum rules where all the indirect and the resonant indirect contributions are absent. For any physical observable θ, we have

$$\sum_H \theta_H\int_0^1 D_{q\to H}(Z)dZ=\theta_q, \tag{23}$$

where θ_H, θ_q are the values of this observable for a hadron H or a quark q.

Let us first consider the charges of the normal quarks u and d, which give two independent equations, containing two variables n_{uu} (for π production) and n_{us} (for K production). The separation

$$\int_0^1 dz\int_z^1 h(z/y)g(y)\frac{dy}{y}=\int_0^1 h(y)dy\cdot\int_0^1 g(z)dz \tag{24}$$

of the convolution integral for the resonant part allows us to write:

$$\int_0^1\{D_{u\to\pi^+}(Z)-D_{u\to\pi^-}(z)\}dZ=2\int_0^1 D^{\text{dir}}_{u\to\pi^+}(Z)dZ+\frac{2}{3}\int_0^1 D^{\text{dir}}_{u\to K^+}(Z)dZ \tag{25}$$

Table 2. The first moment of the direct fragmentation function, the charge, isospin and strangeness for the u, d, and s quark jets for our choice for the behaviour near $Z=0$

n_{if}	first m^t	Q	I_3	S
$n_{uu}=-0.25$	$\int_0^1 D^{\text{dir}}_{u\to\pi^+}(Z)dZ=0.19$	$Q_d=-0.38$	$I_d=-0.48$	$S_d=0.20$
$n_{us}=+0.08$	$\int_0^1 D^{\text{dir}}_{u\to K^+}(Z)dZ=0.10$	$Q_u=0.59$	$I_u=+0.48$	$S_u=0.20$
$n_{su}=+0.25$	$\int_0^1 D^{\text{dir}}_{s\to K^+}(Z)dZ=0.18$	$Q_s=-0.36$	$I_s=0$	$S_s=-0.72$
$n_{ss}=+0.58$	$\int_0^1 D^{\text{dir}}_{s\to\phi}(Z)dZ=0.115$			

$$\int_0^1 \{D_{u\to K^+}(Z)-D_{u\to K^-}(Z)\}dZ=\frac{4}{3}\int_0^1 D^{\text{dir}}_{u\to K^+}(Z)dZ \tag{26a}$$

$$\int_0^1 \{D_{d\to K^+}(Z)-D_{d\to K^-}(Z)\}dZ=\frac{2}{3}\int_0^1 D^{\text{dir}}_{d\to K^0}(Z)dZ=\frac{2}{3}\int_0^1 D^{\text{dir}}_{u\to K^-}(Z)dZ \tag{26b}$$

From the charges of u and d we get

$$2\int_0^1 D^{\text{dir}}_{u\to\pi^+}(Z)dZ+2\int_0^1 D^{\text{dir}}_{u\to K^+}(Z)dZ\leqq\frac{2}{3} \tag{27}$$

$$2\int_0^1 D^{\text{dir}}_{d\to\pi^-}(Z)dZ\geqq\frac{1}{3};\qquad D^{\text{dir}}_{u\to\pi^+}(Z)=D^{\text{dir}}_{d\to\pi^-}(Z) \tag{28}$$

The inequalities in (27) and (28) come from baryon production being neglected. The baryon contributions are known to be small and cannot lead to important departures from equalities. We make the choice of 0.40 as an upper bound to (28), corresponding to a baryon production of order 20% and write:

$$0.40\geqq 2\int_0^1 D^{\text{dir}}_{u\to\pi^+}(Z)dZ\geqq\frac{1}{3}. \tag{29}$$

Together with the parametrization (6) this gives for the power n_{uu} (recall that in n_{if} the first subscript i stands for the initial quark and the latter one f for the final quark) the following range of variation:

$$n_{uu}=\{-0.28;\ -0.18\}\quad\text{or}\quad n_{uu}=-0.23\pm0.05. \tag{30}$$

The use of these values of n_{uu} in (27) is not enough constraining for n_{us}. Hence we add the multiplicity sum rule of the initial quark:

$$\sum_H \int_0^1 D_{q\to H}(Z)dZ=1\quad\text{with}\quad H=(qf). \tag{31}$$

This rule has a simple meaning: if one sums the multiplicities of all the hadrons *containing* the original quark, one finds the multiplicity of the initial quark, which is equal to one. Again in this formula, the indirect and the resonant indirect fragmentations do not contribute. Using (24–26) one obtains:

$$4.15\int_0^1 D^{\text{dir}}_{u\to\pi^+}(Z)dZ+2\int_0^1 D^{\text{dir}}_{u\to K^+}(Z)dZ\leqq 1 \tag{32}$$

substituting the formula (29) in (32), we get the inequality

$$0.09\leqq\int_0^1 D^{\text{dir}}_{u\to K^+}(Z)dZ\leqq 0.15 \tag{33}$$

which determines the range of variation of n_{us}:

$$n_{us}=\{+0.17;\ -0.05\}\quad\text{or}\quad n_{us}=0.06\pm0.11. \tag{34}$$

Following the same procedure for a s quark jet, we obtain:

$$0.40\geqq 2\int_0^1 D^{\text{dir}}_{s\to K^-}(Z)dZ\geqq\tfrac{1}{3} \tag{35}$$

$$n_{su}=\{0.17;\ 0.32\}\quad\text{or}\quad n_{su}=0.25\pm0.07 \tag{36}$$

and for the last n_{if}, namely n_{ss},

$$0.09\leqq\int_0^1 D^{\text{dir}}_{s\to\phi}(Z)dZ\leqq 0.20 \tag{37}$$

$$n_{ss}=\{0.80;\ 0.16\}\quad\text{or}\quad n_{ss}=0.48\pm0.32. \tag{38}$$

We remark that the calculation of n_{us} and n_{ss} require the knowledge of n_{uu} and n_{su} respectively, which are independently determined only by fixing the range of variation of the averaged charge of the jet. However, in the absence of experimental data on the variation of the charge Q, the third component of the isospin I_3 and the strangeness S versus Z or versus the rapidity y we have compared our results to Field-Feynman ones. This comparison is not very sensitive to the variation of n_{if} in the determined ranges (30), (34), (36), and (38). Therefore we have fixed them to the following values:

$$\begin{aligned} n_{uu}&=-0.25 & n_{su}&=+0.25\\ n_{us}&=+0.08 & n_{ss}&=+0.58 \end{aligned} \tag{39}$$

which on one hand are almost equal to the central values of the different allowed ranges and on the other hand obey the following empirical linear parametrization:

$$n_{if}=1-1.5\alpha_i-\alpha_f. \tag{40}$$

According to (39), we give for Q, I_3, and S the differential distributions in Figs. 5–7, and the mean values, in addition to the first moment of the direct parts of a jet initiated either by u, d or s quark, in Table 2.

However, within this choice (39), the determination of the normalization N_q of the indirect parts is straight-

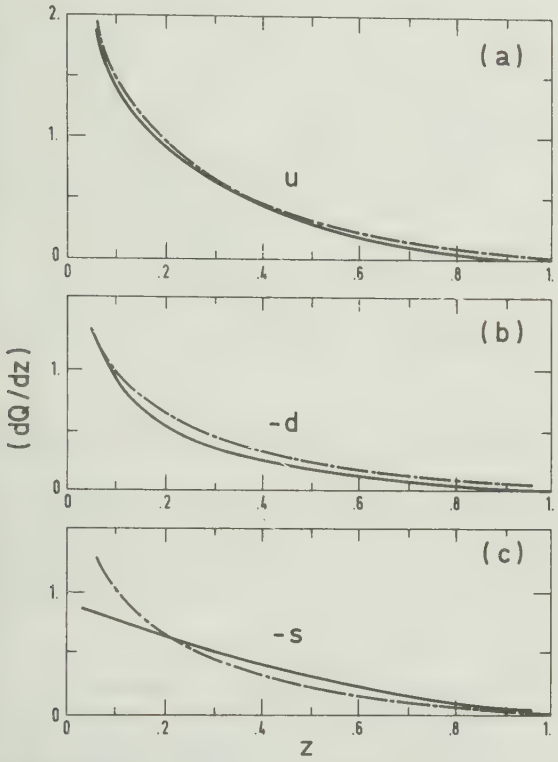

Fig. 5. The differential charge distribution for **a)** u quark, **b)** d quark, **c)** s quark. Full lines are predictions whereas the dotted ones are those of *FF*

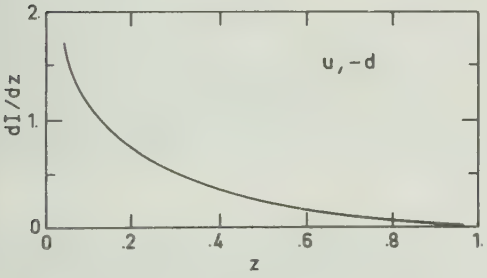

Fig. 6. The differential distribution for the isospin ($u=-d$). The s case is compatible with zero

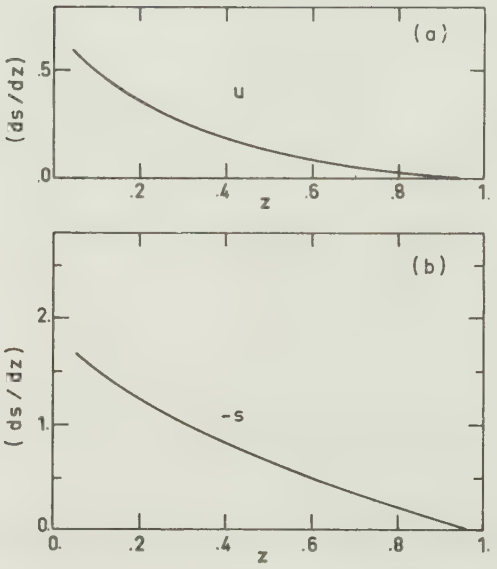

Fig. 7. The differential distribution for the strangeness **a)** for u or d quark; **b)** s quark

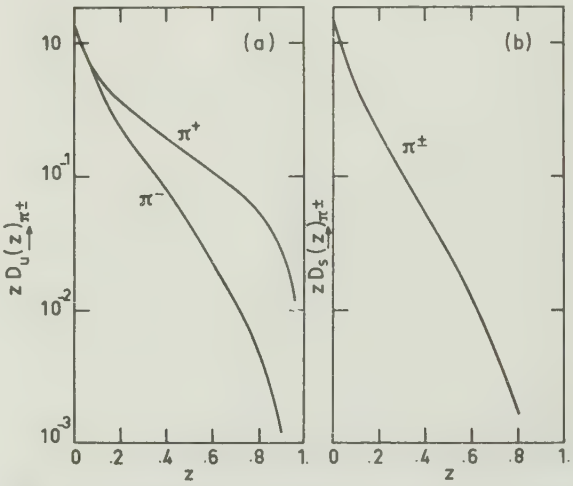

Fig. 8. The fragmentation functions into π^+ or π^- **a)** u quark, **b)** s quark

forward. Indeed, taking the momentum conservation law:

$$\sum_H \int_0^1 Z D_{q\to H}(Z)dZ=1 \tag{41}$$

and using (6), (13), (16), (20–22), (24), and (40) we get for u and s jets that;

$$N_u=0.069 \qquad N_s=0.068 \tag{42}$$

It is exactly the result that we must expect. For a given hadron H, the height of the plateau in a quark jet is independent on the flavor of this quark. In other words the production of a given particle H in the central region, where the indirect parts dominate must not be related to the initial quark. In order to take roughly into account the existence of a small baryon production, we shall use

$$N=N_u=N_s=0.06 \tag{43}$$

in numerical applications of our model.

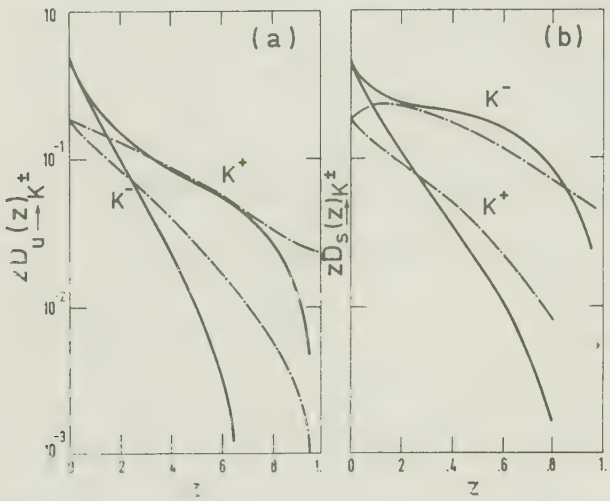

Fig. 9. The same as in Fig. 8 for K^+ and K^- production. The full lines and the dotted ones are our results and those of *FF* respectively

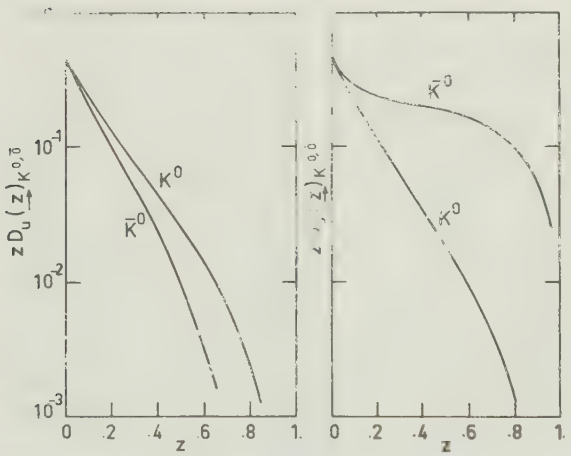

Fig. 10. The same as in Fig. 8 for K^0 and $\bar{K}^0$ production

Table 3. The total longitudinal fraction, of a u or s quark momentum, carried by the pseudoscalar mesons (π and K)

	u-quark	s-quark
π^+	0.246	0.145
π^0	0.216	0.153
π^-	0.158	0.145
K^+	0.099	0.070
K^-	0.060	0.177
K^0	0.070	0.060
$\bar{K}^0$	0.060	0.173
TOT, π	62%	44%
TOT, K	29%	48%
TOT	91%	92%

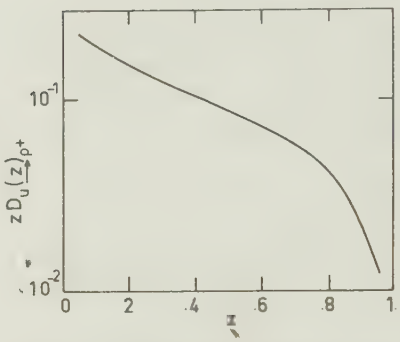

Fig. 11. The fragmentation function of u into ϱ^+

4.2. Predictions for the Quark Fragmentation Functions

A clean test of our predictions for quark fragmentation functions is not possible in the absence of sufficient experimental data on individual quark fragmentation into a given hadron. Nevertheless we give the following predictions and comparisons:

i) We show our results for quark fragmentation functions in Figs. (8)–(10) for u or s quark into (π^+, π^-), (K^+, K^-), and $(K^0, \bar{K}^0)$. The interesting fact to note is that the distributions for $s \to K(\bar{K})$ (Fig. 9b and 10b) are higher at $Z \neq 0$ than for $u \to K(\bar{K})$ (Figs. 9a and 10a). In FF model this effect exists and it is done by setting by hand a different normalization in the direct quark fragmentation. In our model this quark leading effect is automatically taken into account by Regge dynamics which distinguish various flavors by different trajectories and, as consequences, different normalization and different power behaviours near $Z=1$. For these reasons, our curves for $s \to K(\bar{K})$ are higher than those of FF.

ii) We give an example of resonances production namely u quark fragmentation into ϱ^+ meson (Fig. 11).

iii) We give the fractions of the total momentum of u and s quarks carried by each produced hadron (π or K) in Table 3.

iv) We compare our results for production of charged particles $H^+ + H^-$ (Fig. 12), charged pions $\pi^+ + \pi^-$ (Fig. 13) and neutral kaons $K^0 + \bar{K}^0$ (Fig. 14) with experimental data on e^+e^- annihilation taken from [20]. The agreement is good. Note, however, that the available experimental data, with which we compare our predictions correspond to energies beyond the threshold for charm production; and therefore they contain an excess of pions and kaons coming from hadronic and semi-leptonic decays of these charmed particles. This effect is not taken into account in our model.

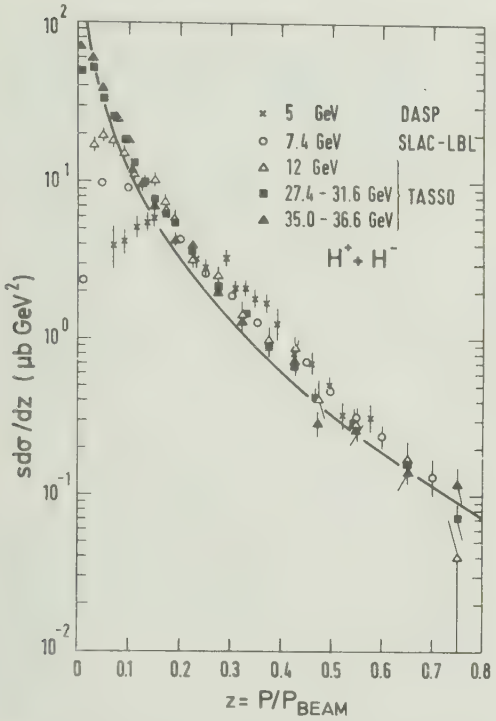

Fig. 12. The production of all charged hadrons in e^+e^- annihilation. The experimental points are from Ref. [20]. The curve is our prediction

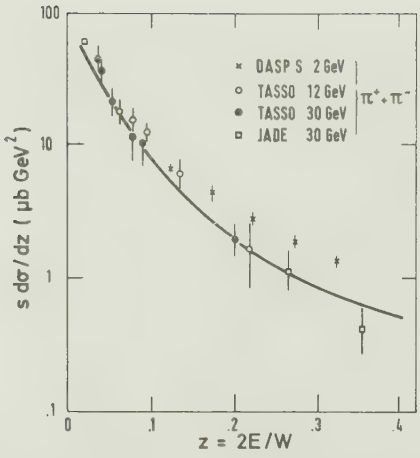

Fig. 13. The same as in Fig. 11 for $\pi^+ + \pi^-$ production

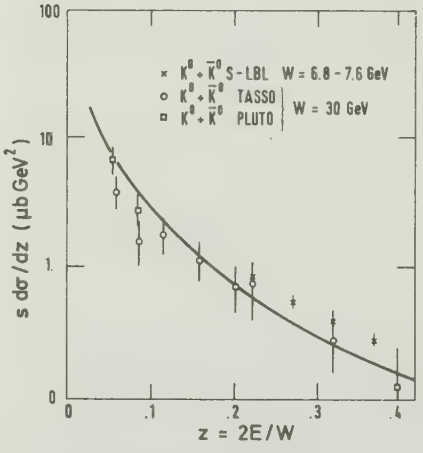

Fig. 14. The same as in Fig. 11 for $K^0 + \bar{K}^0$ production

V. Charm Fragmentation Functions

Since the contributions of charm to the already calculated quark (u, d, s) fragmentation functions cannot be large, we can extend our previous results to include charm in the quark set considered up to now. We proceed in the following way:

i) Since the behavior near $Z=1$ is known as before, we only need to determine the $Z\simeq 0$ behaviour. We choose to use the empirical relation established in Sect. 4.1 [Eq. (40)]. We get:

$$D^{\text{dir}}_{c\to cu}(Z)=4.36\,Z^{3.72}(1-Z) \tag{44}$$

$$D^{\text{dir}}_{c\to cs}(Z)=6.20\,Z^{4.06}(1-Z)^{1.33} \tag{45}$$

$$D^{\text{dir}}_{c\to cc}(Z)=33.97\,Z^{6.37}(1-Z)^{3.65} \tag{46}$$

$$D^{\text{dir}}_{s\to sc}(Z)=1.05\,Z^{2.90}(1-Z)^{3.65} \tag{47}$$

$$D^{\text{dir}}_{u\to uc}(Z)=0.39\,Z^{2.40}(1-Z)^{3.65}. \tag{48}$$

In these equations, as it was done for the $\phi=s\bar{s}$ trajectory ($\alpha_s=0.17$), the hidden charm trajectory intercept is determined by a linear fit to the ψ and χ masses: $\alpha_\psi=\alpha_c=-2.15$. The notation (ij) exhibits the quark content of the observed particle H.

We observe on (44–48) the well-known quark leading effect. Starting from (46) ($D^{\text{dir}}_{c\to\psi}(Z)$), which is piked for intermediate Z values, if one keeps the final (initial) quark fixed the fragmentation function increases in the small (large) Z region when the initial (final) quark changes from a heavy quark to a lighter one.

ii) The parameter of the indirect fragmentation part (13) for the charm is N_c. As we have discussed it in Sect. 4.1, we take the same value for all flavors, i.e. $N_c=0.06$.

iii) The decay functions $f_{H^*\to H}$ are also obtained by application of (16) and the $\beta_{H^*\to H}$ branching ratios are taken from experiment.

One of the consequences of this generalization is a slight change in the average values of the quantum numbers, namely of the charges:

– The charge of the u quark is still the same since there is no direct fragmentation of u into $D^{\pm}$ and no charged decay of $\bar{D}^{*0}$

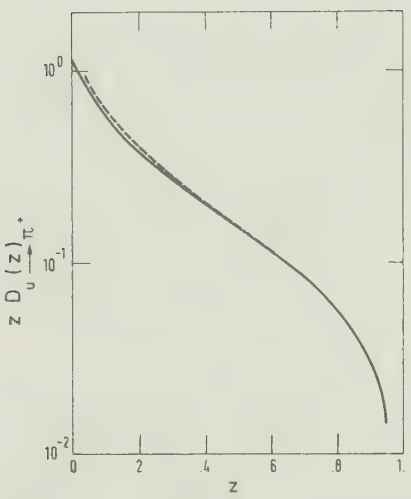

Fig. 15. The u quark fragmentation function into π^+ before (full line) and after (dotted line) the introduction of charm, without the non planar hadronic decay of charmed particles

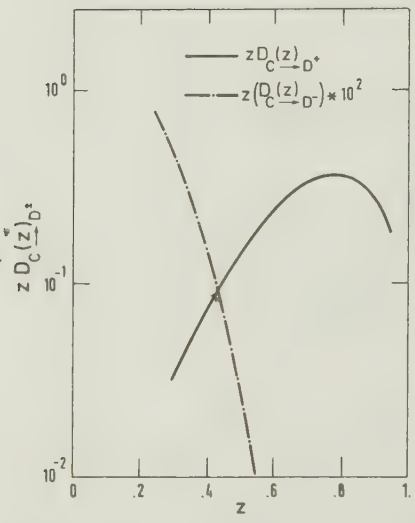

Fig. 16. The c quark fragmentation functions into D^+ (full line) and D^- (dotted line). The latter curve is multiplied by a factor 10^2

– The charge of the d quark gets an additional term given by:

$$\Delta Q_d = -\int_0^1 \{D^{\text{dir}}_{d\to D}(Z) + D^{\text{dir}}_{d\to D}(Z)\,[\beta_{D^{*-}\to\pi^-} + \beta_{D^{*-}\to D^-}]\}\,dZ = -0.006 \qquad (49)$$

– In the same way, the charge of the s quark is changed by: -0.01. Although all these contributions do not change the previous results appreciably, they lead to reasonable values for the charge, the third component of isospin, the strangeness and the charm of c quark jet. In particular, we find:

$$Q_c = +0.58 \qquad C_c = 0.80. \qquad (50)$$

As an example of our results from this extension, we show in Fig. 15 the change of $ZD_{u\to\pi^+}(Z)$ distribution, which is negligible for large Z and small for small Z. Actually, experiments show a more important enhancement, which is essentially due to non planar hadronic decays as $D\to K\pi$. These decays are not yet included in our model as we have pointed in Sections 3-2-4 and 4-2-4. In addition Figs. 16 and 17 exhibit the fragmentation of c into D^+ or D^- and the production of charged $(D^+ + D^-)$ and neutral $(D^0 + \bar{D}^0)$ particles compared with experimental data from [21]. The agreement is fairly good.

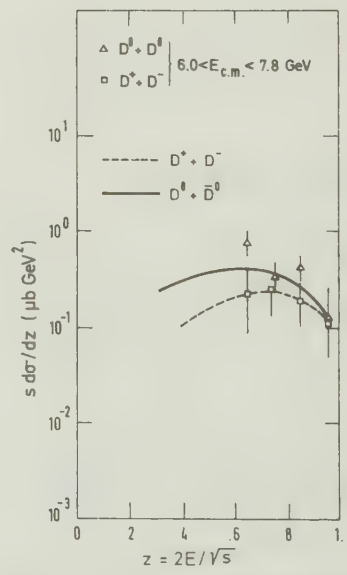

Fig. 17. Our predictions for the charged $(D^+ + D^-$, dotted line) and neutral $(D^0 + \bar{D}^0$, full line) in e^+e^- annihilation. Experimental data are from Ref. [21]. A cut off of order 0.35 is taken into account $(Z \geqq 0.35)$

VI. Conclusions and Outlooks

The use of DTU scheme in general and the rules of topological correspondence in particular allows us to derive a model for quark fragmentation functions by considering them as the product appropriately normalized of the behaviours near $Z=0$ and $Z=1$. The two unknown parameters of the model are not extracted from experiments, but rather a priori determined from the physical constraints of quantum numbers conservation. Furthermore, the various powers obtained for different quarks in the behaviour near $Z=0$ suggests

an empirical relation, which, when applied to the charm sector, leads to reasonable success. Hence we get all quark (u, d, s, and c) fragmentation functions into mesons without any free parameters. The comparison of our results, with experimental data gives satisfactory agreement.

The dual quark fragmentation model we propose here brings a new element in an effort to exploit *complementarity* between the two approaches of hadron physics, QCD and DTU. We mean that, while QCD predicts scaling violations in the quark fragmentation functions but gives no information on the non perturbative part of these functions, the dual approach appears as a good candidate to describe the soft effects.

For the time being the present results can be taken as the non perturbative input (a scaling parton model) of a QCD quark fragmentation functions, which can be used in a typical range of Q^2 where the scaling violations can be neglected. Incorporating Q^2-dependences requires the determination of $p_\perp$ dependence of the parton function and the knowledge of the gluon fragmentation functions. These questions are under present investigation.

Acknowledgements. We thank stimulating discussions with Bo. Anderson, G. Cohen-Tannoudji, M. Fantanaz, R. Lacaze, and H. Navelet. We acknowledge A. Morel for fruitful discussions and reading of the manuscript.

References

1. Aachen-Berlin CERN-Cracow-London (I.C.)–Vienna-Warsaw collaboration IC/HENP/79/27 preprint, July (1980); M. Basile et al.: CERN-EP/80–113 preprint June (1980); P. V. Chliapnikov: Contribution to Bruge Symp. Belgium (1980); W. Kittel: rapporteur's Review at the X Int. Symp. on multiparticles dynamics, GOA, September 1979
2. For a complete review on DTU see G. F. Chew, E. Rosenzweig: Phys. Rep. **41**, 263 (1978)
3. R. K. Ellis, H. Georgi, M. Machacek, H. D. Politzer, G. G. Ross: Phys. Lett. **78** B, 281 (1978); Nucl. Phys. B**152**, 285 (1979); A. J. Buras: Rev. Mod. Phys. **52**, 199 (1980)
4. a) G. Cohen-Tannoudji, F. Hayot, R. Peschanski: Phys. Rev. D**17**, 2930 (1978)
   b) G. Cohen-Tannoudji, A. El Hassouni, J. Kalinowski, R. Peschanski: Phys. Rev. D**19**, 3397 (1979)
   c) G. Cohen-Tannoudji, A. El Hassouni, J. Kalinowski, O. Napoly, R. Peschanski: Phys. Rev. D**21**, 2699 (1980)
   d) A. El Hassouni, R. Peschanski, Contribution to the XIVth rencontre de Moriond, March 11–23 (1979); Tran-Than-Van (ed.)
   e) G. Cohen-Tannoudji, O. Napoly: Contribution to the XVth rencontre de Moriond (1980); Tran-Than-Van (ed.)
5. A. El Hassouni, O. Napoly: Phys. Rev. D**23**, 193 (1981)
6. For an application of DTU for $D(Z)$ function see:
   J. Dias de Deus, S. Jadach: Acta Physiol. Pol. B**9**, 249 (1978);
   F. Hayot, S. Jadach: Phys. Rev. D**17**, 2307 (1978).
   For other works on $D(Z)$ see for example
   U. Sukhatme: Phys. Lett. **73** B, 478 (1978);
   B. O. Anderson, G. Gustafson, T. Sjostrand: Z. Phys. C – Particles and Fields **6**, 235 (1980);
   J. Dias de Deus, N. Sakai: Phys. Lett. **86** B, 321 (1979)
7. G. Altarelli, G. Parisi: Nucl. Phys. B**126**, 298 (1977)
8. An interesting discussion on the relation DTU–QCD can be found in M. Bishari: WIS 79/63-Ph. preprint and therein
9. V. N. Gribov, L. N. Lipatov: Yad. Fiz. **15**, 1218 (1972), and Sov. J. Nucl. Phys. **15**, 675 (1972)
10. R. D. Field, R. P. Feynman: Nucl. Phys. B**136**, 1 (1978)
11. A. H. Muller: Phys. Rev. D**2**, 2963 (1970);
    P. Salin in the Proc. of the summer school of Gif-sur-Yvette France (1973)
12. J. Kwiecinski, N. Sakai: Nucl. Phys. B**106**, 44 (1976);
    N. Sakai: Nucl. Phys. B**99**, 167 (1975)
13. J. Badier et al.: CERN preprint CERN/EP 80–48 (April 1980)
14. G. H. Thomas: Phys. Rev. D**5**, 2212 (1972);
    C. E. De Tar, K. Kang, C.-I. Tan, J. H. Weis: Phys. Rev. D **4**, 425 (1971)
15. The color factor 1/3 comes from the fact that in one case one sums over the quark color while in the other case one averages
16. G. Zech: Contribution to the XIVth Rencontre de Moriond (1979); Tran-Than-Van (ed.)
17. A. Seiden: Phys. Lett **68** B, 157 (1977)
    C. Cochet et al.: Nucl. Phys. B**155**, 333 (1979);
    France-USSR and CERN – USSR collaborations, Z. Phys. C – Particles and Fields **6**, 101 (1980)
18. Since in our model the behaviours near $Z=0$ and $Z=1$, the product of which determines the quark fragmentation, only depend on the flavor of the quarks involved; we assume that the pseudoscalars and vectors are generated by the same direct and indirect fragmentation functions
19. S. Okubo: Phys. Lett. **5**, 165 (1963);
    G. Zweig: CERN report TH. 412 (unpublished) (1964);
    I. Iizuka Prog Theor. Phys. Suppl. **37–38**, 21 (1966)
20. V. Lüth et al.: Phys. Rev. Lett. **30**, 120 (1977)
    D. Pandoulas: rapporteur talk at the 1980 Wiscons in Conference, and ref. therein
21. P. A. Rapidis et al.: Phys. Lett. **84** B, 507 (1979);
    M. Piccolo et al.: Phys. Lett. **86** B, 220 (1979)

Z. Phys. C - Particles and Fields 13, 219–227 (1982)

Zeitschrift für Physik C Particles and Fields
© Springer-Verlag 1982

Model for Nucleon Valence Structure Functions at All x, All $p_\perp$ and All Q^2 from the Correspondence Between QCD and DTU

G. Cohen-Tannoudji, A. El Hassouni[1]
DPH-T, CEN Saclay, Orme des Merisiers, BP No. 2, F-91190 Gif-sur-Yvette, France

A. Mantrach[1]
L.P.T.H.E., Université de Paris-sud Orsay, Laboratoire associé au CNRS, Bât. 211, F-91405 Orsay, France

E.G. Oudrhiri-Safiani[1]
L.P.T.H.E., Université de Paris VII Tour 33, Laboratoire Associé au CNRS LA 280, 2 Place Jussieu, F-75261 Paris Cedex 05, France

Received 10 July 1981; in revised form 26 November 1981

Abstract. We propose a simple parametrization of the nucleon valence structure functions at all x, all $p_\perp$ and all Q^2. We use the DTU parton model to fix the parametrization at a reference point ($Q_0^2 = 3\,\mathrm{GeV}^2$) and we mimic the QCD evolution by replacing the dimensioned parameters of the DTU parton model by functions depending on Q^2. Excellent agreement is obtained with existing data.

1. Introduction

It is well known that QCD predicts scaling violations in deep inelastic processes, in agreement with experimental observations. However it has been shown that at leading order in α_s these scaling violations (logarithmic evolution of the moments of the structure functions) do not affect the general structure of the parton model, that is the factorization [1] of inclusive cross sections into the product of a cross section of a process involving point like constituents with parton densities. At leading order, all scaling violation effects can be incorporated by substituting functions depending on x and Q^2 to the parton densities taken at some reference point Q_0^2 (Q^2 is here the transfer momentum squared for the considered deep inelastic process).

To be specific we consider the difference of neutrino and anti-neutrino cross sections, which singles out the non singlet structure function

$$x\frac{d\sigma}{dx}(\nu N \to \mu^- + x) - x\frac{d\sigma}{dx}(\bar{\nu} N \to \mu^+ + x) = xF_3^\nu \equiv xF^{NS}. \tag{1}$$

1 On leave of absence from the laboratoire de Physique Théorique, Faculté des Sciences de Rabat, Av Ibn Battota BP No. 1014, Rabat, Maroc

$N = \frac{1}{2}(n+p)$ is an isoscalar target and F^{NS} is the non singlet structure function, related to the difference of quark and antiquark distributions inside the nucleons.

Renormalization group equations [2] allow to predict the evolution of this non singlet structure function, via that of its moments:

$$F^{NS}(n, Q^2) = \int_0^1 dx\, x^{n-1} F^{NS}(x, Q^2)$$

$$= F^{NS}(n, Q_0^2) C_n^{NS}\left(\frac{Q^2}{Q_0^2}, g^2\right) \tag{2}$$

$$C_n^{NS}(Q^2/Q_0^2, g^2) = C_n^{NS}(1, g(Q^2)) \cdot \exp\left\{ -\int_{g(Q_0^2)}^{g(Q^2)} \frac{\gamma_n^{NS}(g')}{\beta(g')} dg' \right\}. \tag{3}$$

The functions $C_n^{NS}\left(\frac{Q^2}{Q_0^2}, g^2\right)$ are the Wilson coefficients, $g(Q^2)$ is the running coupling constant whose evolution is governed by the usual $\beta(g)$ function and $\gamma_n^{NS}(g)$ is the anomalous dimension of the non singlet quark operator. If $g(Q_0^2)$ is small enough, one can use the perturbative expansion of the exponent, and at the lowest order one obtains:

$$F^{NS}(n, Q^2) = F^{NS}(n, Q_0^2) \exp(-d_n^{NS} V(Q^2)) \tag{4}$$

where

$$V(Q^2) = \ln\left(\ln\left(\frac{Q^2}{\Lambda^2}\right) \Big/ \ln\left(\frac{Q_0^2}{\Lambda^2}\right)\right)$$

$$d_n^{NS} = \frac{4}{3\beta_0}\left[1 - \frac{2}{n(n+1)} + 4\sum_{j=2}^{n}\frac{1}{j}\right] \tag{5}$$

$$\beta_0 = 11 - \tfrac{2}{3}N_f$$

0170-9739/82/0013/0219/$01.80

Here N_f is the number of flavors and Λ is the QCD scale parameter (we have taken it equal to 0.6 GeV) [3]. In (4), all non perturbative effects are contained in $F^{NS}(n, Q_0^2)$, which, in current approaches, is extracted from experiment.

We propose to use the so called DTU parton model [4] to determine this non perturbative component. The DTU parton model is based on the parton interpretation of the planer topology in the dual topological unitarization (DTU) scheme. Let $F_0^{NS}(x, \{\alpha'_\varphi\})$ be the non singlet structure function in the DTU parton model. $\{\alpha'_\varphi\}$ is the set of dimensioned physical parameters which characterizes this DTU parton model, namely the slope of the Regge trajectories, and the masses of the external and exchanged particles. The DTU parton model obeys scaling and compares well with data [4–9] at moderate value of $Q^2 (1 \lesssim Q^2 \lesssim 4\,\text{GeV}^2)$. Now it has been shown, in the so called preconfinement approach [10], that, in an axial gauge, at the leading logarithm approximation the sum of planar diagrams in the $1/N$ expansion of QCD (N is the number of colors or flavors) accounts for the leading contribution to scaling violations. One can establish a topological correspondence between DTU and $\frac{1}{N}$ QCD provided that:

i) One identifies each topological component of DTU with the component of the same topology of $\frac{1}{N}$ QCD, but taken at $Q^2 = Q_0^2$, a value of Q^2 which characterizes the transverse cut off of the DTU parton model, and which has to be determined phenomenologically;
ii) One replaces, in the topological correspondence for other values of Q^2, the dimensionned parameters of DTU $\{\alpha'_\varphi\}$ by Q^2 dependent functions, which somehow amounts to "renormalize" DTU.

The justification of this procedure lies in confinement which implies that the parameters of QCD, that is Λ and N and those of DTU, that is $\{\alpha'_\varphi\}$ and N *cannot be independent.* If there exists a relation between them, such as:

$$f(\Lambda, \{\alpha'_\varphi\}, N) = 0, \tag{6}$$

one can adopt one of the two following point of view:
i) Consider $\{\alpha'_\varphi\}$ as fixed, but then Λ depends on N and thus one looses the topological correspondence; the planar topology in $\frac{1}{N}$ QCD has no reason to correspond to the planar topology in DTU; scaling violations in DTU are related to higher topologies.
ii) Consider Λ as fixed and maintain the topological correspondence by replacing $\{\alpha'_\varphi\}$ by running cutoffs $\{\alpha'(Q^2)\}$ and identify:

$$\frac{1}{N}(\text{QCD})_{Q^2} \text{ and } \frac{1}{N_f}(\text{DTU})_{\alpha'(Q^2)}.$$

Let us extend the set $\{\alpha'_\varphi\}$ to a set of running cut off $\{\alpha'(Q^2)\}$ with the condition

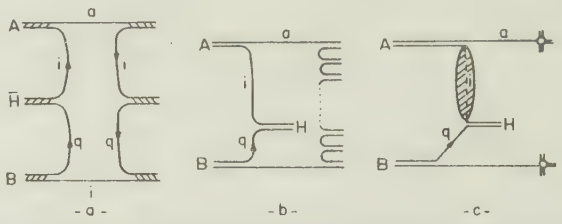

Fig. 1a–c. The parton interpretation of planar one particle inclusive cross sections (valence structure function)

$$\{\alpha'(Q_0^2)\} = \{\alpha'_\varphi\}, \tag{7}$$

and defined by the identity

$$F^{NS}(x, Q^2) \equiv F_0^{NS}(x, \{\alpha'(Q^2)\}). \tag{8}$$

F^{NS} is a known function of x and $\{\alpha'\}$ and the Q^2 evolution of the left hand side is known from QCD.

Our aim is to find a parametrization of $\{\alpha'(Q^2)\}$ such that the correct evolution of F^{NS} is insured, and hence its explicit form predicted.

In Sect. 2 we recall from which topological component of inclusive cross section one can extract, in the DTU parton model, the valence structure function. In Sect. 3 we discuss the properties of the six point dual function which has the same topology as the topological component discussed in Sect. 2. In Sect. 4, we derive an ansatz which approximately reproduces the behaviour of the six point dual function in the full range of the variables. From this ansatz we obtain a model for the valence structure function of the nucleon which is fixed at the reference point in Sect. 5, 'renormalized" in Sect. 6, and compared with data in Sect. 7.

2. The Valence Structure Function in the DTU Parton Model

The DTU parton model consists on the interpretation of some specific topological components of one particle inclusive cross sections ($A + B \to H + X$), in terms of structure functions, as shown in Fig. 1.

According to these interpretations, and in order to get a model for the structure function, one is led to calculate the inclusive cross sections ($A + B \to H + X$), or, thanks to the generalized Mueller's [11] optical theorem, the discontinuity in the missing mass M^2 of the forward $3 \to 3$ amplitude. As a model for this discontinuity, we use the six point dual function [12–14] which has the required topological properties.

It leads to an explicit form, valid in the central region as well as in the fragmentation region, of the invariant hadronic density. This density is defined as:

$$\frac{E_H}{\sigma_{AB}} \frac{d\sigma(A + B \to H + X)}{d^3 p_H} = f(s, M^2, t) \tag{9}$$

where $t = (P_B - P_H)^2$, $M^2 = (P_A + P_B - P_H)^2$ and $s = (P_A + P_B)^2$.

Up to terms of order m^2/s, the Mandelstam variables can be reexpressed in the B fragmentation region as:

$$M^2 = (1-x)s \quad \text{(a)}$$
$$u = -xs \quad \text{(b)}$$
$$t = m_B^2 + m_H^2 - (p_\perp^2 + m_H^2 + m_B^2 x^2)/x \quad \text{(c)} \qquad (10)$$

where x is the usual Feynman scaled momentum. Feynman's scaling implies that:

$$f(s, M^2, t) \xrightarrow[\substack{s, M^2 \to \infty \\ x, p_\perp \text{ fixed}}]{} f_{B \underset{A}{\to} H}(x, p_\perp) \qquad (11)$$

The parton interpretation in Fig. 1 relates the limiting distribution $f_{B \underset{A}{\to} H}(x, p_\perp)$ to the valence quark structure function $G^V_{B \to q}(x, p_\perp)$ of particule B:

$$E_H \frac{d\sigma(A + B \to H + X)}{d^3 p_H} = \sigma(A + q \underset{i}{\to} H + a) \cdot x G^V_{B \to q}(x, p_\perp). \qquad (12)$$

On an other hand,

$$\sigma(A + q \underset{i}{\to} H + a) \simeq g^2 \left(\frac{xs}{s_0}\right)^{\alpha_i - 1}, \qquad (13)$$

where α_i is the intercept of ($i\bar{i}$) Regge trajectory, so that we obtain

$$x G^V_{B \to q}(x, p_\perp) = x^{1-\alpha_q} f_{B \underset{A}{\to} H}(x, p_\perp) \qquad (14)$$

where α_q is the intercept of the $q\bar{q}$ Regge trajectory. The next step is to achieve a convenient parametrization of the distribution $f_{B \underset{A}{\to} H}(x, p_\perp)$.

3. The Six Point Dual Function [13–14]

With the notation indicated on the diagrams of Fig. 2, the form of the six point dual function is given by

$$B_6 = \int_0^1 dx_1 \int_0^1 dx \int_0^1 dx_2 \, x_1^{-\alpha_{23}-1}(1-x_1)^{-\alpha_{12}-1} x^{-\alpha_{13}-1} (1-x)^{-\alpha_{61}-1} x_2^{-\alpha_{45}-1}(1-x_2)^{-\alpha_{56}-1} \cdot (1 - x x_1)^{-\alpha_{62}+\alpha_{12}+\alpha_{61}} (1 - x x_2)^{-\alpha_{51}+\alpha_{56}+\alpha_{61}} \cdot (1 - x_1 x x_2)^{-\alpha_{34}+\alpha_{62}+\alpha_{51}-\alpha_{61}} \qquad (15)$$

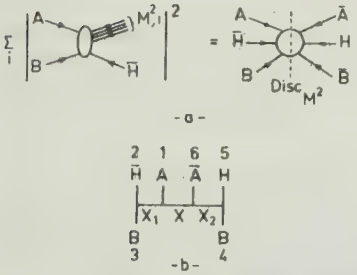

Fig. 2. a The definition of the six point dual function, b the variables in the fragmentation region of the incident particle B

where

$$\alpha_{ij} = \alpha(s_{ij}) = \alpha_{ij}^0 + \alpha'(p_i + p_{i+1} + \ldots p_j)^2 \qquad (16)$$

Taking the scaling limit $|\alpha_{13}|, |\alpha_{12}|, |\alpha_{56}| \to \infty$, we obtain:

$$f_{B \underset{A}{\to} H}(x, p_\perp) = \left(\frac{\alpha_{13}}{s}\right)^{\alpha_{61}} \left(-\frac{\alpha_{12}}{\alpha_{13}}\right)^{2\alpha_{23}+1} \int_0^1 dy_1 \int_0^{1-y_1} dy_2 \cdot y_1^{-\alpha_{23}-1} y_2^{-\alpha_{45}-1} \left(1 - \frac{\alpha_{13}}{\alpha_{12}} y_1\right)^{\alpha_{23}-\alpha_{34}-\alpha_{62}} \cdot \left(1 - \frac{\alpha_{13}}{\alpha_{56}} y_2\right)^{\alpha_{45}-\alpha_{34}-\alpha_{51}} \cdot \left(1 - \frac{\alpha_{13}}{\alpha_{12}} y_1 - \frac{\alpha_{13}}{\alpha_{56}} y_2\right)^{-\alpha_{61}-\alpha_{34}+\alpha_{62}+\alpha_{51}} \cdot (1 - y_1 - y_2)^{\alpha_{61}} \qquad (17)$$

The following remarks are in order:

i) from $s_{61} = s_{34} = 0$, we have $\alpha_{61} = \alpha_i$, $\alpha_{34} = \alpha_q$ (18)

ii) $\alpha_{13} \simeq \alpha' M^2$, $\alpha_{12} \simeq \alpha' u$ and $\alpha_{23} = \alpha_0 + \alpha' t$ (19)

The Regge slope α' is usually taken equal to 1 GeV^{-2}.

iii) $\alpha_{51} = \alpha_{62} = O(m^2) \simeq 0.$ (20)

iv) It is of physical interest [15] that the squared transfer momentum between the incoming particle B and the outgoing particle H may well reach a positive value, close to that of the location of the first pole on the t-channel (see Fig. 3). We define x_{max} as the solution of

$$\frac{dt}{dx} = -m_B^2 + (m_H^2 + p_\perp^2)/x^2 = 0$$

so that

$$x_{max} = \frac{\sqrt{m_H^2 + p_\perp^2}}{m_B} = \frac{m_{H\perp}}{m_B} \qquad (21)$$

and

$$t(x_{max}) = -p_\perp^2 + (m_B - m_{H\perp})^2. \qquad (22)$$

Therefore, at the point $x = x_{max}$, independent on the energy s, we expect that the contribution to the density $f(x, p_\perp)$ of the first pole in the t-channel to be maximal. In the case of interest, which is relative to the nucleon structure function, the fragmentation to be considered is

$$P \underset{\pi^\pm}{\longrightarrow} \pi^\pm \qquad (23)$$

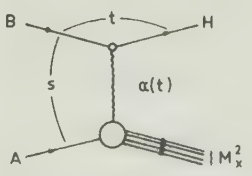

Fig. 3. The exchange of the pole in the t-channel ($B\bar{H}$)

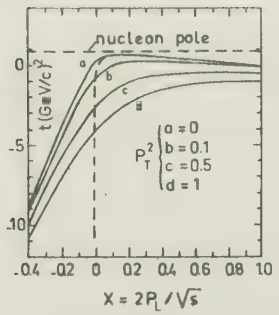

Fig. 4. The transfer momentum t, in the t-channel depending on x, and for different values of $p_\perp^2$ in the case of $p \to \pi$

The corresponding value of x_{max} at $p_\perp = 0$, and of the transfer momentum (see Fig. 4) are

$$x_{max}(p_\perp = 0) = \frac{m_\pi}{m_N} = 0.15 \tag{24}$$

$$t(x_{max}, p_\perp = 0) \simeq .64\ \text{GeV}^2 \tag{25}$$

We remark, on one hand, that $x \simeq .15$ is close to the position of the maximum of the valence nucleon structure functions ($x G^V_{p\to u}$ and $x G^V_{p\to d}$), and on the other hand, that the corresponding maximal value of t is close to the value of the nucleon pole namely $0.88\ \text{GeV}^2$.

Unfortunately the form (15) of the six point dual function is not simple enough for practical use since the integration cannot be done explicity except in some particular cases. We are thus led to search for more tractable approximate form which will be required to exhibit the triple Regge and double Regge behaviours of the full dual six point function.

4. An Approximate Form for the Limiting Distribution

In the limit $x \to 1$ the limiting distribution takes on the form

$$f^{T.R} \simeq (1-x)^{\alpha_{61}-2\alpha_{23}} \frac{\Gamma^2(-\alpha_{23})\Gamma(\alpha_{61}+1)}{\Gamma(-2\alpha_{23}+\alpha_{61}+1)} \tag{26}$$

which corresponds to the standard tripple Regge behaviour

$$\gamma(t)\left(\frac{s}{M^2}\right)^{2\alpha(t)} \frac{1}{|\alpha(t)|^2}\left(\frac{M^2}{s}\right)^{\alpha_i} \tag{27}$$

Using the triple Regge vertex $\gamma(t)$ determined by Thomas [14] in order to reproduce the behaviour of the actual dual six point function as well as possible, and taking into account the double Regge limit of (17), i.e.

$$f^{D.R} p_{\perp \to \infty} \simeq (p_\perp)^{-\alpha_{61}-\alpha_{34}-3} \exp(-4\alpha' p_\perp^2). \tag{28}$$

we propose the following ansatz for the valence

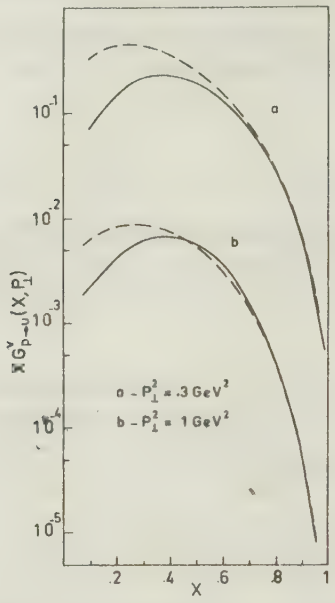

Fig. 5. The dashed line (---) is our approximate form for the structure function (29). The solid line is the one given by (17). The normalization is arbitrary

structure function:

$$G^V_{B\to q}(x, p_\perp) = \beta x^{-\alpha_q} \frac{(1-x)^{\alpha_i - 2\alpha(t)}}{|x(\alpha(t)-J)|^2}$$
$$\cdot e^{-2\alpha' m^2_{H\perp}} (1+x)\alpha'^2 m^2_{H\perp} \tag{29}$$

J is the spin of the particle corresponding to the lowest lying pole in the t-channel, and β a normalization coefficient. In Fig. 5 we compare the proposed ansatz with the six point dual function, in the case of the fragmentation $p \underset{\pi^+}{\to} \pi^+$. The non singular factor $(1+x)$ in (29) is necessary to achieve such a good agreement.

5. Valence Structure Function at the Reference Point Q_0^2

In order to probe a u quark (resp. d quark) in a nucleon, one must take a π^+ (resp π^-) as H particle. Accordingly, the trajectory in the $B\bar{H}$ channel is a mixture of the nucleon and Δ trajectories (resp a pure Δ trajectory). In [7] it was shown that one can reproduce the behaviour of the $u(\sim(1-x)^3)$ and $d(\sim(1-x)^4)$ valence structure functions by assuming that the Δ trajectory decouples and by replacing its contribution by the contribution of its first daughter (with intercept $\alpha_\Delta - 1$). We shall do the same assumption here.

Our method for building a parametrization is that the DTU parton model provides a good approximation to the structure functions at a certain value Q_0^2 of Q^2, the Q^2 evolution being then obtained by replacing the dimensioned parameters by Q^2 dependent

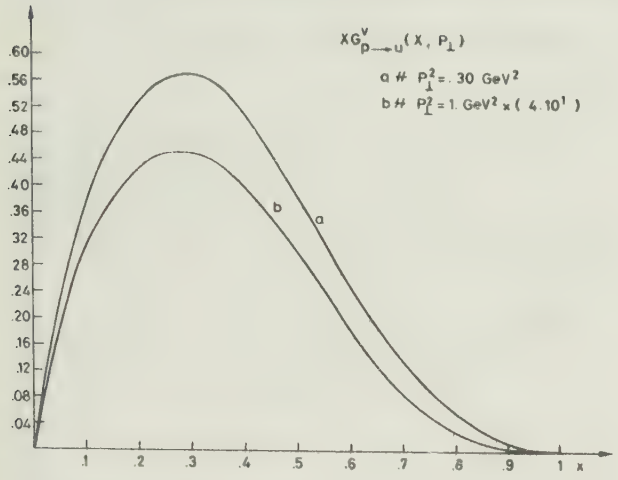

Fig. 6. Structure function $x G^{V}_{p\to u}(x, p_\perp)$ as function of x at fixed $p_\perp^2$. At $p_\perp^2 = 1$ GeV^2, the structure function is multiplied by a factor 40

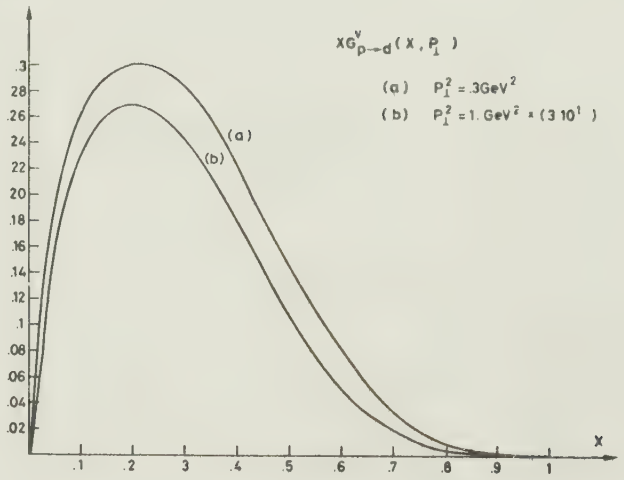

Fig. 8. Structure function $x G^{V}_{p\to d}(x, p_\perp)$ as function of x at fixed $p_\perp^2$. At $p_\perp^2 = 1$ GeV^2, our prediction is multiplied by a factor 30

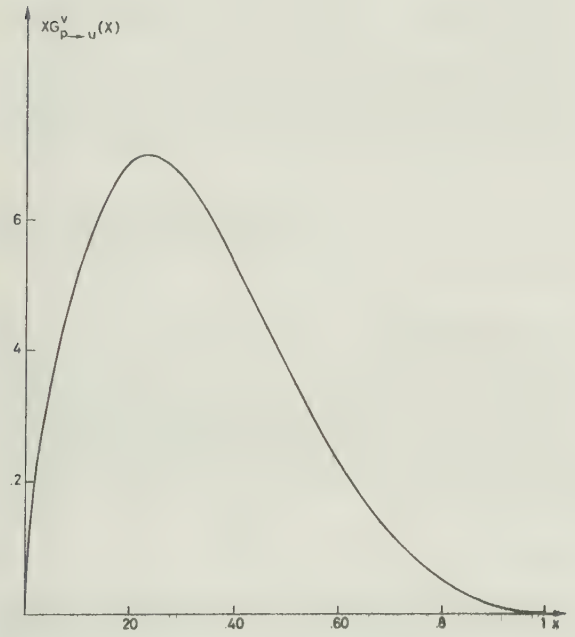

Fig. 7. The integration of structure functions over $p_\perp$: $x G^{V}_{p\to u}(x)$

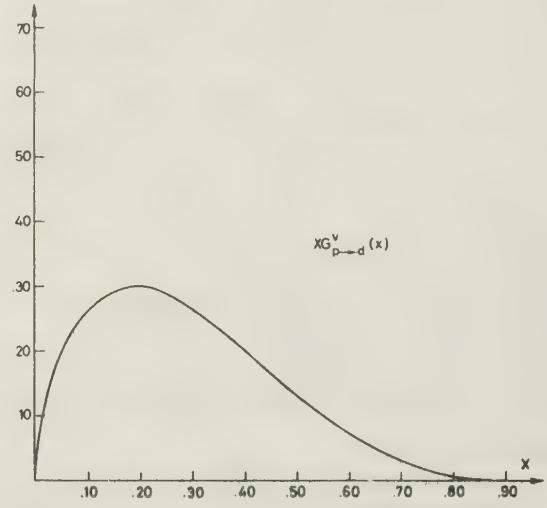

Fig. 9. The integration of structure functions over $p_\perp$: $x G^{V}_{p\to d}(x)$

ones. The problem is that one has no constraint on the precise value of Q_0^2, nor on the value of m_H.

Indeed, in the DTU parton model, the hadronic system $A\bar{H}$ represents the virtual photon in deep inelastic processes. Particle H has no reasons to be a physical pion. On the other hand particle B, the probed particle has to be a physical nucleon at Q_0^2.

We have adopted the following method; we fix Q_0^2 at 3 GeV^2, a value at which it is expected that α_s is already small. Then we determine m_H by a fit to the valence structure functions measured in deep inelastic experiments at $Q^2 = Q_0^2 = 3$ GeV^2.

The structure functions are obtained by integrating the expression of (29) over $p_\perp$. Neglecting contributions which behave like $e^{-Q_0^2\delta}$, we find

$$G^{V}_{B\to q}(x) = \beta x^{-\alpha_q}(1-x)^{\alpha_i - 2J}(1+x)e^{-2h(x)} \cdot\left[\mathrm{EXPI}(y_0) + (y_0 + \alpha' m_H^2 g(x))(\mathrm{EXPI}(y_0) - e^{-y_0}/y_0)\right] \tag{30}$$

where EXPI is the exponential integral function and:

$$h(x) = \alpha' x(m_B^2(1-x) + m_H^2 - m_{\mathrm{pole}}^2) \tag{31}$$

$$g(x) = \frac{2}{x}(\ln(1-x) - x), \tag{32}$$

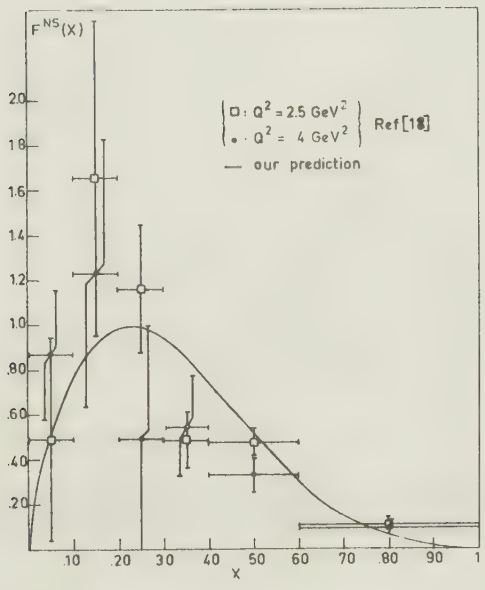

Fig. 10. The function $x F_0^{NS}(x) = x G^V_{p\to u}(x) + x G^V_{p\to d}(x)$

$$y_0 = \alpha' g(x)\left[(1-x)(x m_B^2 - m_H^2) - x m^2_{\text{pole}}\right] \tag{33}$$

β is a normalization coefficient determined by $\int_0^1 G^V_{p\to u}(x)dx = 2$ and $\int_0^1 G^V_{p\to d}(x)dx = 1$. For

$$q = u \quad m^2_{\text{pole}} = m_N^2, \quad J = 1/2 \tag{34}$$

$$q = d \quad m^2_{\text{pole}} = m_\Delta^2, \quad J = 1/2 \tag{35}$$

The best fit has been obtained with

$m_H(Q_0^2) = 0.35$ GeV for the u valence quark distribution (Figs. 6, 7) and

$m_H(Q_0^2) = 0.64$ GeV for the d valence quark distribution (Figs. 8, 9).

In Fig. 10, we show the total valence distribution $x F_0^{NS}$ obtained with our model. With the parametrization (30) for the structure function $G^V_{B\to q}$, at the reference point Q_0^2, we are now ready to study its Q^2 evolution.

6. Scaling Violations

As explained above we are led to us to mimic the QCD corrections due to gluon radiative emissions through redefinition of the set of the dimensioned parameters of the DTU parton model $\{\alpha'\}$.

Within QCD, the evolution with Q^2 of the parton densities is known through that of their moments, given by (4).

We thus use the Q^2 evolution predicted by QCD for the moments from their values at the reference point Q_0^2, as a way to constrain the parametrization of all dimensioned parameters, that is

$m_H^2, m_B^2, m^2_{\text{pole}}$, and α'

as functions of Q^2.

In order to perform this parametrization we shall take, as a guiding line, the results of the moment inversion method [16]. If one assumes that the behaviours of the valence structure functions near $x = 0$ and $x = 1$ are respectively:

$$x^r \text{ and } (1-x)^\nu \tag{36}$$

we obtain [16]

$$r(Q^2) = r(Q_0^2) \tag{37}$$

$$\nu(Q^2) = \nu(Q_0^2) + \frac{16}{3\beta_0} V(Q^2) \tag{38}$$

The expression given in (30) is dimensionless since all the dimensioned quantities appear in the form of the product $(\alpha' m^2)$. The behaviour near $x = 0$ is essentially controlled by $x^{-\alpha_q}$. In order to satisfy (37), we take α_q independent on Q^2. The behaviour near $x = 1$ is governed by:

a) the values of α_i and J, which are independent of α' and m^2, which we take independent of Q^2.

b) The value of the exponential integral function EXPI(y_0) i.e. the value of y_0.

In the limit $x \to 1$, y_0 is proportional to $(\alpha' m^2_{\text{pole}})$ and then in order to reproduce the behaviour of (38) we one led to set

$$(\alpha' m^2_{\text{pole}})_{Q^2} = (\alpha' m^2_{\text{pole}})_{Q_0^2} + \frac{1}{2}\frac{16}{3\beta_0} V(Q^2). \tag{39}$$

On the other hand, since the quantum numbers of the pole and of the probed particle B may be identical, we use the same parametrization for the quantity $(\alpha' m_B^2)$, i.e.:

$$(\alpha' m_B^2)_{Q^2} = (\alpha' m_B^2)_{Q_0^2} + \frac{1}{2}\frac{16}{3\beta_0} V(Q^2) \tag{40}$$

As for the last quantity which controls y_0 namely $\alpha' m_H^2$ let us first recall that the ratio m_H/m_B governs the value of t which approaches the most closely the pole position (21–22). Now QCD [16] tells us, through the inverse moment method, when powers of x and $(1-x)$ respectively near $x = 0$ and $x = 1$ are assumed, that for increasing Q^2, the maximal value of $x G^V_{B\to q}(x, Q^2)$ decreases and that the position of this maximum moves towards smaller x values. To get an identical effect, in our parametrization we propose:

$$\left(\frac{\alpha' m_H^2}{\alpha' m_B^2}\right)_{Q^2} = \left(\frac{\alpha' m_H^2}{\alpha' m_B^2}\right)_{Q_0^2} \Big/ (1 + \mu V(Q^2)) \tag{41}$$

where μ is a free parameter. In practice we have constrained this parameter by the requirement that the evolution of the low moments obtained from our parametrization coincides with the one predicted

from QCD. Indeed we note that the parametrization of $\frac{m_H}{m_B}$ does not affect the behaviour of y_0 (33) near $x = 1$ and thus does not affect the behaviour of higher moments.

It turns out that with

$$\mu = 2.\frac{16}{3\beta_0}, \tag{42}$$

we get a good agreement with the QCD evolution of the moments $n = 2$ and $n = 4$ (see Fig. 11).

To summarize we notice that when $Q^2 \to \infty$

$\alpha' m_H^2 \to ct$

$\alpha' m_B^2 \sim ct\, v(Q^2)$

$\alpha' m_{pole}^2 \sim ct\, v(Q^2)$

α_q, α_i, J are constant.

Such behaviours would be obtained if one assumes that the system of spectator quarks (the valence quarks of the nucleon which are not probed) acquires an invariant mass, increasing with Q^2. This picture is compatible with the physical interpretation of scaling violations in QCD: the emission of hard gluons induces an increasing invariant mass for the system of spectator partons.

7. Comparison with Data

a) Longitudinal Momentum Distribution

Once μ is constrained by the above mentioned argument, we are left with no free parameter for the comparison with experimental data on valence structure functions integrated over $p_\perp$.

Our predictions are shown in Table 1 and in Figs. 12–16; they all are in good agreement with existing data [17–18].

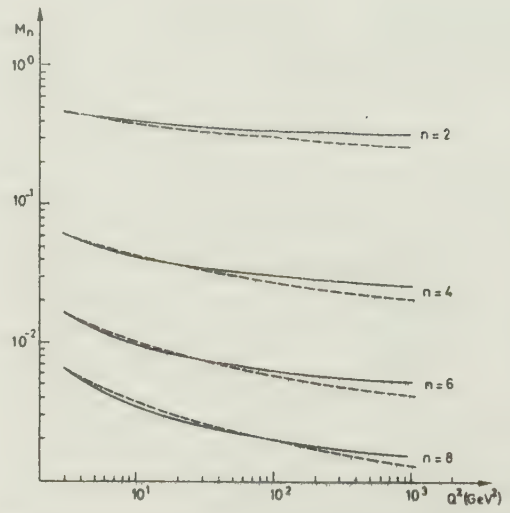

Fig. 11. The dashed lines (– –) show the QCD evolution of moments of F^{NS} from our inputs (30). The solid lines show the evolution resulting from our parametrization

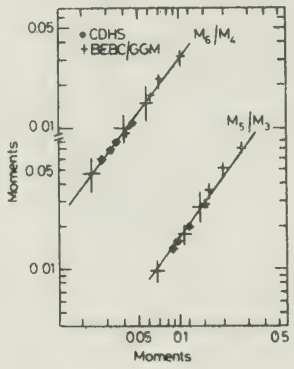

Fig. 12. ln M_i versus ln M_j plots as obtained by CDHS and BEBC/GGM [17], the lines represent our predictions

Table 1. Values of slopes of (ln M_n/ln M_m), for first and second order in QCD, for experiment (CDHS) and for our parametrization of ($\alpha' m^2$)

Slope of M_n/M_m	QCD (first order)	QCD (second order)	Experiments	Parametrization
M_6/M_4	1.29	1.39	$1.45 \pm .15$	1.40
M_8/M_4	1.50	1.69	$1.71 \pm .18$	1.70
M_{10}/M_4	1.66	1.94	$1.86 \pm .20$	1.95
M_8/M_6	1.16	1.22	——	1.22
M_{10}/M_6	1.29	1.40	——	1.40
M_5/M_3	1.46	——	$1.58 \pm .12$	1.62
M_7/M_3	1.76	——	$1.84 \pm .20$	2.06

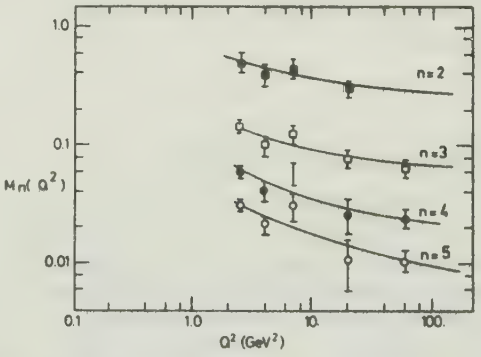

Fig. 13. The moments of $xF^{NS}(x, Q^2)$ VS Q^2. The data are from [18]. The solid lines represent our predictions

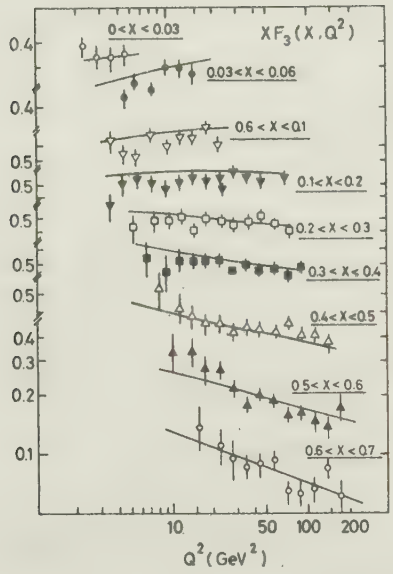

Fig. 14. $xF^{NS}(x, Q^2)$ as measured by the CDHS group [17] with the results of our parametrization

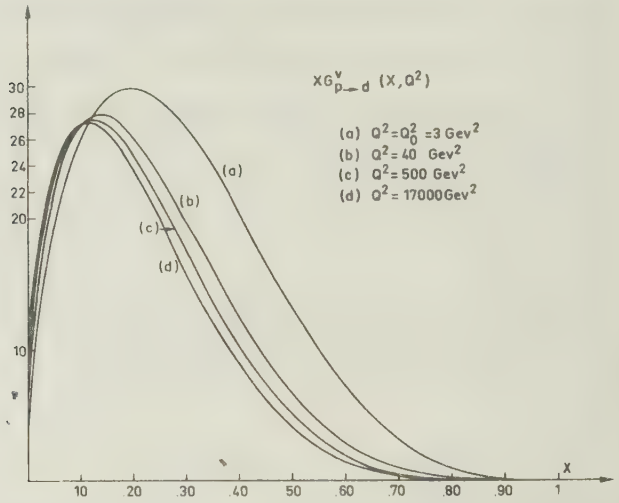

Fig. 16. $xG^{\nu}_{p\to d}$ as a function of x for (a) $Q^2 = Q_0^2 = 3\,\mathrm{GeV}^2$, (b) $Q^2 = 40\,\mathrm{GeV}^2$, (c) $Q^2 = 500\,\mathrm{GeV}^2$ and (d) $Q^2 = 17000\,\mathrm{GeV}^2$ (our parametrization)

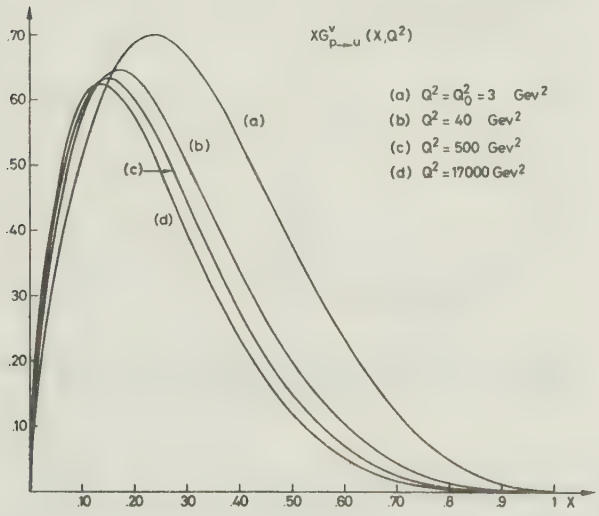

Fig. 15. $xG^{\nu}_{p\to u}$ as a function of x for (a) $Q^2 = Q_0^2 = 3\,\mathrm{GeV}^2$, (b) $Q^2 = 40\,\mathrm{GeV}^2$, (c) $Q^2 = 500\,\mathrm{GeV}^2$ and (d) $Q^2 = 17000\,\mathrm{GeV}^2$ (our parametrization)

b) Transverse Momentum Distribution

In order to predict the variation of $p_\perp^2$ as a function of Q^2, we now need another parametrization, that of α'. The slope of Regge trajectories. In fact, in our previous comparison, our predictions did not depend on the Q^2 evolution of the slope α': all the discussed quantities (structure functions and their moments) are dimensionless and involve only the dimensionless products $(\alpha' m^2)$. On the contrary the average value of $p_\perp^2$ is proportional to $\frac{1}{\alpha'}$. Starting from (29) which gives $x G^{\nu}_{B\to q}(x, p_\perp)$, we have

$$\langle p_\perp^2 \rangle = \frac{1}{\alpha' g(x)} \left\{ (1 + y_0) - \frac{\mathrm{EXPI}(y_0) - \alpha' m_H^2 g(x) e^{-y_0}/y_0}{\mathrm{EXPI}(y_0) + (y_0 + \alpha' m_H^2 g(x)) \left(\mathrm{EXPI}(y_0) - \frac{e^{-y_0}}{y_0} \right)} \right\} \tag{43}$$

In order to get the QCD prediction for the behaviour of $\langle p_\perp^2 \rangle$,

$$\langle p_\perp^2 \rangle \simeq Q^2 / \ln Q^2, \tag{44}$$

We propose for the slope α' the following parametrization:

$$(\alpha')_{Q^2} = (\alpha')_{Q_0^2} \Big/ \left(1 + \rho \frac{(Q^2/Q_0^2 - 1)}{(\ln Q^2/\Lambda^2)} \right), \tag{45}$$

where ρ is a free parameter to be determined experimentally. Equation (45) shows that α' is a decreasing function of Q^2, which reduces the exponentional cutoff in $p_\perp^2$, without changing the previous results.

Furthermore, (43) implies a "seagull" effect with a maximal value of $p_\perp^2$ of order $(0.20\,\mathrm{GeV}^2)$, for $Q^2 = Q_0^2$. The variation of $\langle p_\perp^2 \rangle$ as a function of x and Q^2 arises from a combination of (43) and (45). The absence of experimental data on $\langle p_\perp^2 \rangle$ prevents to obtain a determination of the parameter ρ, however we estimate it to be of order of 0.1.

To summarize we can say that our model leads to

an extremely simple parametrization of valence structure functions which agrees well with available data at all values of x and Q^2 explored till now. We hope that this parametrization will be useful for many phenomenological purposes such as QCD tests, extrapolations of data out of the x range experimentally reached, Monte Carlo analysis, etc..

We want to stress that although our parametrization is constrained by comparison with QCD at first order, it fits better the predictions of higher order corrections and experimental results than the predictions of the first order.

As a by product we predict the $p_\perp$ distribution of valence quarks. It would be interesting to test our predictions by comparison with experimental quantities which are sensitive to this distribution. Such are the $p_\perp^{out}$ distribution in large $p_\perp$ collisions and the transverse momentum distribution in large mass lepton pair inclusive production.

Acknowledgements. We thank A. Morel for careful reading of the manuscript.

References

1. D.J. Gross, F. Wilczek: Phys. Rev. Lett. **30**, 1323 (1973); Phys. Rev. **D8**, 3633 (1973); H.D. Politzer: Phys. Rev. Lett. **30**, 1346 (1973)
2. For general review on QCD results see G. Altarelli, G. Parisi: Nucl. Phys. **B126**, 298 (1977); E. de Rafaël: In the Proc. of summer School of Gif-sur-Yvette France (1978); V. Alessandrini: Second Rencontre de Rabat Maroc (1979); A.J. Buras: Rev. Mod. Phys. **52**, 199 (1980); and invited talk presented at symposium on topical questions in QCD, Copenhagen, July (1980)
3. H.L. Anderson, H.S. Matis, L.C. Myrianthopoulos: Phys. Rev. Lett. **40**, 1061 (1978)
4. G. Cohen-Tannoudji, F. Hayot, R. Peschanski: Phys. Rev. **D17**, 2930 (1978)
5. G. Cohen-Tannoudji, A. El Hassouni, J. Kalinowski, R. Peschanski: Phys. Rev. **D19**, 3397 (1979)
6. G. Cohen-Tannoudji et al. : Phys. Rev. **D21**, 2699 (1980)
7. A. El Hassouni, O. Napoly: Phys. Rev. **D23**, 193 (1981)
8. A. El Hassouni, A. Mantrach, E.G. Oudrhiri-Safiani: Z. Phys. C—Particles and Fields **9**, 185 (1981)
9. A. El Hassouni, R. Peschanski: Contribution to the XIVth recontre de Moriond, March 11–23 (1979, Tran-Than-Van, ed. Dreux: Frontieres
10. D. Amati, G. Veneziano: Phys. Lett. **83B**, 87 (1979)
11. A.H. Mueller: Phys. Rev. **D2**, 2963 (1970); P. Salin: In Proc. of the summer school of Gif-sur -Yvette France (1973)
12. R.C. Brower, C.E. Detar, J.H. Weis: Phys. Rep. **146**, 260 (1974)
13. C.E. Detar, Kyungsik Kang, Chung-I Tan, J.H. Weis; Phys. Rev. **D4**, 425 (1971)
14. G.H. Thomas: Phys. Rev. **D5**, 2212 (1972)
15. E.L. Berger, Ph. Salin, G.H. Thomas: Phys. Lett. **38B**, 265 (1972) Ph. Salin, G.H. Thomas: Nucl. Phys. **B38**, 375 (1972)
16. F. Martin: Phys. Rev. **D19**, 1382 (1979); C. Lopez, F.J. Yndurain: Nucl. Phys. **B171**, 231 (1980); CERN preprint TH-2930-CERN, 19 August (1980); A.J. Buras, K.J.F. Gaemers: Nucl. Phys. **B132**, 249 (1978); E. Reya: DESY 79/88 DO-TH 79/20 December (1979)
17. J.G.H. de Groot et al. : Z. Phys. C—Particles and Fields **1**, 143 (1979)
18. P.C. Bossetti et al. : Nucl. Phys. **B142**, 1 (1978)

Z. Phys. C – Particles and Fields 14, 171–177 (1982)

Zeitschrift für Physik C Particles and Fields
© Springer-Verlag 1982

Model For Nucleon Gluon and Sea Quark Structure Functions at All x and All Q^2 from the Correspondence Between QCD and DTU

G. Cohen-Tannoudji

DPH-T, Cen Saclay, Orme des Merisiers, F-91191 Gif-sur-Yvette, Cedex, France

A. Mantrach[1]

L.P.T.H.E., Université de Paris-sud Orsay, Laboratoire Associé au CNRS, Bât. 211, F-91405 Orsay, France

E.G. Oudrhiri-Safiani[1]

L.P.T.H.E., Université de Paris VII Tour 33, Laboratoire Associé au CNRS LA280, 1er étage, 2 Place Jussieu, F-75261 Paris Cedex 05, France

Received 21 January 1982; in revised form 23 March 1982

Abstract. We propose a simple parametrization of the nucleon gluon and sea quark structure functions at all x, and all Q^2. We use the DTU parton model to fix the parametrization at a reference point ($Q_0^2 = 1.25\,\mathrm{GeV}^2$ and $\Lambda^2 = 0.01\,\mathrm{GeV}^2$) and we mimic the QCD evolution by replacing the dimensioned parameters of the DTU parton model by functions depending on Q^2.

I. Introduction

In the paper of [1] (hereafter denoted as paper I) we have proposed a parametrization of valence structure functions which reproduces the dependence in x and Q^2. This parametrization is based on the so-called DTU parton model [2], that is the parton interpretation of the lowest topology component of the topological expansion of DTU (Dual Topological Unitarization). The Q^2 dependence, constrained by the renormalization group equations of QCD [3], is implemented by replacing, in the structure function of the DTU parton model, all the dimensionned parameters (e.g. Regge slopes and masses) by functions depending on Q^2.

According to the DTU parton model, the valence structure function can be extracted from a simple topological component of one particle inclusive distribution. The duality properties of this component are those of a well studied dual six point functions which is the starting point of the parametrization of the paper I.

The purpose of the present paper is to generalize the procedure of paper I to sea quark and gluon structure functions.

In Sect. II we derive the parametrization of the singlet structure functions at the reference scale. In Sect. III we introduce scaling violations and in Sect. IV we show the comparison with experimental data in deep inelastic scattering and lepton pair production in $p\,p$ collisions.

II. Sea Quarks and Gluons in the DTU Parton Model

1. Topological Characterization

The topological characterization of sea quark structure function has been studied in [4]. Figure 1 shows the topological component of one particle inclusive distribution which involves the sea quark structure function, and its parton interpretation, similar to the one of the valence case [5, 6].

We propose now the topological characterization of gluon structure function. The starting point is the parton interpretation of the cylindrical Pomeron exchange cross section, in terms of wee gluon exchange. Since in Fig. 2 the valence quarks of the

[1] On leave of absence from the laboratoire de Physique Théorique, Faculté des Sciences de Rabat, Av Ibn Battota BP n° 1014, Rabat, Maroc

0170-9739/82/0014/0171/$01.40

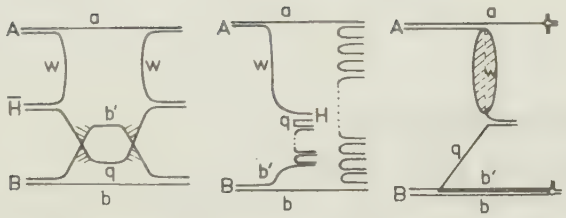

Fig. 1. Topological characterization of the sea quark structure function

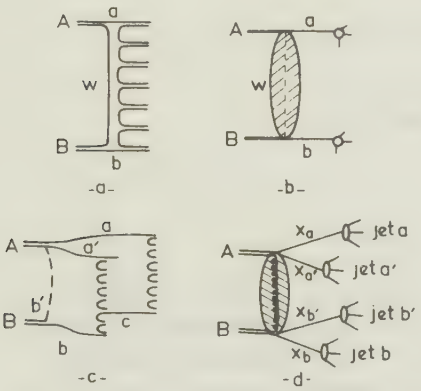

Fig. 2. a, b The parton interpretation of planar total cross sections. c, d The parton interpretation of cylindrical total cross sections

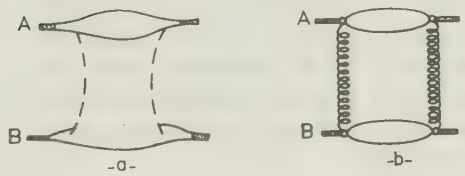

Fig. 3. a The cylindrical pomeron exchange. b The two gluon exchange

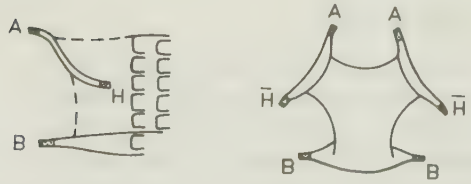

Fig. 4. Topological characterization of the gluon structure function

Fig. 5. Parton interpretation of Fig. 4

initial particles belong the different sheets, it is natural to interpret the interaction mechanism as the exchange of octet, that is a wee gluon. Therefore a pomeron exchange in the t-channel is interpreted as the exchange of two gluons Fig. 3 (in a way similar to the model proposed by Low and Nussinov [7]).

Thanks to this parton interpretation of Pomeron exchanges we can now exhibit the topological component of one particle inclusive cross section which involves a gluon structure functions.

This component is depicted in Figs. 4 and 5. It corresponds to a triple Pomeron coupling since a Pomeron is exchanged in the three channels $A\bar{H}$, $H\bar{A}$, and $B\bar{B}$, but in order to exhibit the gluon structure function this component has to be evaluated in the non diffractive region (H is in the B fragmentation region).

2. *Behaviours in the Double and Triple Regge Regions*

We write here the parton intepretation of the topological components of Figs. 1 and 5

$$f^2(B_{bb'} \xrightarrow[A_{wa}]{} H_{qw}) = \sigma(q + A_{wa} \xrightarrow[w]{} H_{qw} + a) \cdot G_{B_{bb'} \to q}(x, P_\perp) \tag{1}$$

$$f^3(B_{bb'} \xrightarrow[A_{aa'}]{} H_{aa'}) = \sigma(g + A_{aa'} \xrightarrow[(a,a')]{} H_{aa'} + g) \cdot G_{B_{bb'} \to g}(x, P_\perp). \tag{2}$$

The superscripts in (1) and (2) denoted the number of boundaries of the topological component of the six point functions associated with the considered inclusive processes. The subscripts denote the quark content of each involved hadron (supposed to be mesons for simplicity; in case of a baryon one of the subscripts would be replaced by a diquark subscript). The indexes below the arrows in the parton-hadron cross sections denote the exchange of wee parton which induces the reactions, namely a wee quark in the quark-hadron cross-section and a pair of wee quarks in the gluon-hadron cross sections.

Whereas wee quark exchange leads to a Regge pole behaviour for the quark-hadron cross section,

$$\sigma(q + A_{wa} \xrightarrow[w]{} H_{qw} + a) \sim (x\,s)^{\alpha_w - 1} \tag{3}$$

where α_w is the intercept of the $(w\bar{w})$ Regge trajectory, $\alpha_w = \alpha_{w\bar{w}}(0)$. The exchange of a pair of wee quarks leads to a Regge cut behaviour:

$$\sigma(g + A_{aa'} \xrightarrow[(a,a')]{} H_{aa'} + g) \sim (x\,s)^{\alpha^c_{a,a'} - 1} \tag{4}$$

where $\alpha^c_{a,a'}$ is the intercept of the Regge cut build out of the $(a\bar{a})$ and $(a'\bar{a}')$ trajectories,

$$\alpha^c_{a,a'} = \alpha^c_{a\bar{a},a'\bar{a}'}(0) = \alpha_{a\bar{a}}(0) + \alpha_{a'\bar{a}'}(0) - 1 = \alpha_a + \alpha_{a'} - 1. \tag{5}$$

Since both f^2 and f^3 involve a pomeron in the double Regge or central region, both structure functions behave like $1/x$ when x goes to zero. The behaviour in the triple Regge region involves Regge cuts. As shown in Figs. 1 and 5 f^2 involves a cut-pole-cut coupling and f^3 a cut-cut-cut coupling.

$$f^2(B_{bb'} \xrightarrow[A_{wa}]{} H_{qw})_{x\to 1} \sim \left(\frac{s}{M^2}\right)^{2\alpha^c_{qb',wb}(t)} \left(\frac{M^2}{s_0}\right)^{\alpha_w} \tag{6}$$

$$f^3(B_{bb'} \xrightarrow[A_{aa'}]{} H_{aa'})_{x\to 1} \sim \left(\frac{s}{M^2}\right)^{2\alpha^c_{ab,a'b'}(t)} \left(\frac{M^2}{s_0}\right)^{\alpha^c_{a,a'}}. \tag{7}$$

Note that when one combines linear pole trajectories one obtains linear cut trajectory

$$\alpha^c_{ij,kl}(t) = \alpha_{ij}(0) + \alpha_{kl}(0) - 1 + \alpha'_c t \tag{8}$$

where

$$\alpha'_c = \frac{\alpha'_{ij}\alpha'_{kl}}{\alpha'_{ij}+\alpha'_{kl}}$$

3. Parametrization

In paper I the properties of six point function in the narrow resonance dual model were used as a guiding line to derive the parametrization of the valence structure function. This parametrization was obtained by means of the behaviour of the six point function in the double and triple Regge limits; a simplified form was shown to reproduce the behaviour of the six point function in the full range of x and $P_\perp$, namely

$$G^V_{B\to q}(x, P_\perp) = \beta x^{-\alpha_q} \frac{(1-x)^{\alpha_i - 2\alpha(t)} e^{-2\alpha' m^2_{H\perp}}}{|x(\alpha(t)-J)|^2} (1+x)\alpha'^2 m^2_{H\perp}. \tag{9}$$

For the purpose of parametrizing sea quark and gluon structure functions one cannot rely any more on the guiding line of an explicit six point functions provided by the narrow resonance dual model since the involved topologies are much more complicated than the planar one. Nevertheless we propose a parametrization, similar to (9) which takes into account the Regge cut behaviours of f^2 and f^3 in the triple Regge limit, namely

$$G_{B\xrightarrow[b,(b'b'')]{} q^s}(x, P_\perp) = \delta_S x^{-\alpha_{\mathbb{P}}} \frac{(1-x)^{\alpha_w - 2\alpha^c_{bw,q(b'b'')}(t)}(1+x)\, e^{-2\alpha'_c m^2_{H\perp}}\alpha'_c}{|x(\alpha^c_{bw,q(b'b'')}(t) - J^c_{bw,q(b'b'')})|} \tag{10}$$

$$G_{B\xrightarrow[b,(b'b'')]{} g}(x, P_\perp) = \delta_g x^{-\alpha_{\mathbb{P}}} \frac{(1-x)^{\alpha^c_{a,a'} - 2\alpha^c_{ab,a'(b'b'')}(t)}(1+x)\, e^{-2\alpha'_c m^2_{H\perp}}\alpha'_c}{|x(\alpha^c_{ab,a'(b'b'')}(t) - J^c_{ab,a'(b'b'')})|} \tag{11}$$

$B_{b,(b'b'')}$ stands for the proton and $J^c_{ij,k(ll')}$ is the value of $\alpha^c_{ij,k(ll')}(t)$ for $t = t_c = (m_{H_{ij}} + m_{B_{k(ll')}})^2$ which is the t-channel threshold associated with the Regge cut $\alpha^c_{ij,k(ll')}$. A simple pole in the structure function reflects a $(t-t_c)^{1/2}$ behaviour near threshold in the amplitudes. Since one can choose arbitrarily the quark w, a, q, and a' in (10) and (11) and if one assume a symmetrical sea quark distribution, it is possible to use the same Regge cut trajectory in both expression. The only difference between them is then due to the difference between α_w and $\alpha^c_{a,a'}$

$$\alpha_w = 0.5$$
$$\alpha^c_{a,a'} = 0. \tag{12}$$

In (10) and (11) δ_S and δ_g are dimensionless normalization factors. In contrast with the valence case, in which the normalization is fixed by a quark number sum rule for each flavor of quarks, we have in the singlet case only one sum rule, the energy momentum conservation sum rule. One thus needs an additional assumption. We thus assume that gluons carry 45% of the momentum at the point $(Q^2 = Q^2_0)$.

The results concerning $xG_{P\to g}(x)$ and $xG_{P\to q^s}(x)$ are shown respectively in Figs. 6 and 7. These two results are obtained after an integration over $P_\perp$ of

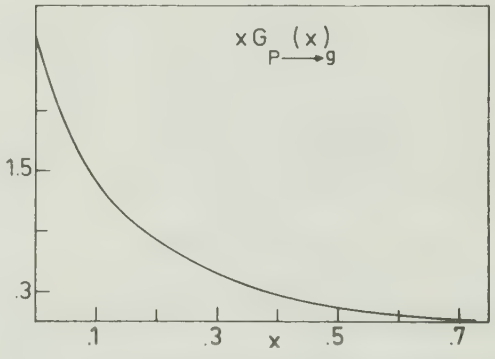

Fig. 6. Gluon structure function $xG_{P\to g}(x)$ in the proton at the reference scale Q^2_0

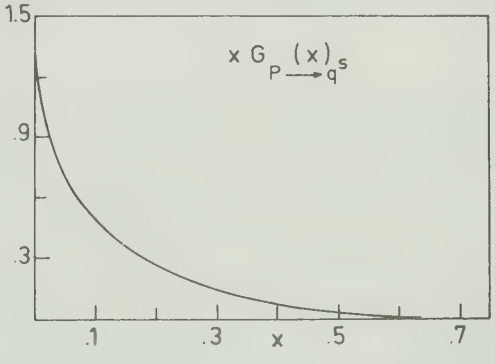

Fig. 7. Sea quark structure function $xG_{P\to q^s}(x)$ in the proton at the reference Q^2_0

(10) and (11).

$$xG_{P\to q^s,\,g}(x)=\delta_{S,g}(1+x)(1-x)^{\alpha_A-J^c_{ij,k(ll')}}$$
$$\cdot e^{-2h(x)}[h(x)\,\mathrm{EXPI}(y_0)-e^{-y_0}/g(x)] \tag{13}$$

where EXPI is the exponential integral function and:

$$h(x)=\alpha'_c\,x(m_B^2(1-x)+m_H^2-t_c) \tag{14}$$

$$g(x)=\frac{2}{x}(\ln(1-x)-x) \tag{15}$$

$$y_0=\alpha'_c\,g(x)\,[(1-x)(x\,,m_B^2-m_H^2)-x\,t_c] \tag{16}$$

$$\alpha_A=\alpha_w,\alpha^c_{a,a'}. \tag{17}$$

III. Q^2 Dependence of Sea Quark and Gluon Structure Functions

In this section we extend to the singlet distributions the method, derived in paper I, to implement scaling violations in the DTU parton model. The structure functions derived in the preceding section are identified with the structure functions at the reference point $Q^2=Q_0^2$ and the Q^2 dependence is introduced by parametrizing the dimensionned quantities in terms of Q^2 dependent functions. The parametrization, very similar to the one introduced in paper I is constrained to reproduce for the moments of the structure functions the evolution predicted by QCD.

The solution of the Altarelli-Parisi moment [3] equations for the singlet quark ($\Sigma(n,Q^2)$) and the gluon ($G_{B\to g}(n,Q^2)$) distribution is given by:

$$\Sigma(n,Q^2)=\{(1-a_n)\,\Sigma(n,Q_0^2)-\tilde{a}_n G_{B\to g}(n,Q_0^2)\}$$
$$\cdot\exp(-d^n_+\,v(Q^2))+\{a_n\Sigma(n,Q_0^2)+\tilde{a}_n G_{B\to g}(n,Q_0^2)\}$$
$$\cdot\exp(-d^n_-\,v(Q^2)) \tag{18}$$

$$G_{B\to g}(n,Q^2)=\{a_n G_{B\to g}(n,Q_0^2)-b_n\Sigma(n,Q_0^2)\}$$
$$\cdot\exp(-d^n_+\,v(Q^2))+\{(1-a_n)\,G_{B\to g}(n,Q_0^2)+b_n\Sigma(n,Q_0^2)\}$$
$$\cdot\exp(-d^n_-\,v(Q^2)) \tag{19}$$

where

$$a_n=\frac{\gamma^{0,n}_{qq}-\lambda^n_+}{\lambda^n_--\lambda^n_+},\qquad \tilde{a}_n=\frac{\gamma^{0,n}_{qg}}{\lambda^n_--\lambda^n_+}$$

$$b_n=\frac{\gamma^{0,n}_{gq}}{\lambda^n_--\lambda^n_+},\qquad d^n_\pm=\frac{\lambda^n_\pm}{2\beta_0}$$

$\lambda^n_\pm$ are the eigenvalues of the one-loop anomalous dimension matrix

$$(q,G)\,\gamma^{0,n}_{ij}=\frac{16\pi^2}{g^2}\cdot\gamma^n_{ij}(g^2)$$

($\gamma^n_{ij}(g^2)$ are the anomalous dimension). Their explicit values were calculated in [8].

The Eqs. (18) and (19), with those of the non singlet part determine the evolution of the moments of structure functions. However to obtain the structure functions themselves (i.e. those depending on x and Q^2), we have to call for the moment inversion method. In addition to the technical difficulty of this method, one is also faced, in the case of quark and gluon singlet structure function, with coupled moment equations.

Nevertheless, assuming of the quark and the gluon singlet part that the behaviours near $x=0$ and $x=1$ are respectively powers of x and $(1-x)$, the results of this inversion to the first order of QCD are [9]

i) The power of x, like in the valence case, is independent of Q^2

ii) Each singlet structure function is expressed in terms of a sum of powers of $(1-x)$ of the quark and gluon singlet. All the powers of $(1-x)$ acquire a linear dependence in $v(Q^2)$; therefore the coefficient of $v(Q^2)$ are different. We shall use these results as a guide to establish our parametrizations for the sea quark and the gluon structure function.

The method of paper I leads to the following parametrization:

$$(\alpha'_c\,t_c)_{Q^2}=(\alpha'_c\,t_c)_{Q_0^2}+\lambda_S\,v(Q^2) \tag{20}$$

$$\left(\frac{(m_H^{S,g})^2}{m_B^2}\right)_{Q^2}=\left(\frac{(m_H^{S,g})^2}{m_B^2}\right)_{Q_0^2}\Big/(1+\mu_S\,v(Q^2)) \tag{21}$$

where $v(Q^2)=\mathrm{Log}(\mathrm{Log}\,Q^2/\Lambda^2/\mathrm{Log}\,Q_0^2/\Lambda^2)$, m_H^S is the mass of particle H for the sea, m_H^g is the mass of particle H for the gluon and Λ is the Q.C.D. scale parameter ($\Lambda=0.1$ GeV, $Q_0^2=1.25\,\mathrm{GeV}^2$). The best fit of the moment evolution will determine the λ_S, μ_S and $m_H^{S,g}$ parameters.

However, one question is still standing up, namely the normalization of the sea quark and gluon structure functions. At the point Q_0^2, we have use the hypothesis of 45% of momentum carried by the gluons, to answer this question. To generalise this answer to all Q^2, we propose to normalize the second moment of the gluon as QCD predicts (19) and in agreement with the hypothesis made at Q_0^2.

A comment is in order about the applicability of our parametrization. In contradiction with the non singlet case, the gluon and sea quark distributions become strongly singular near $x=0$ when Q^2 increases as a consequence of gluon self interactions. Our parametrization does not exhibit this effect; we thus have to be cautious that our parametrization does not work in the very small x region.

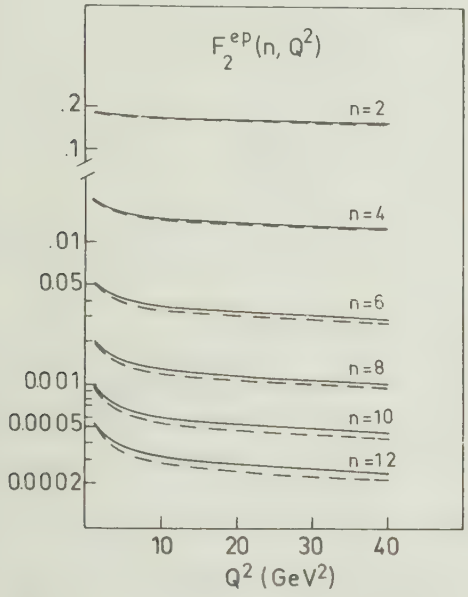

Fig. 8. The solid lines show the QCD evolution of moments of F_2^{ep} from our inputs. The dashed lines (- -) show the evolution resulting from our parametrization

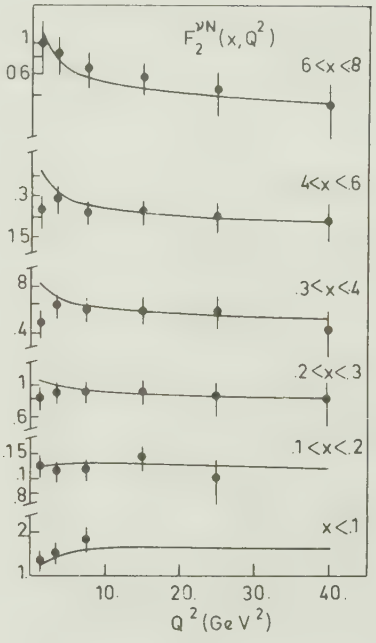

Fig. 9. Comparison of our predictions for $F_2^{\nu N}(x, Q^2)$ with data [10]

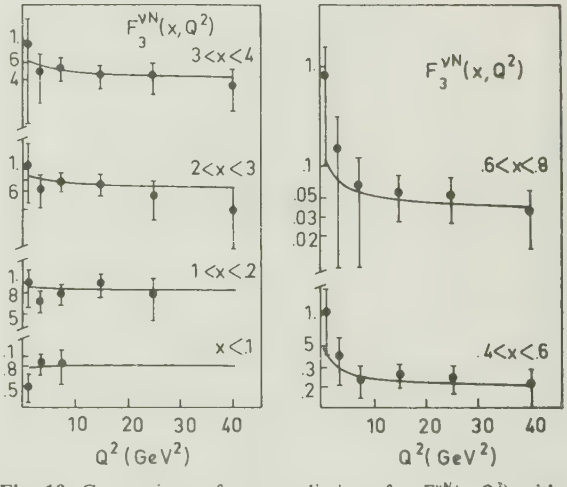

Fig. 10. Comparison of our predictions for $F_3^{\nu N}(x, Q^2)$ with data [10]

λ_S, μ_S and $m_H^{S,g}$ constrained by the evolution of the moments. As shown in Fig. 8 our parametrization reproduce well the QCD evolution with

$$\lambda_S = 3\frac{16}{3\beta_0}, \quad \mu_S = 8\frac{16}{3\beta_0}, \quad (\beta_0 = 11 - \tfrac{2}{3}N_f) \tag{22}$$

and $m_H = 10\,\text{MeV}$ (70 MeV) for the sea quark (the gluon) distribution.

For comparison, the corresponding parameters for the valence distribution where determined in paper I to be

$$\lambda = \frac{1}{2}\frac{16}{3\beta_0}, \quad \mu = 6\frac{16}{3\beta_0} \tag{23}$$

$m_H = 0.3\,\text{GeV}$ (0.6 GeV) for the $u(d)$ valence quark distribution.

IV. Comparison With Data

With these values of λ, μ and m_H parameter, we can predict the x and Q^2 dependence of $F_2^{\nu N}$, $F_3^{\nu N}$ and $F_2^{\mu P}$ Figs. 9–11. The agreement with experiments [10, 11] are satisfactory. Furthermore Figs. 12 and 13 exhibit our predictions respectively of $xG_{P\to q^S}(x, Q^2)$ and $xG_{P\to g}(x, Q^2)$ for $Q^2 = 6$, 40 and 2,000 GeV^2.

A clean text of our model is provided by lepton pair production in pp collision (the so called Drell Yan process)

$$pp \to \mu^+ \mu^- + x\,.$$

This process has been studied [12] at first order in $\alpha_S(Q^2)$ (here Q^2 is the square invariant mass of the lepton pair). It involves valence, sea quark and gluon distributions.

In Figs. 14 and 15 we compare the predictions of our model with the Owens and Reya parametrization [13] and with existing data [14, 15] for the inclusive cross section at zero rapidity ($y=0$) and the average squared transverse momentum. The results are satisfactory.

The comparison of our parametrization with data raises the following comments:

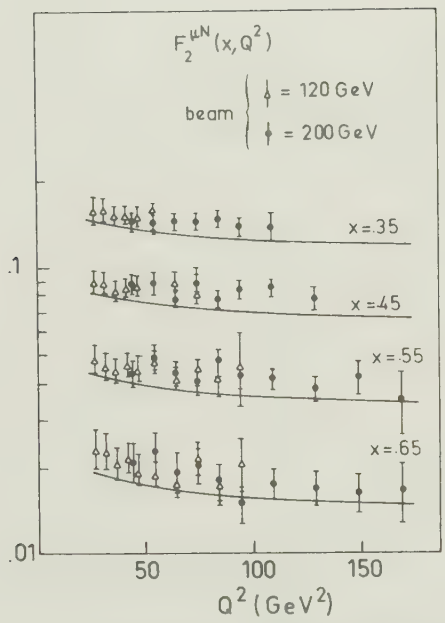

Fig. 11. Comparison of our predictions for $F_2^{\mu N}(x, Q_0^2)$ with data [11]

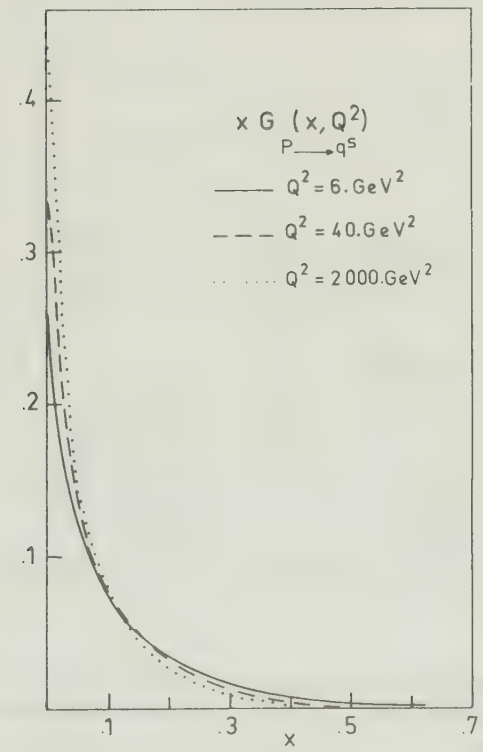

Fig. 12. $xG_{P\to q^S}(x, Q^2)$ as a function of x for $Q^2=6$, 40 and 2,000 GeV^2

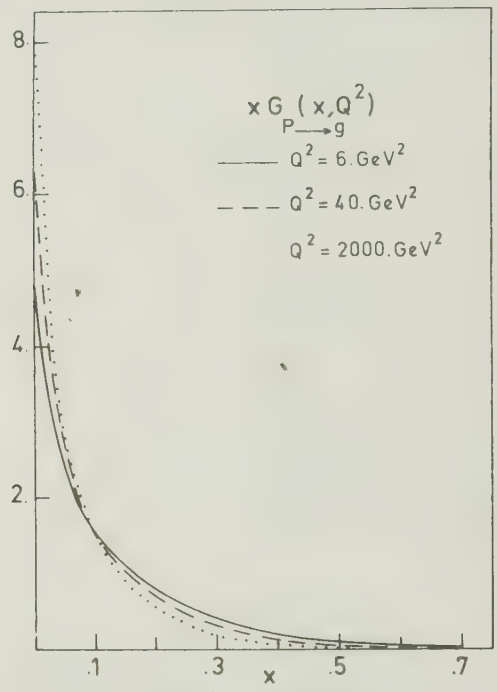

Fig. 13. $xG_{P\to g}(x, Q^2)$ as a function of x for $Q^2=6$, 40 and 2,000 GeV^2

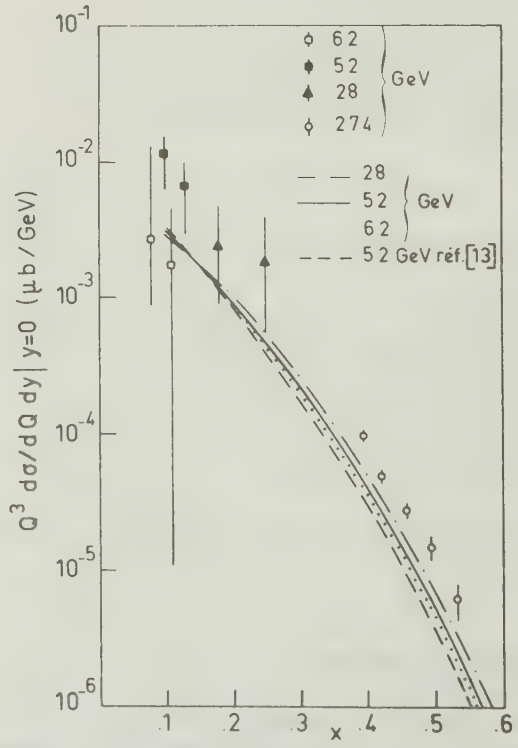

Fig. 14. Comparison of our predictions for $Q^3 \left.\frac{d\sigma}{dQ\,dy}\right|_{y=0}$ with the ones of Owens and Reya [13]. The pp data are from [14] and the pN data are taken from [15]

i) In our parametrization the sea quark and gluon distributions are rather "hard", i.e. the powers of $(1-x)$ are not too large. Naive parametrizations [9] imply on the contrary very high powers of $1-x$ at large Q^2. Because of this feature, these naive parametrizations completely fail in reproducing data.

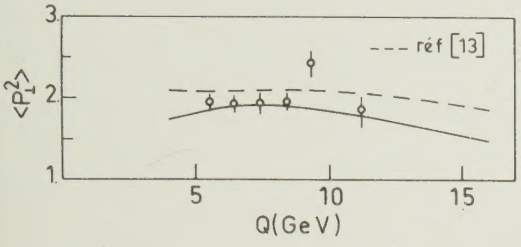

Fig. 15. Comparison of our predictions for $\langle P_\perp^2 \rangle_{y=0}$ with the ones of Owens and Reya [13]. The data are from [14]

ii) Although our parametrization leads to a curve which is above the one resulting of the Owens and Reya parametrization in Fig. 14, we are still below the data by a factor smaller than 2.3.

iii) The experimental point which is not fitted at all in Fig. 15 is not far from the Υ mass.

iv) Our parametrization confirms the smallness of Λ ($\Lambda = 100$ MeV).

References

1. G. Cohen-Tannoudji, A. El Hassouni, A. Mantrach, E.G. Oudrhiri Safiani: preprint DPh-T/81/55 Saclay July (1981) Z. Phys. C - Particles and Fields **13**, 219-227 (1982)
2. G. Cohen-Tannoudji, F. Hayot, R. Peschanski: Phys. Rev. **D17**, 2930 (1978)
3. For general review on QCD results see: E. de Rafaël: Proc. of summer School of Gif-sur-Yvette France (1978); V. Alessandrini: Second Rencontre de Rabat Maroc (1979); A.J. Buras: Rev. Mod. Phys. **52**, 199 (1980); and invited talk presented at symposium on topical questions in QCD, Copenhagen, July (1980)
4. G. Cohen-Tannoudji, A. El Hassouni, J. Kalinowski, R. Peschanski: Phys. Rev. **D19**, 3397 (1979); G. Cohen-Tannoudji et al.: Phys. Rev. **D21**, 2699 (1980)
5. A. El Hassouni, O. Napoly: Phys. Rev. **D23**, 193 (1981)
6. A. El Hassouni, A. Mantrach, E.G. Oudrhiri-Safiani: Z. Phys. C - Particles and Fields **9**, 185 (1981)
7. F.E. Low: Phys. Rev. **D12**, 163 (1975); S. Nussinov: Phys. Rev. **D14**, 264 (1976)
8. G. Altarelli, G. Parisi: Nucl. Phys. **B126**, 298 (1977)
9. F. Martin: Phys. Rev. **D19**, 1382 (1979); C. Lopez, F.J. Yndurain: Nucl. Phys. **B171**, 231 (1980) and CERN preprint TH-2930-CERN, 19 August (1980); A.J. Buras, K.J.F. Gaemers: Nucl Phys. **B132**, 249 (1978)
10. J. Morfin et al.: Phys. Lett. **104B**, 235 (1981)
11. D. Bollini et al.: Phys. Lett. **104B**, 403 (1981)
12. H.D. Politzer: Nucl. Phys. **B129**, 301 (1977); G. Altarelli, G. Parisi, R. Petronzio: Phys. Lett. **76B**, 351, 356 (1978); F. Halzen, D.M. Scott: Phys. Rev. **D18**, 3378 (1978); K. Kajantie, R. Raitio: Nucl. Phys. **B139**, 72 (1978)
13. J.F. Owens, E. Reya: Phys. Rev. **D17**, 3003 (1978)
14. J.H. Cobb et al.: Phys Lett. **72B**, 273 (1977)
15. D. Antreasyan et al.: Phys. Rev. Lett. **39**, 906 (1977); D.M. Kaplan et al.: Phys. Rev. Lett. **40**, 435 (1978)

RESUME :

Cette thèse est une contribution à l'étude de la chromodynamique quantique (QCD) à l'approximation des logarithmes dominants (ALD). Nous avons utilisé l'interprétation de l'ALD en terme de modèle des partons généralisés pour proposer des tests des processus élémentaires de QCD dans les réactions de photoproduction à grand moment transverse. Nous avons utilisé l'ALD pour sommer les effets de radiation de gluons induits dans une collision hadronique à haute énergie. Nous avons obtenu ainsi une montée de 15 mb de la section efficace totale nucleon-nucleon entre 60 GeV et 540 GeV. Nous avons utilisé l'existence d'une transition de préconfinement dans l'ALD pour étudier les brisures d'invariance d'échelle dans le modèle dual des partons.

Sujet : INTERACTIONS FORTES ET CHROMODYNAMIQUE
A L'APPROXIMATION DES LOGARITHMES DOMINANTS

MOTS CLES

QCD, Aproximation des logarithmes dominants, modèle des partons généralisés, photoproduction à grand P_T, radiation des gluons, préconfinement, modèle dual des partons.

MANTRACH ABDELHAQ